CCM-82-03

COMPRESSIVE FLOW OF VISCOELASTIC MATERIALS

SEUNG JONG LEE

CENTER FOR COMPOSITE MATERIALS

College of Engineering
University of Delaware
Newark, Delaware

```
@str6/@str6
!!


--    1  OF    1
--                      **ITIC DOES NOT HAVE THIS ITEM**
-- 1 -  AD NUMBER: D412811
-- 5 -  CORPORATE AUTHOR: DELAWARE UNIV NEWARK CENTER FOR COMPOSITE
--      MATERIALS
-- 6 -  UNCLASSIFIED TITLE:     COMPRESSIVE FLOW OF VISCOELASTIC MATERIALS.
--10 -  PERSONAL AUTHORS: LEE,E. S. ;
--11 -  REPORT DATE:      JUN   , 1961
--12 -  PAGINATION:    20P
--14 -  REPORT NUMBER:    CCM-61-03
--20 -  REPORT CLASSIFICATION:  UNCLASSIFIED
--21 -  SUPPLEMENTARY NOTE:     PH.D THESIS SUBMITTED TO UNIVERSITY OF
--      DELAWARE.
--22 -  LIMITATIONS (ALPHA):    APPROVED FOR PUBLIC RELEASE; DISTRIBUTION
--      UNLIMITED. AVAILABILITY: CENTER FOR COMPOSITE MATERIALS, UNIVERSITY
--      OF DELAWARE, NEWARK, DE. 19711.
--33 -  LIMITATION CODES:  1  24
--******
--                  END OF DISPLAY LIST

--                ((ENTER NEXT COMMAND))
```

COMPRESSIVE FLOW OF VISCOELASTIC MATERIALS

by

Seung Jong Lee

A dissertation submitted to the Faculty of the University of Delaware in partial fulfillment of the requirements for the degree of Doctor of Philosophy in Chemical Engineering

June, 1982

ACKNOWLEDGMENTS

I would like to express my sincere gratitude to my academic advisors, Drs. A. B. Metzner and M. M. Denn for their considerate guidance, invaluable inspiration, and encouragement during the pursuit of present work.

I am indebted to Dr. M. J. Crochet of Universite Catholique de Louvain, Belgium for his support, and suggestions concerning with the finite element calculations and for allowing me to use his finite element codes throughout the course of this work.

I am thankful to Dr. K. F. Wissbrun of Celanese Research Corporation for providing rheological measurements on some of the testing materials.

Special thanks are extended to Drs. C. D. Denson, R. L. McCullough, A. V. Rama Murthy, and R. K. Gupta for their many helpful commemts and suggestions.

The silicone polymer and TLA-227 used in this study were donated by F. N. Cogswell of ICI, England and Texaco, Inc., respectively. This generosity are highly appreciated.

I am also grateful for having had the opportunity to

work with an excellent student, G. Riggins, who carried out most of squeezing experiments and capillary measurements.

Financial support by the Center for Composite Materials, University of Delaware is deeply acknowledged. I am also grateful to Dr. R. B. Pipes, the Director of the Center, who was a source of constant help and encouragement throughout this work.

Finally, I wish to express my gratitude to my parents, who have given me the best education possible both at home and at school, and to my brother and sisters for their encouragement from Seoul.

TABLE OF CONTENTS

LIST OF FIGURES

Figures

LIST OF TABLES

Tables

ABSTRACT

The compressive flow of viscoelastic materials between two parallel flat disks under a constant load has been investigated analytically, numerically, and experimentally. This process simulates a number of compression molding and lubrication experiments; the purpose of our study was to assess the effects of fluid viscoelasticity and of temperature gradients in these applications.

A dimensionless group S ($= \frac{\eta_{max} H^2}{\eta_{min} R^2}$) has been found very useful for determining the flow regimes when there exists a substantial transverse viscosity gradient in the fluid charge, such as in the nonisothermal compression molding processes.

Compressive flow of linear viscoelastic materials has been analyzed analytically. It shows that the squeezing motion becomes oscillatory when the ratio of the Deborah number to the Reynolds number is larger than a critical value, and that the linear viscoelastic materials are squeezed faster than the corresponding Newtonian cases.

Compressive flow of various non-linear model fluids has also been analyzed numerically. The Maxwell fluid

behaves much like linear viscoelastic materials, except under extraordinarily high loading conditions. But, the Johnson- Segalman model and the Marrucci structural model show that slower squeezing may arise after the initial rapid transient under moderate loading conditions. This slower squeezing must be due to the special features of these models, which the Maxwell model does not exhibit, such as stress overshoot in the transient flows.

Experimentally two different observations have been made. A silicone polymer shows the oscillatory and the faster squeezing, which is predictable by the Maxwell type of model fluid. Two other polymer solutions show an inflection point, which probably reflects a very weak oscillation, and a slower squeezing than for the corresponding inelastic cases. The slower squeezing of these solutions seems to be due to the transient behavior of these materials such as stress overshoot. The use of those models, which can predict the transient behavior more precisely, is recommended to describe the transient responses of these materials.

NOMENCLATURE

Symbols

a	acceleration of the top plate
a_T	horizontal shift factor
C_i	constants
$\underline{d}$, d_{ij}	deformation rate tensor, and its components
f	function f defined by (4.3)
F	force on the top plate
g	gravitational acceleration
G	shear modulus
G_o	G at the equilibrium in (3.67)
G'	storage modulus
G''	loss modulus
H	half of the total film thickness
H_o	half of the initial film thickness at t=0
K	consistency factor of power-law fluid
m	mass of the load on the top plate
n	power-law index of power-law fluid
p	pressure
r	radial position
R	radius of the disk
R_o	initial radius of the disk

S	dimensionless number defined by (2.14)
t	time
$\bar{t}$	dimensionless time defined by (2.19)
Δt	time increment
Δt_n	time increment defined by $t_{n+1} - t_n$
T	oscillation period
V	speed of the top plate
$\underset{\sim}{V}$	velocity vector
V_r	radial velocity
V_z	axial velocity
$\underset{\sim}{V}_i$	descritized $\underset{\sim}{V}$ at node i
$\underset{\sim}{V}_n$	descritized $\underset{\sim}{V}$ at $t=t_n$
x	structural variable
$\underset{\approx}{X}$	spacial coordinate
z	axial position

Greek symbols

$\dot{\gamma}$	shear rate in simple shear flow
$\dot{\gamma}_w$	wall shear rate
$\dot{\gamma}_{max}$	maximum shear rate
δ	thickness of the lubricant layer
$\dot{\epsilon}_b$	biaxial extensional rate
ε	material parameter in equation (3.53)
η	viscosity
η_o	zero shear viscosity

η^*	complex viscosity
η_p	viscosity of the polymer
η_{sv}	viscosity of the solvent
η_1	viscosity of the lubricant (less viscous layer)
η_2	viscosity of viscous layer
θ	angular position
λ, λ_1	relaxation time
λ_2	retardation time
λ_o	λ at the equilibrium defined by (3.67)
ξ	material parameter in equation (3.53-55)
ρ	density of the material
ρ_m	pseudo-fluid density defined by (3.47) or (4.24)
ρ^*	apparent density ($=\rho+\rho_m$)
$\underline{\sigma}$, σ_{ij}	total stress tensor, and its components
$\underline{\tau}$, τ_{ij}	extra atress tensor, and its components
$\underline{\tau}_i$	descritized $\underline{\tau}$ at node i
$\underline{\tau}_n$	descritized $\underline{\tau}$ at $t=t_n$
$\underline{\tau}_p$	$\underline{\tau}$ due to the polymer
$\underline{\tau}_{sv}$	$\underline{\tau}$ due to the solvent
$\hat{\underline{\tau}}$, $\hat{\tau}_{ij}$	$\underline{\tau}/G$, τ_{ij}/G
ϕ_i	linear interpolation functions
ψ_i	quadratic interpolation functions
ω	angular frequency
Π_d	second invariant of the deformation rate tensor $\underline{d}$

$\frac{D}{Dt}$	material time derivative
$\frac{\delta}{\delta t}$	contravariant convected Oldroyd time derivative
∇	contravariant convected Oldroyd time derivative
Δ	covariant convected Oldroyd time derivative

CHAPTER 1

INTRODUCTION

1.1 Relevance of the problem

The problem to be considered in this work is that of the compressive flow* of viscoelastic fluids between two horizontal circular flat disks, shown schematically in Fig. 1.1. The test fluid is contained between two disks which are at rest for times $t<0$; at $t=0$ the upper disk is released and falls under the normal load F. The spacing between the disks is measured as a function of time.

This compressive flow between disks is of interest for many reasons.

(1) It is encountered in the popular plastometer method, which has been used to determine the material properties of highly-viscous materials.

(2) It is also encountered in certain polymer

*The term "compressive flow" stands for the flow in the opposite sense of the extensional flow, not for the flow of compressible fluids. It is equivalent to "squeezing flow" or "squeeze film flow" which has been used more often in the literature.

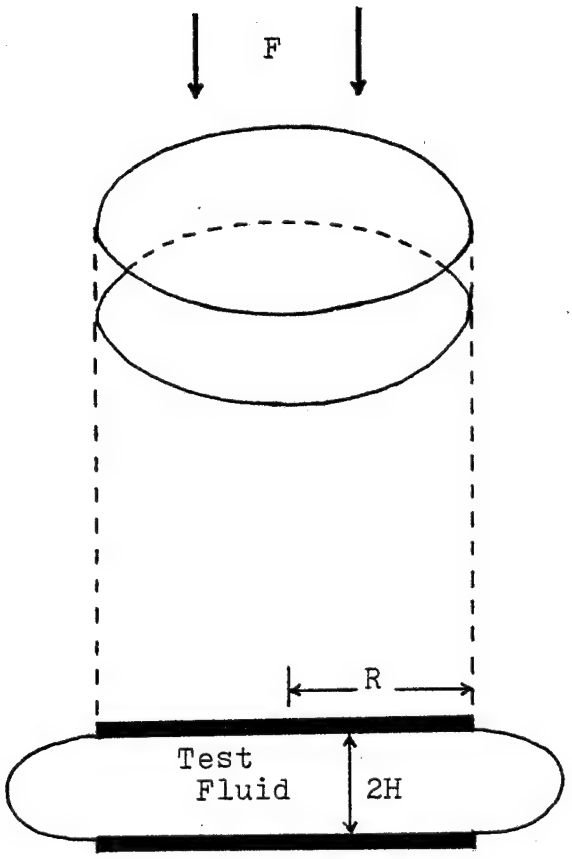

Fig. 1.1 Schematic diagram of the compressive flow.

processing operations such as compression molding, injection molding, stamping, etc. The polymeric charges in these processes are frequently filled with fibers, whose orientation will determine the material properties of final products, and the orientation of the fibers is believed to be determined by the flow behavior of the polymeric medium.

(3) It also arises in lubrication systems, and there has been a controversy as to whether or not viscoelastic lubricants will perform better than Newtonian lubricants, since modern motor oils often contain polymeric additives which render them viscoelastic.

(4) Most of all, this flow is of particular interest to rheologists since both shearing and extensional deformations are present under transient conditions, the flow being dominated by shear near the wall and by extension in the middle of the gap. Therefore, the compressive flow is a good candidate to be used in evaluating proposed constitutive equations, especially transient responses, and further improving them.

It will be assumed throughout that the fluid is incompressible.

1.2 Review of previous work

In this section we will review the principal

theoretical studies and experimental work which have been published.

Stefan(1874) appears to be the first to have dealt with this problem. He analyzed the flow for Newtonian fluids and derived the equation

$$H(t) = \left[\frac{1}{H_0^2} + \frac{16 F t}{3\pi \eta R^4} \right]^{-\frac{1}{2}} \qquad (1.1)$$

which is known as the Stefan equation after him. A complete list of symbols and their meanings are found in the Nomenclature. A more systematic derivation of equation (1.1), based upon the creeping flow approximation and the parallel squeezing assumption, is given by Denn(1980). Here the term "parallel squeezing" implies that material planes which are initially horizontal remain so during the subsequent deformation. This assumption is not always valid, even though it is very useful in many cases. In Section 2.2, we will consider an example in which the parallel squeezing assumption fails. This has been also mentioned by Brindley et. al.(1976). The Stefan equation has been tested and verified experimentally for Newtonian fluids by many authors, including Parlato(1969), Leider(1974), Brindley et. al.(1976), and Grimm(1977).

In 1931, the squeezing of power-law fluids was analyzed by Scott(1931), who developed an equation similar

to equation (1.1) given by

$$H(t)=\left[\left(\frac{1}{H_0}\right)^{\frac{n+1}{n}}+\frac{2(n+1)}{2n+1}\,\frac{F(n+3)}{\pi K R^{n+3}}\,t\right]^{-\frac{n}{n+1}} \qquad (1.2)$$

where K and n are the consistency factor and the power-law index of the given power-law fluid, respectively. The derivation of equation (1.2) will not be repeated here since complete developments of the Scott equation are given elsewhere (Scott,1931; Leider and Bird,1974; Grimm,1977). Experimental work on power-law fluids has been carried out by Parlato(1969), Leider(1974), Brindley et. al.(1976), and Grimm(1977). In general, experimental data agree well with the Scott equation.

Various researchers have considered the case of viscoelastic fluids in the compressive flow. All of them except Metzner(1968a) predict that viscoelastic fluids squeeze out faster than the corresponding inelastic fluids, which is the opposite of many available experimental results.

Tanner(1965) analyzed the flow for contravariant convected Maxwell fluids with a power-law viscosity and a constant relaxation time. He argued that the normal stress effects are small compared to the shear stress effects and predicted faster squeezing of viscoelastic fluids than the corresponding power-law fluids.

Metzner(1968a) appears to be the first to have recognized the possible importance of the extensional flow as well as the shearing flow in this problem. He mentioned that extraordinarily high stresses are predicted to be required for rapid extensional deformation of viscoelastic fluids, and he predicted slower squeezing of viscoelastic fluids (contravariant convected Maxwell fluids) based upon the "extensional primary field" approximation (Metzner,1971). Williams and Tanner(1970) also considered a combination of shear and extensional effects but concluded that extensional effects are small compared to the shearing effects.

Kramer's analysis(1974) is unique in that the particle path equations are numerically solved using a convected coordinate system without neglecting any of the normal stresses. He used the integral constitutive equation of Lodge's rubberlike liquid(see Lodge, 1964) with a single exponential memory function, which is identical to the contravariant convected Maxwell fluid. By assuming parallel squeezing and negligible inertia, he predicted an initial instantaneous drop and more rapid squeezing of viscoelastic fluids. The initial drop implies that the material has no resistance at the instant t=0 except its own inertia; no resistance of the material implies zero apparent viscosity, hence infinite Reynolds number. Thus, the inertia should be

taken into account in the compressive flow of viscoelastic materials under a constant load, even though the creeping flow approximation (negligible inertia) is very useful in the inelastic cases.

Leider and Bird(1974) have suggested that the use of a rheological model which can describe stress overshoot in simple shear flow is imperative to explain the slower squeezing of viscoelastic fluids. The models used in the three analyses cited above do predict the presence of a first normal stress difference, but do not predict the stress overshoot phenomena or a second normal stress difference in shear flows. Leider and Bird proposed an empirical equation with an overshoot correction factor to be used in squeeze film problems.

Brindley et. al.(1976) analyzed the flow for the second order fluid and again predicted faster squeezing of viscoelastic fluids. The second order fluid shows the first and second normal stress differences in shear flows, but no stress overshoot. They also presented some very interesting experimental results which show solid-like bouncing behavior under some severe loading conditions, but they did not provide a theoretical explanation of this bouncing behavior.

Experimental studies on viscoelastic materials include those of Parlato(1969), Leider(1974), Brindley

et. al.(1976), and Grimm(1978). In general, with slow squeezing (low Deborah number), the squeezing behavior of viscoelastic fluids is close to the corresponding inelastic case. With fast squeezing (high Deborah number) most of experimental results show that viscoelastic materials squeeze out much slower than the corresponding inelastic fluids, and under very severe loading conditions some materials even bounce back after some amount of squeezing.

Some authors (Leider,1974; Leider and Bird,1974) have used the "half time", which is the time required for the disks to move from a separation H_o to $H_o/2$, to represent their experimental results. The "half time" is very useful in representing the data of purely viscous materials, but it is not recommended in the viscoelastic cases since it may conceal interesting elastic effects. This has been pointed out by Binding et. al.(1976a).

Tichy and Winer(1978) studied constant speed squeezing flow instead of constant load squeezing, using Lodge's rubberlike liquid model with a single relaxation time. They predicted that the load-bearing capacity of a viscoelastic fluid may be increased due to normal stress effects or decreased due to a delayed response of shear stress to a change in shear rate.

Shirodkar(1981), and Shirodkar and Middleman(1982)

also considered constant speed squeezing flow. They used a constitutive equation due to Wagner(1976), which is an empirical modification to the Lodge's rubberlike liquid model. Even though Wagner's model is capable of exhibiting non-Newtonian viscosity, normal stress in simple shear flow, and stress overshoot in transient simple shear flow, the principal drawback in this model is the absence of a general form of the damping function. They predicted that fluid elasticity can increase the force resisting the approach of the boundaries of a squeeze film at high shear rate. They also suggested that generalizations regarding the role of viscoelasticity may be impossible and the effect of polymeric additives on load-bearing capacity appears to depend upon whether the motion is under constant load or constant speed, or some combination thereof.

The properties of polymeric materials responsible for the slower squeezing found experimentally are still in question and need to be studied more systematically.

There has been a somewhat different question in the compression molding process (usually nonisothermal) which concerns the flow in the mold. It is important to identify the portion of the material that flows preferentially to fill the remainder of the mold cavity: the fluid near the wall or that in the central portion of the mold. The answer will depend upon factors such as geometry, material

properties, and temperature gradient in the mold. Both cases have been observed experimentally. There has been no quantitative analysis of this flow.

1.3 Objectives and approaches of present work

Several basic problems in compressive flow remain unsolved. Resolving those problems will be the main objectives of this work, as follows:

(1) We require a better qualitative understanding of the behavior in compressive flow of viscoelastic materials between disks under isothermal conditions.

(2) Furthermore, we wish to analyze this flow quantitatively to explain the experimental observations of slower squeezing and bouncing behavior of viscoelastic materials.

(3) Finally, in the compression molding processes, we wish to understand the preferential flow of some portion of the material in the mold cavity.

In chapter 2 we will consider the compressive flow of purely viscous fluids, including Newtonian and power-law fluids. The flow in the mold cavity will be also examined quantitatively in this chapter.

Compressive flow between disks is not simple; it is a combination of shearing and extensional flow under transient conditions, and the viscoelastic nature of the materials of primary interest makes the problem even more complex. Before dealing with this complex problem we consider a rather simple, but closely related problem in Chapter 3; this is lubricated compressive flow. Since lubricated compressive flow between disks is essentially biaxial extensional flow, various kinds of non-linear viscoelastic constitutive equations can be treated without great difficulty. The unlubricated problem will be considered in Chapter 4. Numerical computation is required in this case. The finite element numerical technique, which will be tested in the simple lubricated problem in Chapter 3, will be applied to solve the continuity, momentum, and constitutive equations simultaneously. In Chapter 5, experimental results will be compared to the theoretical predictions.

CHAPTER 2

COMPRESSIVE FLOW OF PURELY VISCOUS FLUIDS

The compressive flow of purely viscous fluids will be treated in this chapter, focusing on the following:

(1) We will investigate the validity of the Stefan equation (for a Newtonian fluid) and Scott equation (for a power-law fluid) by finite element calculations, in Section 2.1 and 2.3, respectively.

(2) We will analyze the flow in the mold cavity for the compression molding process in Sections 2.2 and 2.4.

(3) Throughout this chapter we will test the finite element and other numerical schemes used to solve compressive flow problems.

2.1 Newtonian fluid

The compressive flow of an isothermal inelastic fluid, neglecting fluid inertia, is governed by the following equations and boundary conditions:

Continuity:

$$\frac{1}{r}\frac{\partial}{\partial r}(rV_r) + \frac{\partial V_z}{\partial z} = 0 \qquad (2.1)$$

Navier-Stokes (variable viscosity, $\eta = \eta(r,z)$):

$$0 = -\frac{\partial p}{\partial r} + \frac{2}{r}\frac{\partial}{\partial r}\left[\eta r \frac{\partial V_r}{\partial r}\right] - \frac{2}{r^2}\eta V_r + \frac{\partial}{\partial z}\left[\eta\left(\frac{\partial V_z}{\partial r} + \frac{\partial V_r}{\partial z}\right)\right] \qquad (2.2)$$

$$0 = -\frac{\partial p}{\partial z} + \frac{1}{r}\frac{\partial}{\partial r}\left[\eta r\left(\frac{\partial V_z}{\partial r} + \frac{\partial V_r}{\partial z}\right)\right] + \frac{\partial}{\partial z}\left(2\eta \frac{\partial V_z}{\partial z}\right) \qquad (2.3)$$

Boundary conditions (see Fig. 2.1 for description of the coordinate system used):

$$V_r = 0\,, \quad \frac{\partial V_z}{\partial r} = 0 \qquad \text{at } r = 0 \qquad (2.4)$$

$$V_z = 0\,, \quad \frac{\partial V_r}{\partial z} = 0 \qquad \text{at } z = 0 \qquad (2.5)$$

$$V_r = 0\,, \quad V_z = -V \qquad \text{at } z = H \qquad (2.6)$$

All the stresses vanish at the free surface (2.7)

The second condition in (2.4) comes from the requirement of zero shear stress along the axis of symmetry. In the case of the parallel squeezing assumption(Section 2.2.1) this condition is automatically satisfied. This problem has been solved, based upon the parallel squeezing assumption, to give the Stefan equation (1.1).

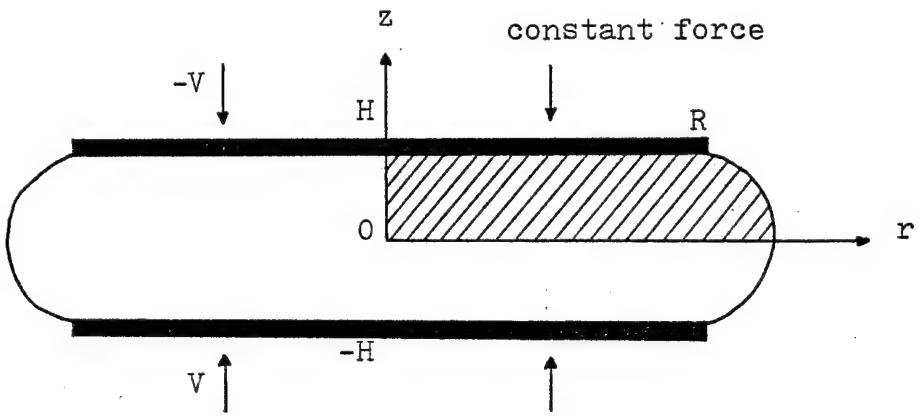

Fig. 2.1 The domain used in the numerical calculations.

We wish to solve the problem numerically with no assumptions in order to compare the solution to the Stefan equation. A finite element technique will be used: the finite element formulation for generalized Newtonian fluids is given in appendix D.I.

Because of flow symmetry, the domain of interest in numerical calculations will be confined to a quarter of entire domain (shaded portion in Fig. 2.1). Neglecting fluid inertia, the problem becomes a quasi-steady state problem even though the flow itself is transient. Therefore, at each time instant we solve the steady state equations (2.1-2.3) under the boundary conditions (2.4-2.7) on the given domain. Then, after a given time increment(Δt), we move the boundary of the domain by $\underset{\sim}{V} \times \Delta t$, solve the problem on the new domain, and proceed to the next time step. The numerical algorithm is given in Fig. 2.2. Between time steps, a predictor-corrector method is used; since the problem is entirely linear, the top plate velocity(V) is adjusted linearly to produce the given constant force.

Numerical calculations have been carried out for three different values of R/H_o(=5,15,50). The results are compared to the Stefan equation in Fig. 2.3, in which dimensionless film thickness(H/H_o) is plotted against dimensionless time, $\bar{t}(=\frac{16}{3}\frac{F}{\pi R^2}(\frac{H_o}{R})^2\frac{t}{\eta})$. At large values of

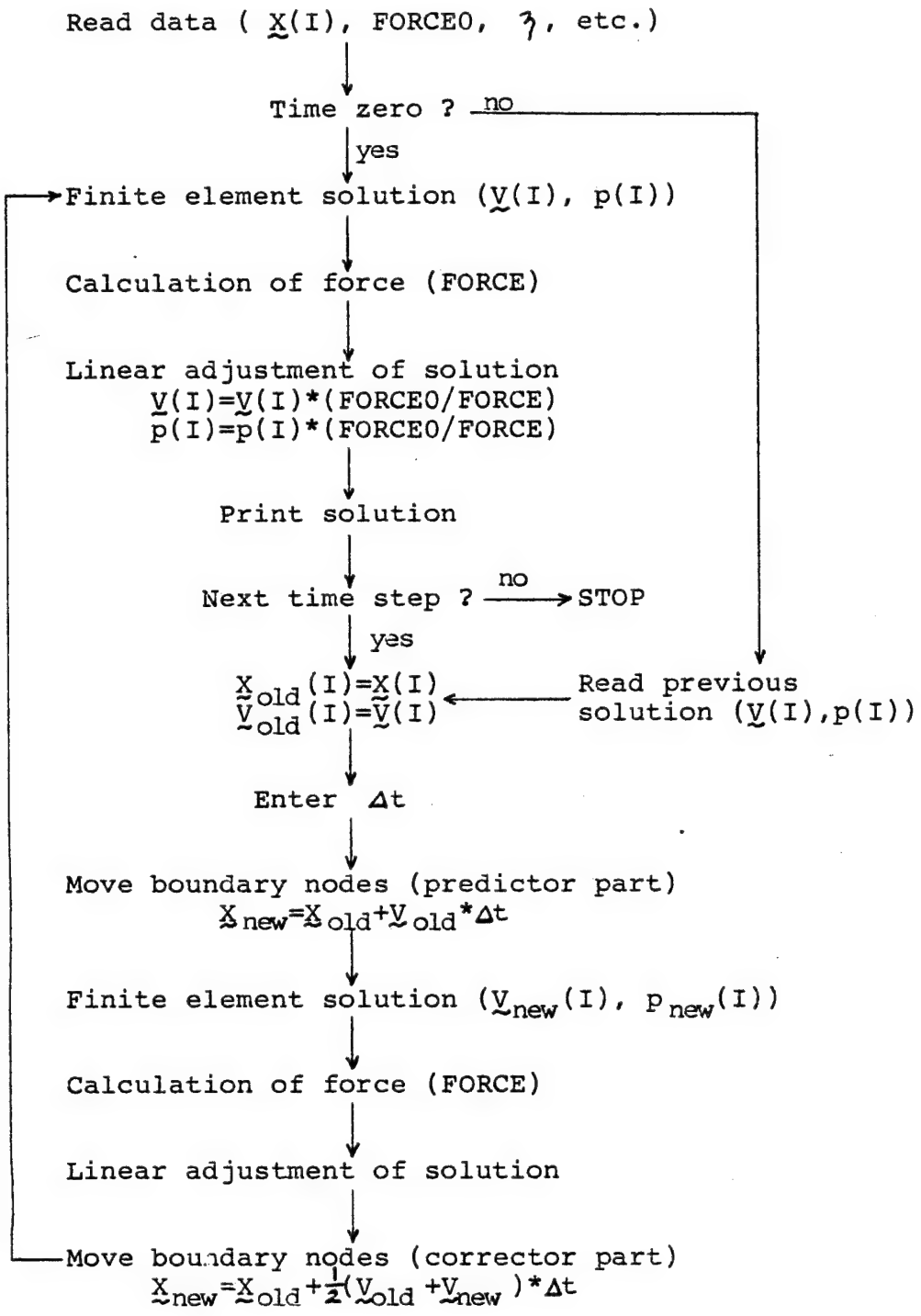

Fig. 2.2 Numerical algorithm to solve compressive flow of Newtonian fluids.

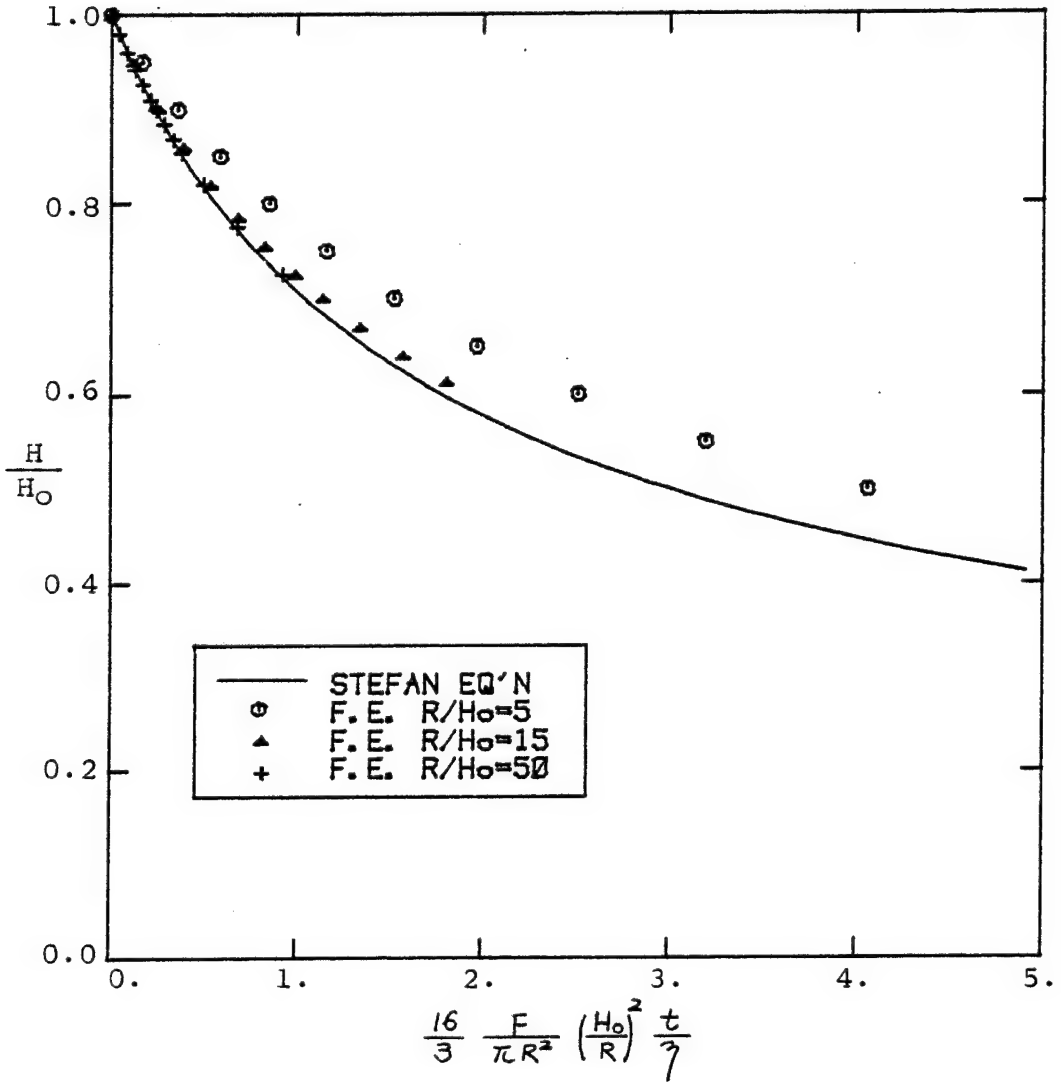

Fig. 2.3 Dimensionless plate spacing versus dimensionless time for isothermal squeezing of Newtonian fluids.

R/H_o, numerical results agree well with the Stefan equation, but as R/H_o decreases the discrepancy between the numerical solution and the Stefan equation increases. This discrepancy is due to the velocity rearrangement caused by the stress singularity at the edge of the disk and becomes small as R/H_o increases, which is also seen in the pressure profiles (see Fig. 6 and 7 in Appendix A). In other words, the parallel squeezing assumption is a good one as long as R/H is large enough.

In the next section we will see a typical example in which the parallel squeezing assumption no longer holds and the boundary condition at the edge of the disk plays an important role.

2.2 Compressive flow between parallel disks with a transverse viscosity gradient

Let us consider the flow in the mold cavity in the compression molding process, which is depicted schematically in Fig. 2.4. There have been two different observations on the flow patterns induced as the mold is closed; Marker and Ford(1977) observed the preferential flow of hot material near the mold faces, while Denton(1981) and Denn, Tadmor, and Edelist(1981) reported no preferential flow of the fluid near the wall and found the maximum velocity at the center plane. These flow patterns are shown schematically in

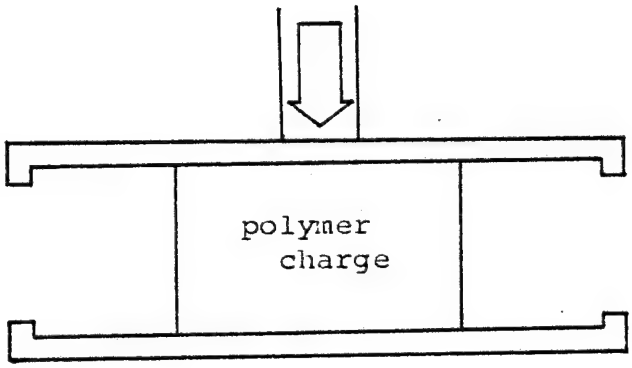

Fig. 2.4 Schematic diagram of the compression molding process.

Fig. 2.5. Qualitatively it is obvious that both cases are possible, depending upon the material properties, geometry, and processing conditions.

A detailed quantitative analysis of this problem is given in Appendix A, and only its essence will be discussed in this section. Here we consider the flow between approaching disks when there is a substantial viscosity gradient in the fluid charge; this viscosity difference may result from the temperature difference caused by the hot plates, or it may represent an approximation to the properties of a viscoelastic charge in which the resistance to a biaxial deformation will be much greater than to shearing.

2.2.1 Parallel squeezing assumption

As already mentioned, The parallel squeezing assumption has been a conventional approach in the squeeze film problem. It can be shown that it is a direct consequence of the parallel squeezing assumption that low viscosity fluid near the disks cannot flow out preferentially, regardless of the viscosity difference between the center plane and the wall (see Appendex A). Therefore, we can see that the parallel squeezing assumption will not be valid when the viscosity difference and geometry are such as to generate a preferential flow of the low

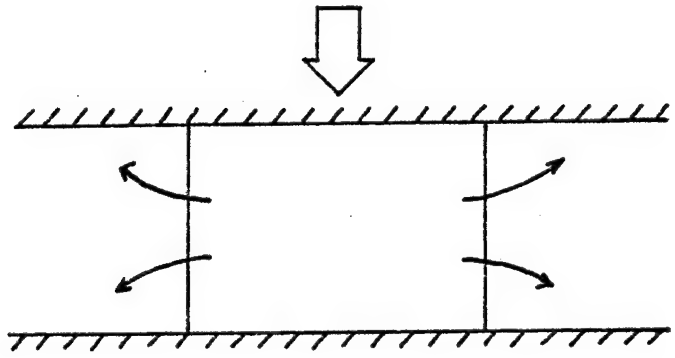

(a)

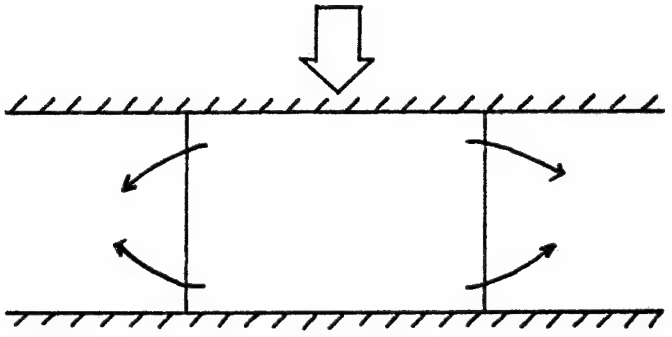

(b)

Fig. 2.5 Flow patterns observed experimentally.
(a) preferential flow of central fluid.
(b) preferential flow of the fluid near the wall.

viscosity fluid near the wall.

2.2.2 Squeezing force and boundary condition

The force required to bring the plates together is obtained by integrating the axial total stress over the surfaces of the disks. The calculation of this force requires a knowledge of the boundary condition at the outer edge of the disks.

The usual boundary condition employed at the disk edge is shown schematically in Fig. 2.6(a); the normal stress at the free surface, $\sigma_{zz}=-p+\tau_{zz}$, is balanced against atmospheric pressure. This gives

$$F = \frac{\pi C_1 R^4}{8} \tag{2.8}$$

where

$$C_1 = V\left[\int_H^0 du \int_H^u \frac{\xi\, d\xi}{\eta(\xi)}\right]^{-1} \tag{2.9}$$

For the case of constant viscosity, we obtain

$$F = \frac{3\pi\eta V R^4}{8H^3} \tag{2.10}$$

At constant force, this leads to the Stefan equation.

This boundary condition gives a paradoxical prediction for the case in which there is a large viscosity difference between the central plane and the walls. From

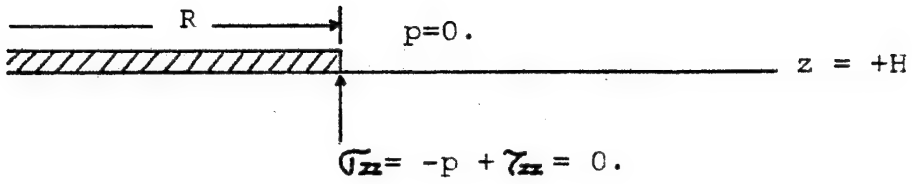

(a)

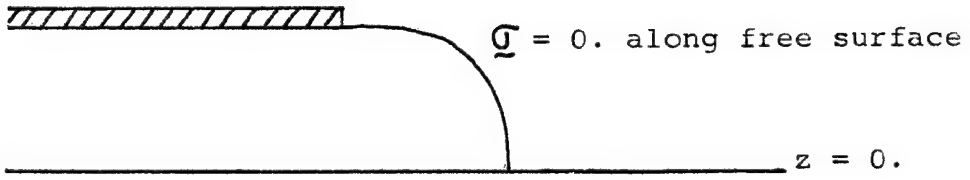

(b)

Fig. 2.6 Boundary condition at the edge of the disk.
(a) conventional one
(b) real situation

(2.8) and (2.9) the force required is of the order of the smallest viscosity that exists over the finite portion of the gap, even if the central portion of the gap contains fluid of arbitrarily large viscosity. Obviously this can not be true.

A better boundary condition at the outer edge is the vanishing of all stresses on the free surface of the extruded sheet, shown schematically in Fig. 2.6(b). Assuming that the velocity rearrangement is restricted to a small neighborhood near the edge, we can approximate this condition by requiring that the net radial force component be zero at r=R; that is,

$$\int_0^H \sigma_{rr}\, dz = 0 \qquad \text{at } r = R \tag{2.11}$$

With the parallel squeezing assumption, this gives

$$F = \frac{\pi C_1 R^4}{8}\left[1 - \frac{8}{3}\left(\frac{H}{R}\right)^2\right] + \frac{3\pi C_1 R^2}{H}\int_H^0 \eta(z)\,dz \int_H^z \frac{\xi\, d\xi}{\eta(\xi)} \tag{2.12}$$

The second term in (2.12) corresponds to the stress from the biaxial extension of the central viscous fluid.

When viscosity is constant,

$$F = \frac{\pi C_1 R^4}{8}\left[1 + \frac{16}{3}\left(\frac{H}{R}\right)^2\right] \tag{2.13}$$

As long as $H/R \ll 1$, (2.10) and (2.13) are identical. Thus, the Stefan equation is unchanged by the alternate boundary

condition.

The situation is quite different, however, when there is a large viscosity variation across the gap. The first term in (2.12) is of order $\frac{\eta_{min} V R^4}{H^3}$ and the second is of order $\frac{\eta_{max} V R^2}{H}$. Thus, the first or second term dominates depending upon whether the group

$$S = \frac{\eta_{max} H^2}{\eta_{min} R^2} \tag{2.14}$$

is small or large, respectively, compared to unity.

2.2.3 The dimensionless group S

When S is small compared to unity, the stress from the biaxial extension of the center fluid is negligible and the maximum velocity occurs at the center plane. Thus the parallel squeezing assumption and the conventional boundary condition are both valid.

As S increases, the new boundary condition is necessary to compute the correct order of magnitude for the force, although the parallel squeezing assumption is still valid.

When S is large compared to unity, the parallel squeezing assumption breaks down since the maximum velocity occurs in the low viscosity fluid near the disks. This has been shown numerically for the case of two fluids; i.e., in

which the viscosity is constant in each of two regions, but changes discontinuously at an interface that is initially planar (see appendix A for the details). Thus, a new analysis is necessary in this case. In the two fluids case, new assumptions other than the parallel squeezing assumption have been made to derive an analytical solution which is found to be in good agreement with the finite element numerical solution.

Thus, we now have a quantitative criterion for the two different flow regimes observed experimentally; that is,

* $S \ll 1$: flow regime of Fig. 2.5(a)

* $S \gg 1$: flow regime of Fig. 2.5(b)

2.3 Power-law fluid

In this section, the Scott equation (for a power-law fluid) will be tested by numerical computation, just as the Stefan equation has been tested in section 2.1.

Governing equations and boundary conditions are the same as in Newtonian case, except that the viscosity is given by

$$\eta(\mathbb{I}_d) = K|4\mathbb{I}_d|^{\frac{n-1}{2}} \qquad (2.15)$$

where

$$\mathrm{II}_d = -\frac{1}{2}\left[(\mathrm{tr}\,\underset{\sim}{d})^2 - \mathrm{tr}(\underset{\sim}{d}^2)\right] \tag{2.16}$$

and

$$\underset{\sim}{d} = \begin{pmatrix} d_{rr} & 0 & d_{rz} \\ 0 & d_{\theta\theta} & 0 \\ d_{rz} & 0 & d_{zz} \end{pmatrix} \tag{2.17}$$

The fluid is assumed to be incompressible, so that

$$\mathrm{II}_d = \frac{1}{2}\mathrm{tr}(\underset{\sim}{d}^2) = \frac{1}{2}\left(d_{rr}^2 + d_{\theta\theta}^2 + d_{zz}^2\right) + d_{rz}^2 \tag{2.18}$$

In solving the problem numerically, an iterative scheme is used to evaluate the viscosity function. That is, the viscosity is initially based on the previous solution for an earlier time step. One then solves for the new velocity and pressure profiles, calculates the viscosity from this new velocity field, and repeats this procedure until the solution (velocity and pressure field) converges within a given error allowance. The numerical algorithm is given in Fig. 2.7.

Numerical computations have been carried out for two different values of R/H_o(5,15) and two different values of the power-law index(0.7,0.5). The results are given in Fig. 2.8, in which the Newtonian case (n=1.0) is also plotted for the comparison. In the figure, the dimensionless time $\bar{t}$ is defined by

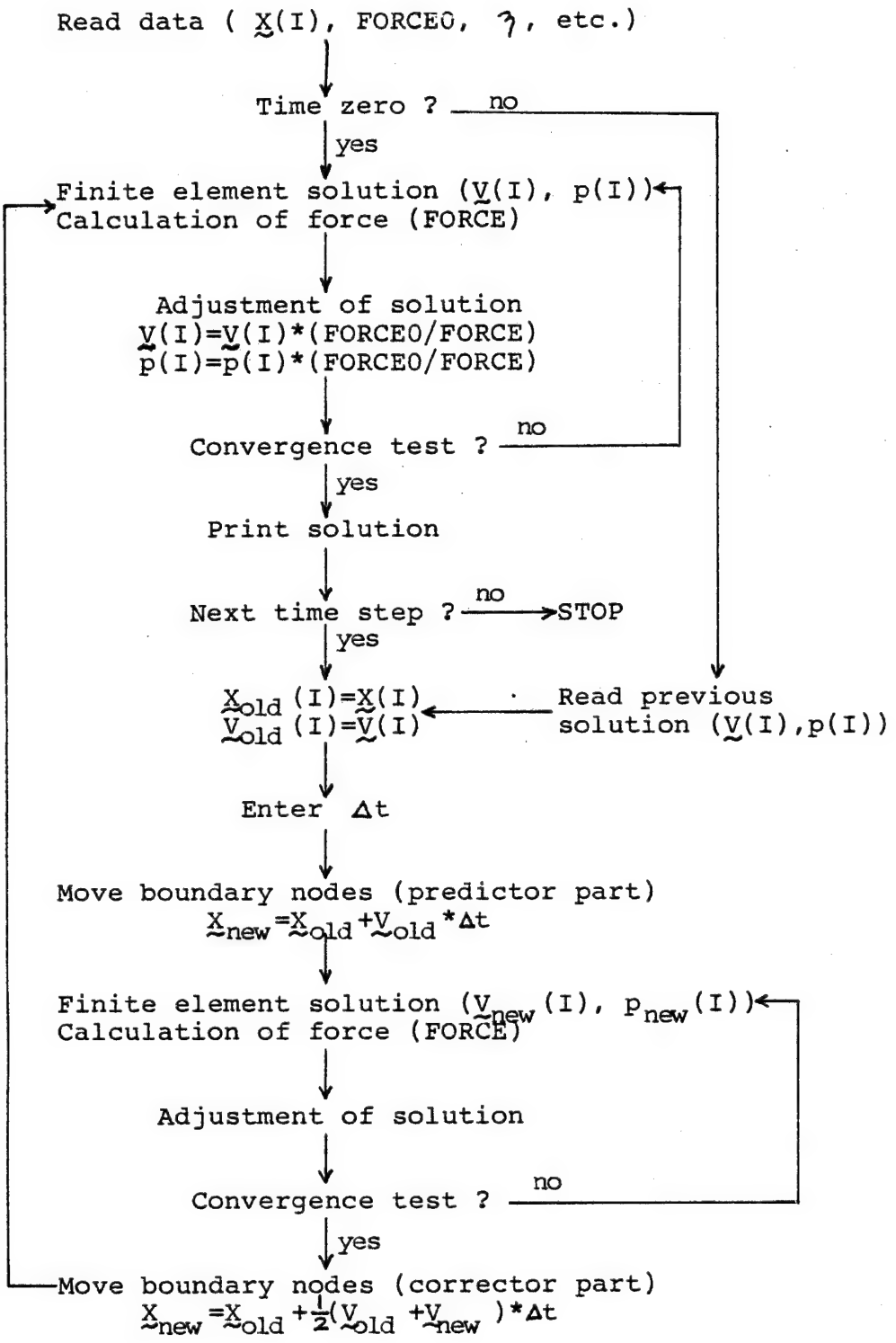

Fig. 2.7 Numerical algorithm to solve compressive flow of power-law fluids.

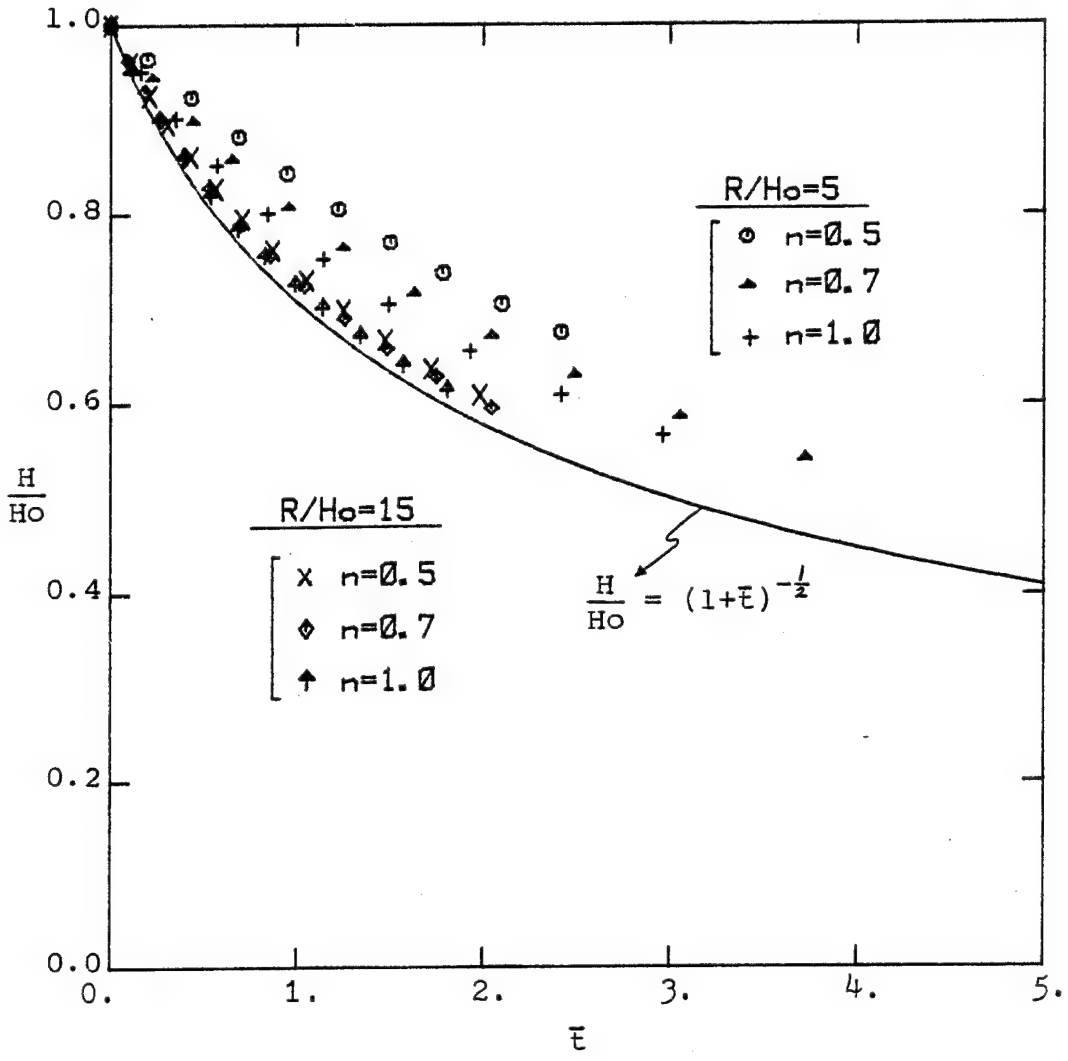

Fig. 2.8 Dimensionless plate spacing versus dimensionless time for isothermal squeezing of power-law fluids.

$$\bar{t} = \left[1 + H_o^{\frac{n+1}{n}} \left(\frac{n+1}{n}\right) kt\right]^{\frac{2n}{n+1}} - 1 \qquad (2.19)$$

$$k = \left[\frac{F}{\pi K R^{n+3}} \left(\frac{2n}{2n+1}\right)^n (n+3)\right]^{\frac{1}{n}} \qquad (2.20)$$

With these definitions, the Scott equation as well as the Stefan equation become

$$\frac{H}{H_o} = (1 + \bar{t})^{-\frac{1}{2}} \qquad (2.21)$$

Again we can see that the edge effect is more significant at smaller values of the R/H_o ratio. The effect increases as the power-law index decreases, or as shear thinning behavior increases. This can be explained by considering the viscosity difference between the fluids inside and outside the edge of the disk. As the power-law index decreases, the fluid outside the edge has a higher viscosity than the fluid inside the edge, which implies that the fluid inside experiences more resistance from the fluid outside. Therefore, the squeezing speed becomes slower as the power-law index decreases. This effect decreases as R/H_o increases, and at large values of R/H_o the Scott equation is still adequate.

2.4 Partially-filled compressive flow of Newtonian fluids.

In this section we consider the flow with a moving front in the mold cavity, depicted in Fig. 2.9. We will focus on the moving free surface and the flow near this

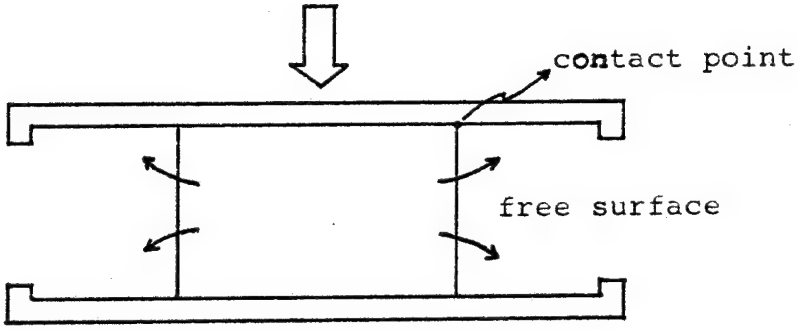

at time = 0.

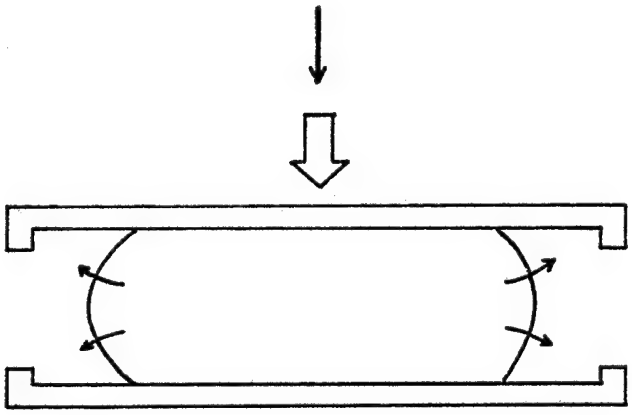

at time = t

Fig. 2.9 Schematic diagram of the flow of a Newtonian fluid in the mold cavity under the isothermal condition.

moving front. Numerical calculations are therefore inevitable, and the proper numerical scheme has to be developed to determine the new contact point between the fluid and the surface, as well as the shape of the free surface, for each time step. It will be assumed that the fluid is Newtonian and isothermal.

2.4.1 Numerical scheme

At any instant of time, the velocity and pressure distributions can be obtained by finite element calculation, as long as the domain is given beforehand At time t=0, we start with a domain of rectangle shape with a flat free surface, as shown in Fig. 2.9, and solve for the velocity and the pressure.

After a small time increment(Δt), the boundary of the domain is changed by

$$\underset{\sim}{X}_{new} = \underset{\sim}{X}_{old} + \underset{\sim}{V} \cdot \Delta t \qquad (2.22)$$

The new contact point is determined by quadratic interpolation of three adjacent nodes, which is shown in Fig. 2.10. That is, after Δt the nodal point 1 moves to $1'$, 2 to $2'$, and 3 to $3'$, etc., and a point p between 1 and 2 will move and just contact the wall; point p' is the new contact point between the fluid surface and the solid wall. The solution and the boundary shape are then improved through

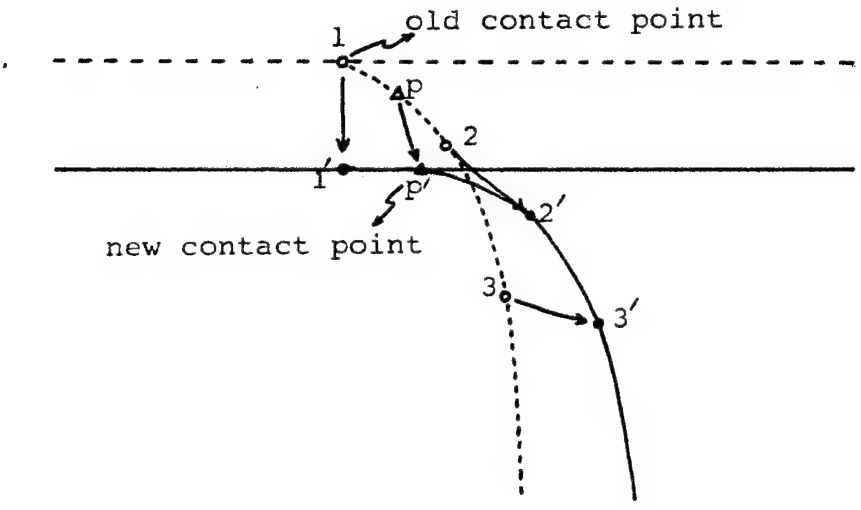

Fig. 2.10 Movement of the frontal nodes and contact point.
------- old front
——— new front after Δt

the predictor-corrector method. These procedures are repeated at each time step. This numerical algorithm is given in Fig. 2.11.

2.4.2 Numerical calculation results

Two sets of calculations have been carried out, one at a small value of R_o/H_o(=5), the other at a large value of R_o/H_o(=15).

In the case of R_o/H_o=5, the movement of the boundary and the frontal free surface are shown in Fig. 2.12 at various stages of squeezing. The radial velocity profiles of the present case are compared in figures 2.13 through 2.16 to the corresponding fully-filled case, which has an extra amount of fluid outside the edge of the disks; the radius for the fully-filled calculation is based on the contact point, p. At the beginning of squeezing (Fig. 2.13), the radial velocity in the partially-filled case is somewhat larger than in the fully-filled case, especially near the centerplane at the edge of the disks(z=0, r=R). This can be understood, considering that the fully-filled case experiences some resistance from the fluid outside the edge of the disks. This difference becomes smaller and smaller as squeezing goes on (see Fig. 2.14 2.16), since the partially-filled case begins to build up a "bulge" of fluid near the front, which acts like

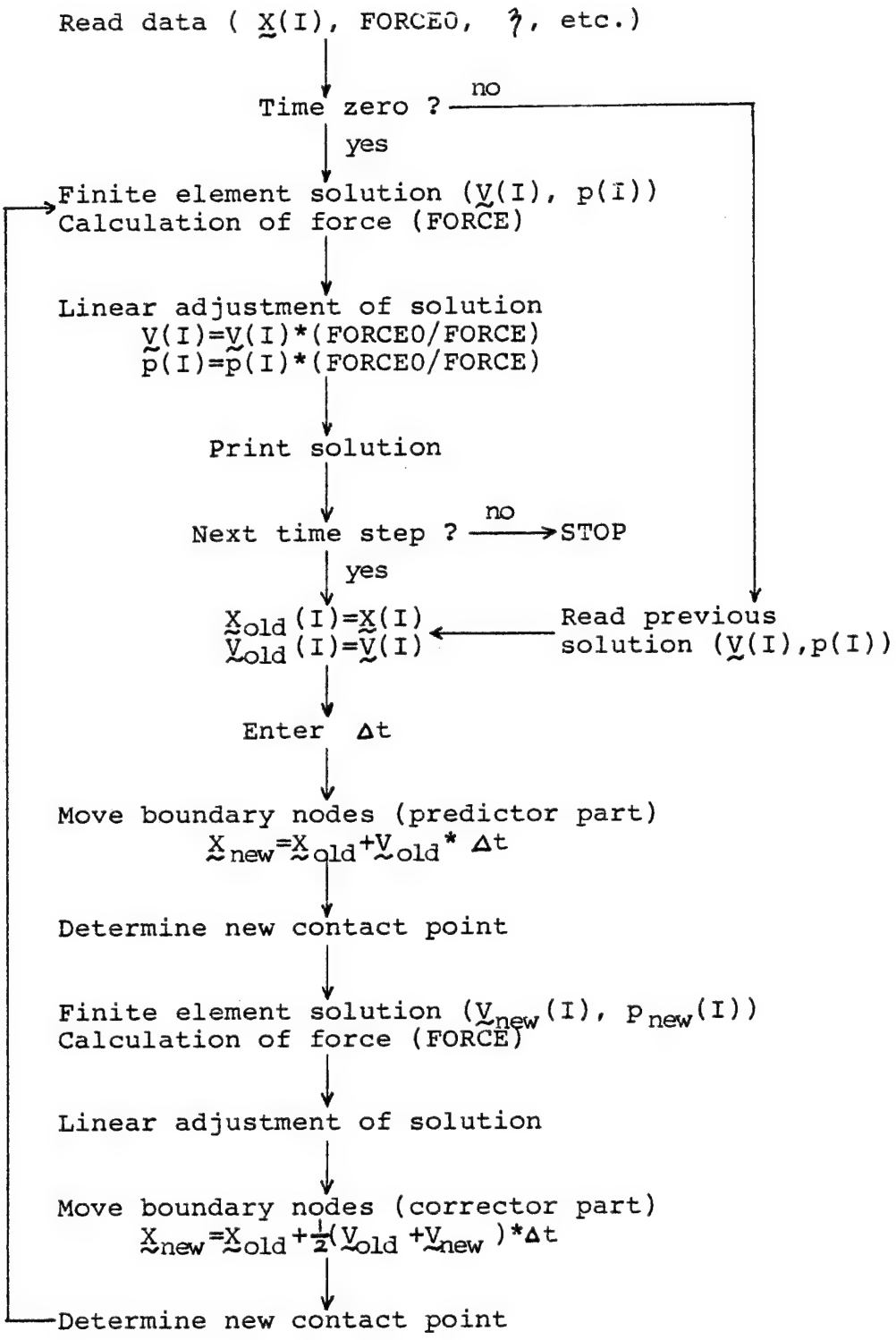

Fig. 2.11 Numerical algorithm to solve the partially-filled comprressive flow of Newtonian fluids.

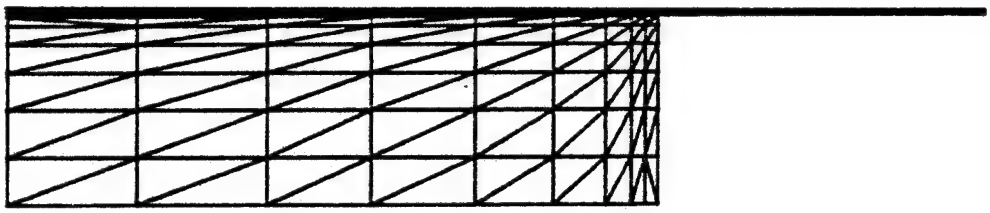

R = 5.
H = 1.

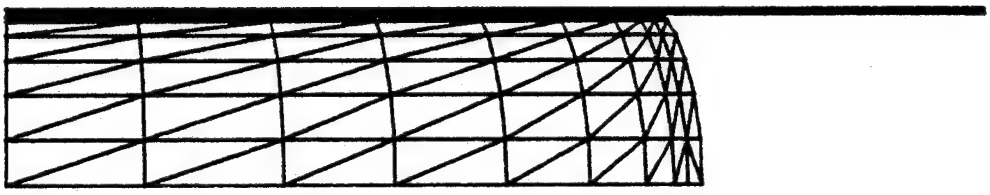

R = 5.042
H = 0.901

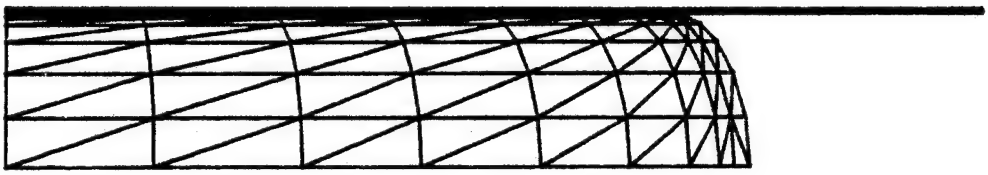

R = 5.199
H = 0.799

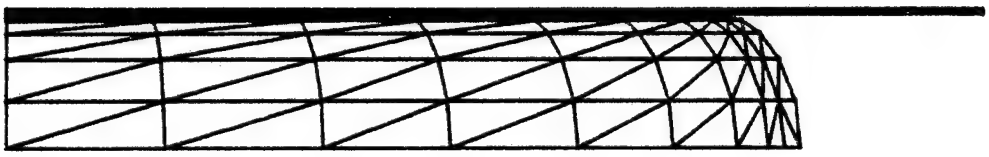

R = 5.517
H = 0.701

Fig. 2.12 Movement of the boundary in the partially-filled compressive flow, $R_o/H_o=5$.

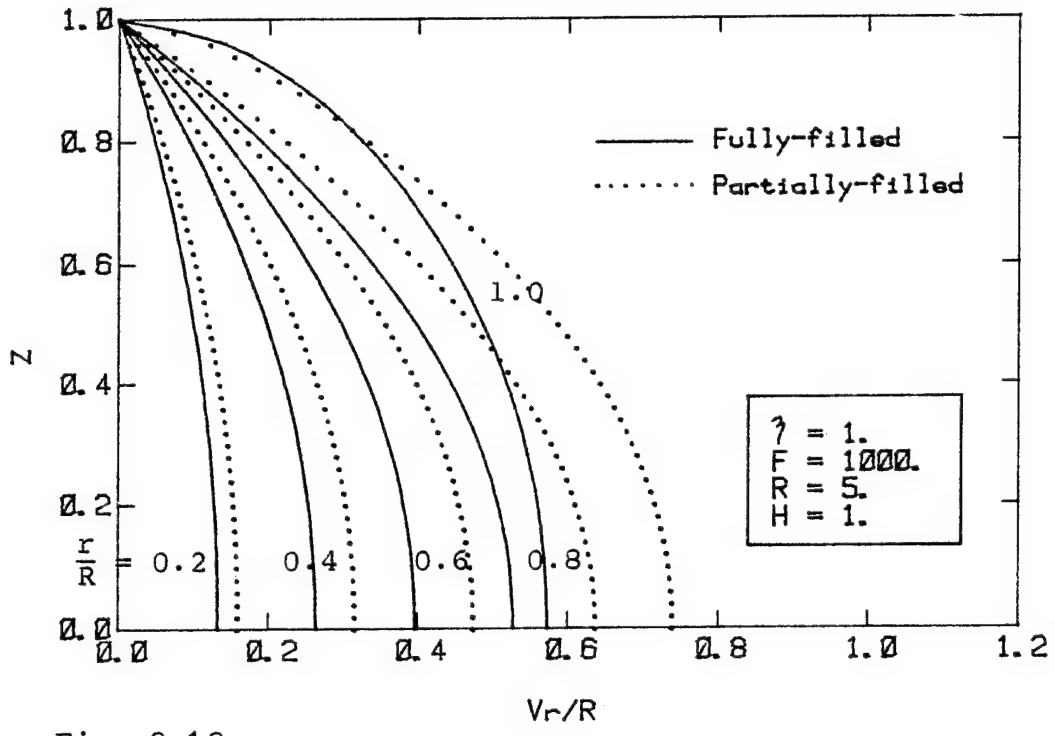

Fig. 2.13

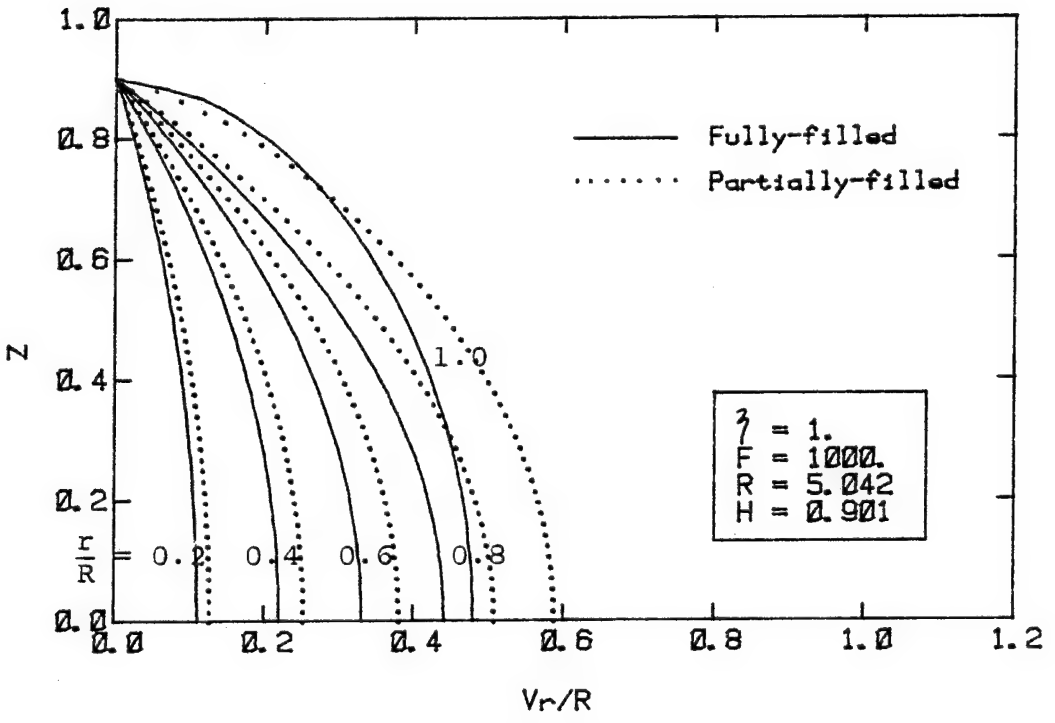

Fig. 2.14 The radial velocity profiles of the partially-filled compressive flow compared to the fully-filled case.

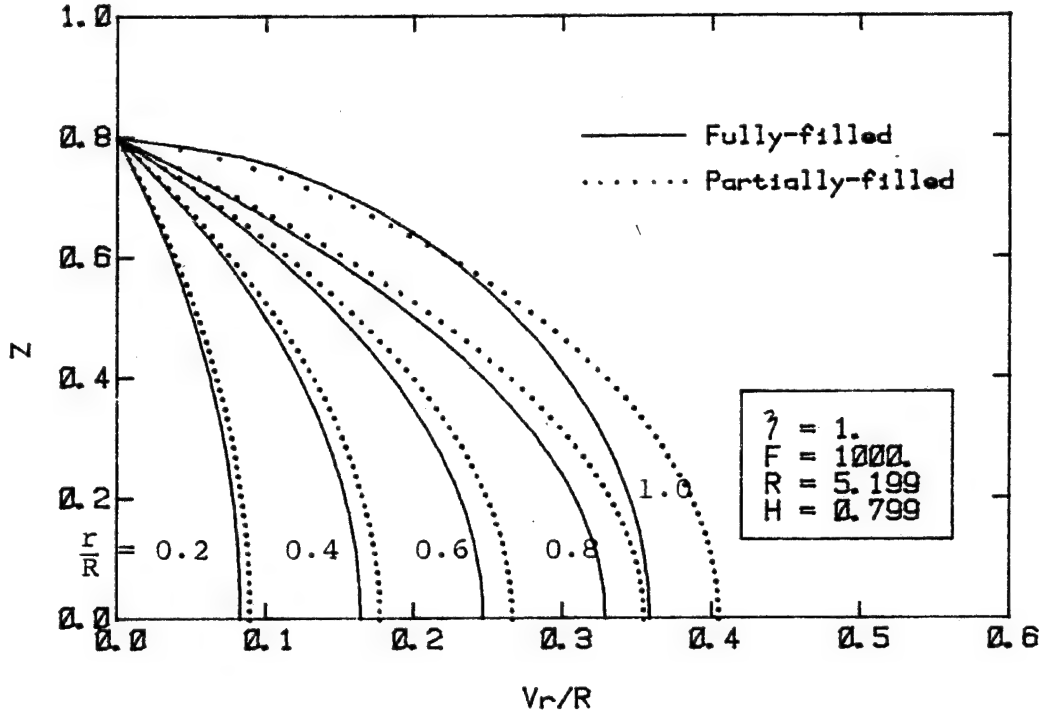

Fig. 2.15

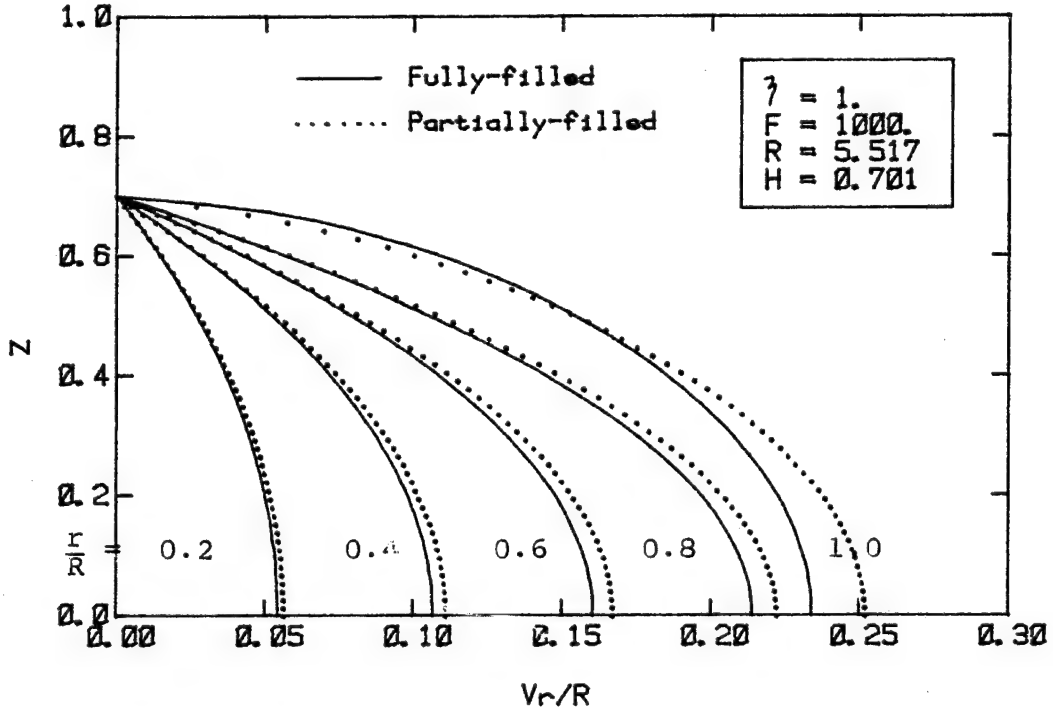

Fig. 2.16 The radial velocity profiles of the partially-filled compressive flow compared to the fully-filled case.

the fluid outside the disks in the full-filled case. Fig. 2.17 shows the pathlines of some material points as the squeezing goes on. The material points near the front are moving upwards, which represents the same phenomenon as observed in the injection molding process, known as the "fountain effect". The term "fountain effect" was coined and discussed by Rose(1961) and is important in determining the quality and morphology of the surface of the molded article.

The movement of the boundary and the comparisons of the radial velocity profiles are shown in figures 2.18 through 2.21 for a large value of R_o/H_o(=15). We see similar phenomena as for R_o/H_o=5, but the effect of the fluid outside the disks is rather small in this case and it becomes much smaller as the squeezing goes on (see Fig. 2.21). We can therefore conclude that as long as R_o/H_o is large enough, the flow patterns in the partially-filled compressive flow are essentially the same as those one observes in the fully-filled case except near the front: here we observe fountain flow phenomenon in the partially-filled case.

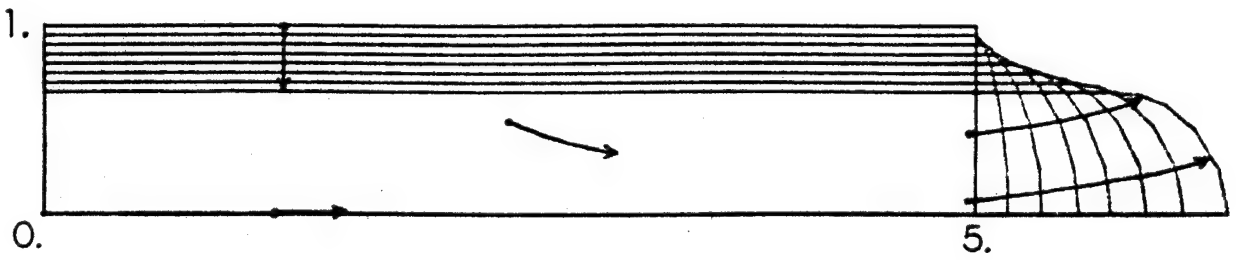

Fig. 2.17 The pathlines of material points in the partially-filled compressive flow of Newtonian fluid : the fountain effect is seen at the moving front.

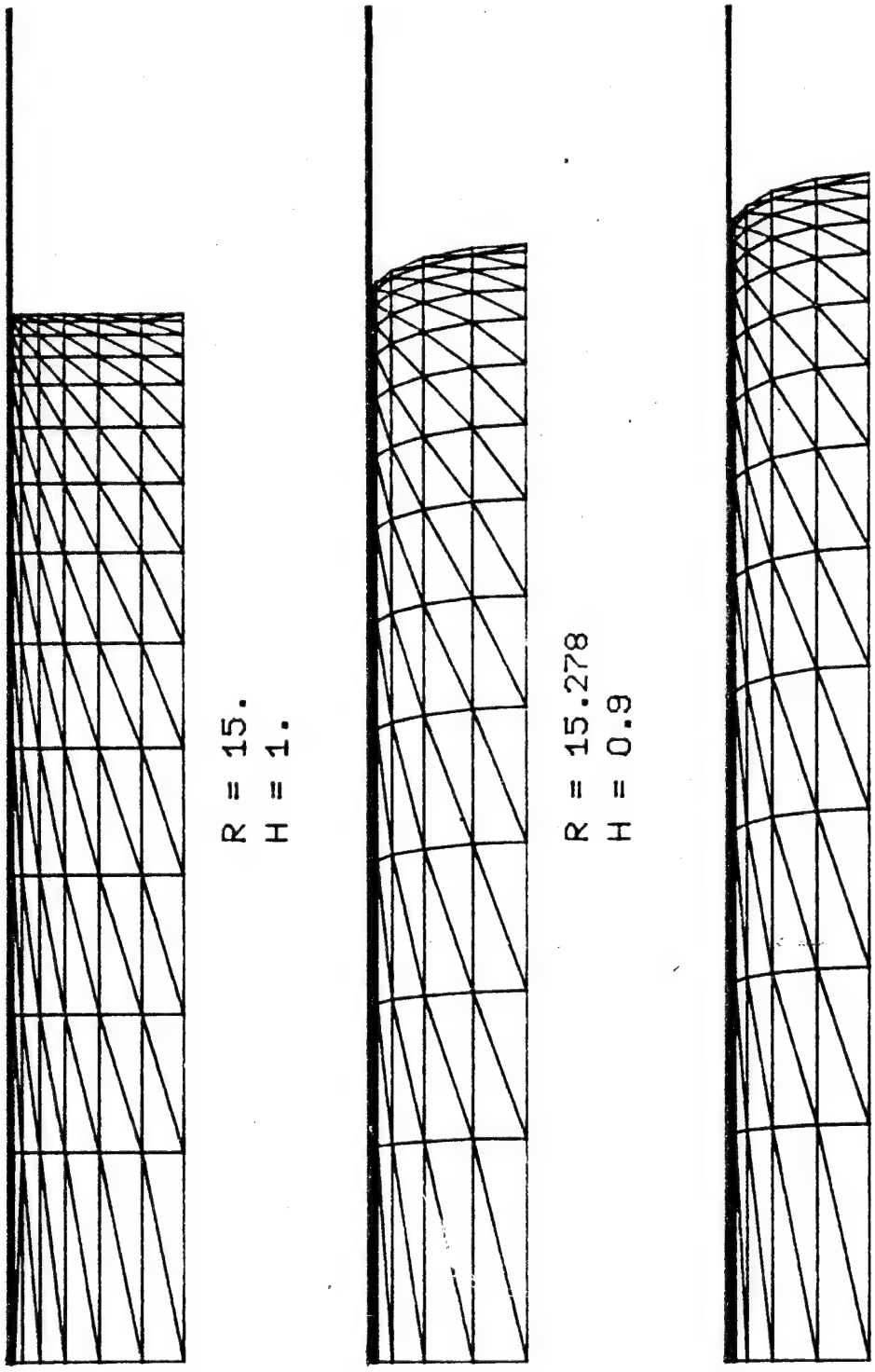

Fig. 2.18 Movement of the boundary, Ro/Ho=15.

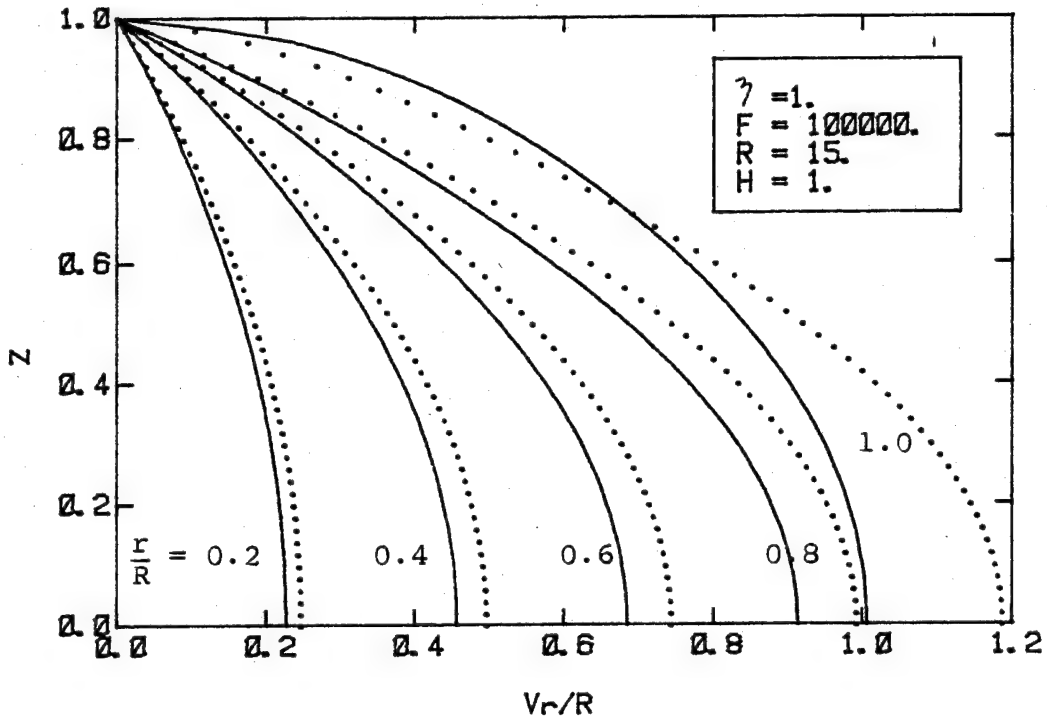

Fig. 2.19

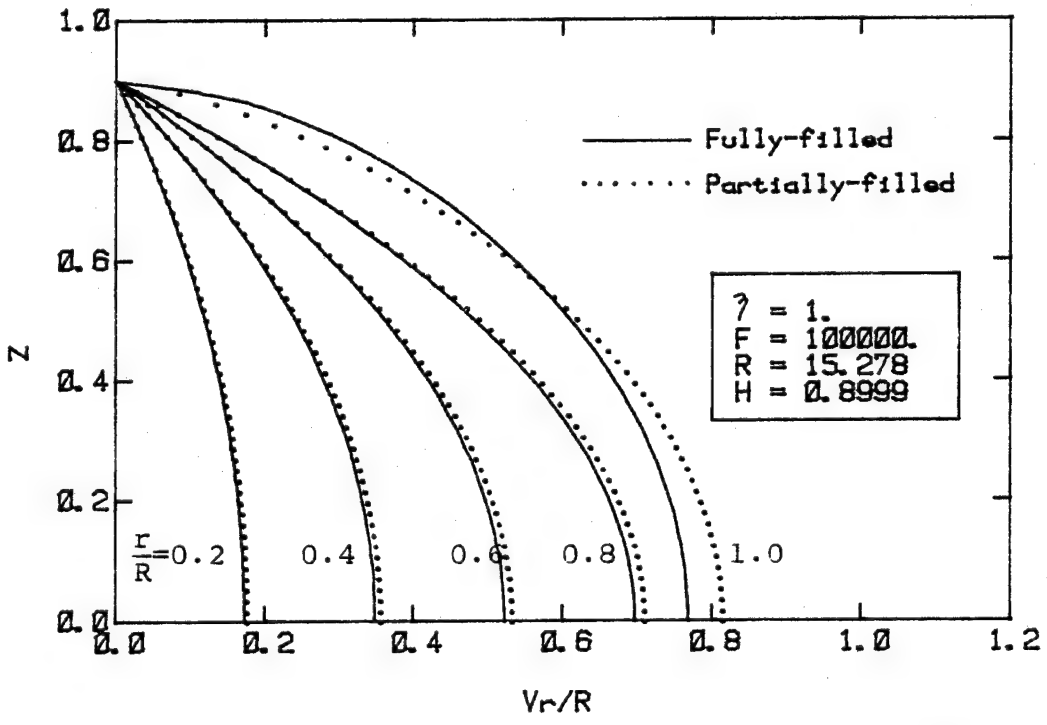

Fig. 2.20 The radial velocity profiles of the partially-filled compressive flow compared to the fully-filled case.

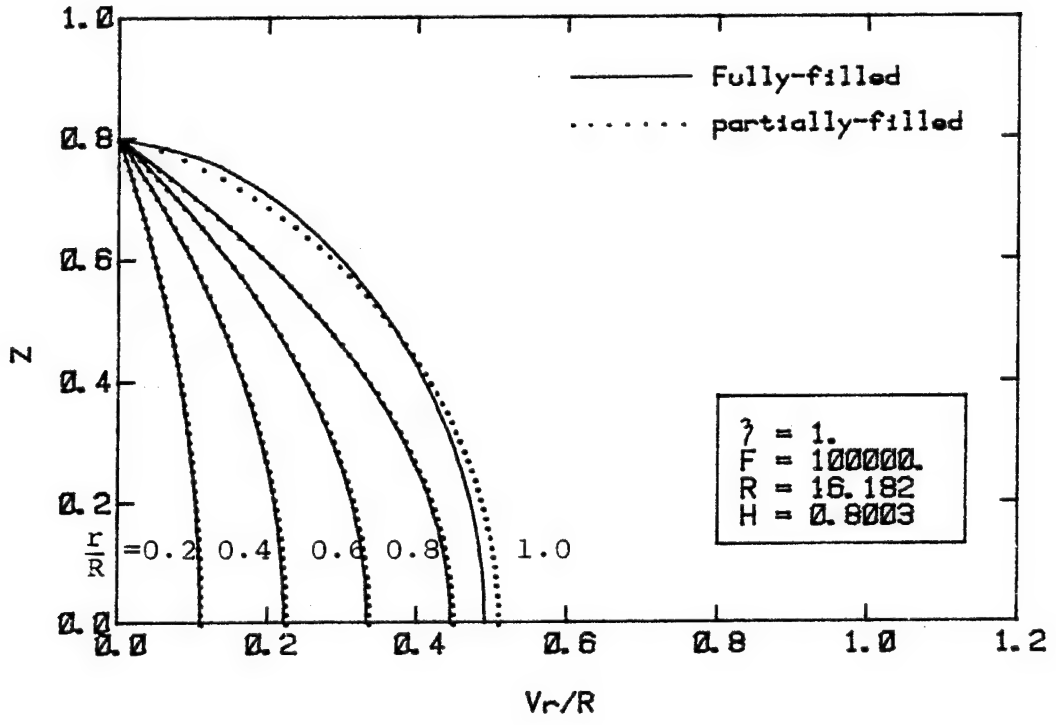

Fig. 2.21 The radial velocity profiles of the partially-filled compressive flow compared to the fully-filled case.

CHAPTER 3

LUBRICATED COMPRESSIVE FLOW OF VISCOELASTIC FLUIDS

3.1 Problem formulation

Let us consider that the material is compressed between two circular disks under a constant load and assume that there exist thin lubricant or low viscosity fluid layers near the wall. The schematic diagram is shown in Fig. 3.1, in which the radius of the disk may or may not vary in time. If the viscosity of the lubricant is given in the proper range, which will be discussed in Section 3.5, the flow in the viscous material may be assumed as biaxial extensional flow with negligible shear. The velocity profile in the cylindrical coordinate is then written as

$$V_r = \dot{\epsilon}_b(t)\, r \tag{3.1}$$

$$V_z = -2\,\dot{\epsilon}_b(t)\, z \tag{3.2}$$

$$V_\theta = 0 \tag{3.3}$$

in which $\dot{\epsilon}_b(t)$ is the biaxial extensional rate and varies in time. The deformation rate tensor $\underset{\sim}{d}$ is given by

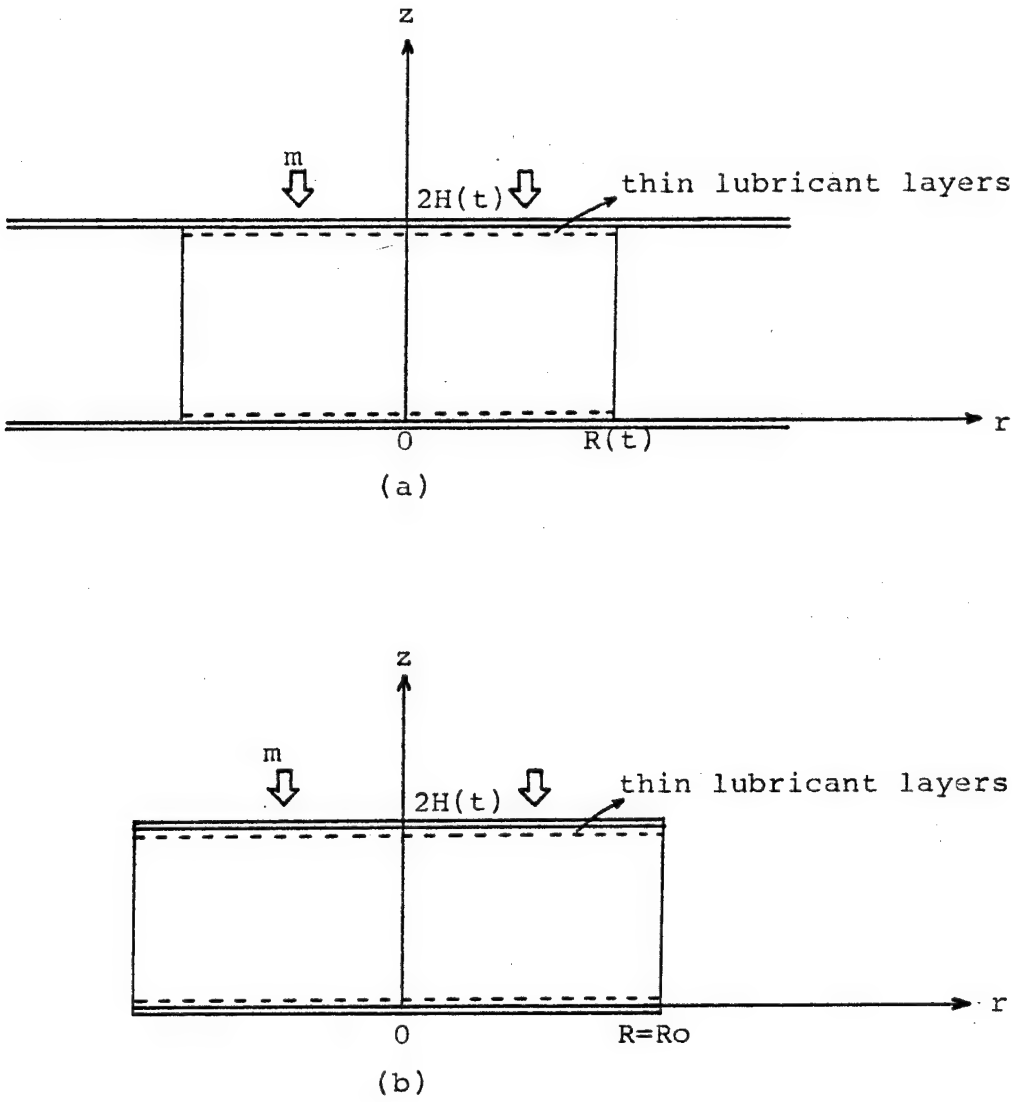

Fig. 3.1 Schematic diagram of the lubricated compressive flow.
(a) R varies in time
(b) R=Ro (constant)

$$\underset{\sim}{d} = \frac{1}{2}(\nabla \underset{\sim}{V} + \nabla \underset{\sim}{V}^{T}) = \begin{pmatrix} \dot{\epsilon}_b(t) & 0 & 0 \\ 0 & \dot{\epsilon}_b(t) & 0 \\ 0 & 0 & -2\dot{\epsilon}_b(t) \end{pmatrix} \tag{3.4}$$

Since $\underset{\sim}{d}$ is uniform in space, the extra stress tensor $\underset{\sim}{\tau}$ may be also assumed uniform in space. Hence,

$$\nabla \cdot \underset{\sim}{\tau} = 0 \tag{3.5}$$

The equations of motion are then reduced to the form

$$\rho \left[r \frac{d\dot{\epsilon}_b}{dt} + r \dot{\epsilon}_b^{\,2} \right] = - \frac{\partial p}{\partial r} \tag{3.6}$$

$$\rho \left[-2z \frac{d\dot{\epsilon}_b}{dt} + 4z \dot{\epsilon}_b^{\,2} \right] = - \frac{\partial p}{\partial z} \tag{3.7}$$

in which the fluid inertia terms are included.

Integrating (3.6) and (3.7), the pressure distribution is obtained as

$$p(r,z,t) = -\frac{1}{2}\rho r^2 \left(\frac{d\dot{\epsilon}_b}{dt} + \dot{\epsilon}_b^{\,2} \right) + \rho z^2 \left(\frac{d\dot{\epsilon}_b}{dt} - 2\dot{\epsilon}_b^{\,2} \right) + p_o(t) \tag{3.8}$$

To determine $p_o(t)$, which is the pressure at r=z=0 (see Fig. 3.1), the boundary condition at the free surface(at r=R) is applied in the following form:

$$\int_0^{2H} (\sigma_{rr})_{r=R} \, dz = 0 \tag{3.9}$$

where $\sigma_{rr} (= -p + \tau_{rr})$ is the radial component of the total

stress tensor $\underset{\sim}{\sigma}$. Evaluating the integration in (3.9),

$$\int_0^{2H} (\sigma_{rr})_{r=R}\, dz$$

$$= \int_0^{2H} \left[\tfrac{1}{2}\rho R^2 \left(\frac{d\dot{\epsilon}_b}{dt} + \dot{\epsilon}_b^2 \right) - \rho z^2 \left(\frac{d\dot{\epsilon}_b}{dt} - 2\dot{\epsilon}_b^2 \right) - p_o + \tau_{rr} \right] dz$$

$$= \rho R^2 H \left(\frac{d\dot{\epsilon}_b}{dt} + \dot{\epsilon}_b^2 \right) - \frac{8}{3}\rho H^3 \left(\frac{d\dot{\epsilon}_b}{dt} - 2\dot{\epsilon}_b^2 \right) - 2p_o H + 2\tau_{rr} H = 0$$

Thus, we obtain the equation for $p_o(t)$,

$$p_o(t) = \tfrac{1}{2}\rho R^2 \left(\frac{d\dot{\epsilon}_b}{dt} + \dot{\epsilon}_b^2 \right) - \frac{4}{3}\left(\frac{d\dot{\epsilon}_b}{dt} - 2\dot{\epsilon}_b^2 \right)\rho H^2 + \tau_{rr} \qquad (3.10)$$

Substituting into (3.8) then gives

$$p(r,z,t) = \tfrac{1}{2}\rho(R^2 - r^2)\left(\frac{d\dot{\epsilon}_b}{dt} + \dot{\epsilon}_b^2 \right) - \tfrac{1}{3}\rho(4H^2 - 3z^2)\left(\frac{d\dot{\epsilon}_b}{dt} - 2\dot{\epsilon}_b^2 \right) + \tau_{rr} \qquad (3.11)$$

The total force exerted by the fluid on the upper disk is calculated through the following integration:

$$F = \int_o^R (-\sigma_{zz})_{z=2H}\, 2\pi r\, dr$$

$$= \int_o^R (p - \tau_{zz})_{z=2H}\, 2\pi r\, dr \qquad (3.12)$$

Substituting equation (3.11) into (3.12) and performing the integration, one obtains

$$F = \tfrac{1}{4}\pi\rho R^4 \left(\frac{d\dot{\epsilon}_b}{dt} + \dot{\epsilon}_b^2 \right) + \frac{8}{3}\pi\rho R^2 H^2 \left(\frac{d\dot{\epsilon}_b}{dt} - 2\dot{\epsilon}_b^2 \right) + \pi R^2 (\tau_{rr} - \tau_{zz}) \qquad (3.13)$$

One of the easiest ways to apply the force on the upper disk is to place a mass on it. In that case, the force is given by

$$F = m(g - a) \tag{3.14}$$

where m = the total mass on and in the disk

g = the gravitational acceleration

a = the acceleration of the disk $\left(= -2\frac{d^2H}{dt^2}\right)$

Equivalently,

$$F = m\left(g - 4H\frac{d\dot{\epsilon}_b}{dt} + 8H\dot{\epsilon}_b^2\right) \tag{3.15}$$

since

$$\frac{dH}{dt} = (V_z)_{z=H} = -2H\dot{\epsilon}_b \tag{3.16}$$

and

$$a = -2\frac{d}{dt}\left(\frac{dH}{dt}\right)$$

$$= 4H\frac{d\dot{\epsilon}_b}{dt} - 8H\dot{\epsilon}_b^2 \tag{3.17}$$

Now, equating equations (3.13) and (3.15), we have

$$m\left(g - 4H\frac{d\dot{\epsilon}_b}{dt} + 8H\dot{\epsilon}_b^2\right) = \frac{1}{4}\pi\rho R^4\left(\frac{d\dot{\epsilon}_b}{dt} + \dot{\epsilon}_b^2\right) + \frac{8}{3}\pi\rho R^2H^2\left(\frac{d\dot{\epsilon}_b}{dt} - 2\dot{\epsilon}_b^2\right) + \pi R^2(\tau_{rr} - \tau_{zz}) \tag{3.18}$$

or

$$\frac{d\dot{\epsilon}_b}{dt} = \frac{m(g + 8H\dot{\epsilon}_b^2) - \frac{1}{4}\pi\rho R^4\dot{\epsilon}_b^2 + \frac{16}{3}\pi\rho R^2H^2\dot{\epsilon}_b^2 - \pi R^2(\tau_{rr} - \tau_{zz})}{\frac{1}{4}\pi R^4\left[\rho + \rho\frac{32}{3}\left(\frac{H}{R}\right)^2 + \frac{16mH}{\pi R^4}\right]} \tag{3.19}$$

Frequently, equations (3.18) or (3.19) can be simplified as follows:

(a) When R>>H, the term including H on the righthand side of (3.18) can be neglected compared to the first term to give

$$\frac{d\dot{\epsilon}_b}{dt} = \frac{m(g+8H\dot{\epsilon}_b^2) - \frac{1}{4}\pi\rho R^4\dot{\epsilon}_b^2 - \pi R^2(\tau_{rr}-\tau_{zz})}{\frac{1}{4}\pi R^4(\rho + \frac{16mH}{\pi R^4})} \tag{3.20}$$

(b) When the compression is not very fast, the inertia of the fluid and the load can be neglected, in which case equation (3.18) is simplified to

$$mg = \pi R^2(\tau_{rr} - \tau_{zz}) \tag{3.21}$$

When the radius of disk varies in time (see Fig. 3.1(a)), the expression for the radius change is obtained from mass conservation; that is,

$$R^2H = \text{constant}$$

or

$$\frac{d}{dt}(R^2H) = 0$$

or

$$\frac{dR}{dt} = R\dot{\epsilon}_b \tag{3.22}$$

Here equation (3.16) has been used.

The next step is to solve equation (3.19) or the

simplified form ((3.20),(3.21)) together with (3.16), (3.22), and appropriate constitutive equations which relate τ_{rr} and τ_{zz} to the deformation. In the next section, we will consider the linear viscoelastic case, since in the limit of small deformations the response of polymeric materials may be considered linear. The non-linear case will be considered in Section 3.3.

3.2 A linearized viscoelastic case

For sufficiently small values of the deformation, the mechanical behavior of polymeric materials is entirely described by the constitutive equation of linear viscoelasticity.

3.2.1 Constitutive equation

A particular case of the constitutive equation of linearized viscoelasticity is given by

$$\underset{\sim}{\tau} + \lambda_1 \frac{\partial \underset{\sim}{\tau}}{\partial t} = 2\eta \left(\underset{\sim}{d} + \lambda_2 \frac{\partial \underset{\sim}{d}}{\partial t} \right) \qquad (3.23)$$

where λ_1 stands for the relaxation time and λ_2 stands for the retardation time. Often λ_2 is set to be zero. Note that as λ_2 approaches λ_1, equation (3.23) approaches the Newtonian equation.*

---

* When $\lambda_2=\lambda_1$, equation (3.23) is simply the sum of the Newtonian constitutive equation and the first time derivative multiplied by λ_1.

In the present problem, the radial and axial components of the constitutive equation are

$$\tau_{rr} + \lambda_1 \frac{d\tau_{rr}}{dt} = 2\eta \left(\dot{\epsilon}_b + \lambda_2 \frac{d\dot{\epsilon}_b}{dt} \right) \tag{3.24}$$

$$\tau_{zz} + \lambda_1 \frac{d\tau_{zz}}{dt} = -4\eta \left(\dot{\epsilon}_b + \lambda_2 \frac{d\dot{\epsilon}_b}{dt} \right) \tag{3.25}$$

from which it follows that

$$\tau_{zz} = -2\,\tau_{rr} \tag{3.26}$$

and

$$\tau_{rr} = \exp\left(-\frac{t}{\lambda_1}\right) \cdot 2 \cdot \frac{\eta}{\lambda_1} \int_0^t \left(\dot{\epsilon}_b + \lambda_2 \frac{d\dot{\epsilon}_b}{dt}\right) \exp\left(\frac{t}{\lambda_1}\right) dt \tag{3.27}$$

3.2.2 Analytical solution

Let us consider the case (b) in Fig. 3.1, in which the radius is constant, and that $R=R_o>>H$. Further assume that the compression is not very fast, so that $\dot{\epsilon}_b^2 << \frac{d\dot{\epsilon}_b}{dt}$, and that the inertia of the load is small compared to the inertia of fluid ($\frac{16\,mH}{\pi R^4} << \rho$ in 3.20). Then equation (3.18) or (3.20) becomes

$$mg = \frac{1}{4}\pi\rho R_o^4 \frac{d\dot{\epsilon}_b}{dt} + 3\pi R_o^2 \tau_{rr}$$

or

$$\frac{d\dot{\epsilon}_b}{dt} = \frac{4mg}{\pi\rho R_o^4} - \frac{12}{\rho R_o^2}\tau_{rr} \tag{3.28}$$

Here equation (3.26) has been used. Substituting (3.27) into (3.28) then gives

$$\frac{d\dot{\epsilon}_b}{dt} = \frac{4mg}{\pi\rho R_o^4} - \frac{24\eta}{\rho R_o^2 \lambda_1} \exp\left(-\frac{t}{\lambda_1}\right) \int_o^t \left(\dot{\epsilon}_b + \lambda_2 \frac{d\dot{\epsilon}_b}{dt}\right) \exp\left(\frac{t}{\lambda_1}\right) dt$$

or

$$\exp\left(\frac{t}{\lambda_1}\right) \frac{d\dot{\epsilon}_b}{dt} = \exp\left(\frac{t}{\lambda_1}\right) \frac{4mg}{\pi\rho R_o^4} - \frac{24\eta}{\rho R_o^2 \lambda_1} \int_o^t \left(\dot{\epsilon}_b + \lambda_2 \frac{d\dot{\epsilon}_b}{dt}\right) \exp\left(\frac{t}{\lambda_1}\right) dt$$

Differentiating this with respect to time gives

$$\exp\left(\frac{t}{\lambda_1}\right) \frac{d^2\dot{\epsilon}_b}{dt^2} + \frac{1}{\lambda_1} \exp\left(\frac{t}{\lambda_1}\right) \frac{d\dot{\epsilon}_b}{dt} = \exp\left(\frac{t}{\lambda_1}\right) \frac{4mg}{\pi\rho R_o^4 \lambda_1} - \frac{24\eta}{\rho R_o^2 \lambda_1} \left(\dot{\epsilon}_b + \lambda_2 \frac{d\dot{\epsilon}_b}{dt}\right) \exp\left(\frac{t}{\lambda_1}\right)$$

or

$$\boxed{\rho\lambda_1 \frac{d^2\dot{\epsilon}_b}{dt^2} + \rho\left(1 + \frac{24\eta\lambda_2}{\rho R_o^2}\right) \frac{d\dot{\epsilon}_b}{dt} + \frac{24\eta}{R_o^2} \dot{\epsilon}_b = \frac{4mg}{\pi R_o^4}} \quad (3.29)$$

which is a second order dynamical equation.

The solution of equation (3.29) is given by

$$\dot{\epsilon}_b = \begin{cases} \dfrac{mg}{6\pi\eta R_o^2} + C_1 \exp(D_1 t) + C_2 \exp(D_2 t) & \text{when } D_1 \neq D_2 \\ \dfrac{mg}{6\pi\eta R_o^2} + \exp(D_1 t) \cdot (C_3 t + C_4) & \text{when } D_1 = D_2 \end{cases} \quad (3.30)$$

where D_1 and D_2 are the roots of the characteristic equation of (3.29), that is,

$$\rho\lambda_1 D^2 + \rho\left(1 + \frac{24\eta\lambda_2}{\rho R_o^2}\right) D + \frac{24\eta}{R_o^2} = 0 \quad (3.31)$$

C_1, C_2, C_3, C_4 are constants to be determined by the following initial conditions:

$$\left.\begin{aligned} \dot{\epsilon}_b(0) &= 0 \\ \left.\frac{d\dot{\epsilon}_b}{dt}\right|_{t=0} &= \frac{4mg}{\pi\rho R_0^4} \quad \text{from (3.28)} \end{aligned}\right\} \tag{3.32}$$

The characteristic feature of the solution (3.30) may be divided into the following three cases, depending upon the values of D_1 and D_2.

$$\text{Case I.} \quad \left(1 - \frac{24\eta\lambda_2}{\rho R_0^2}\right)^2 - \frac{96\eta\lambda_1}{\rho R_0^2} > 0 \tag{3.33}$$

The D_i are real, negative, unequal and given by

$$D_1 = \frac{1}{2\lambda_1}\left[-\left(1+\frac{24\eta\lambda_2}{\rho R_0^2}\right) + \sqrt{\left(1+\frac{24\eta\lambda_2}{\rho R_0^2}\right)^2 - \frac{96\eta\lambda_1}{\rho R_0^2}}\right]$$

$$D_2 = \frac{1}{2\lambda_1}\left[-\left(1+\frac{24\eta\lambda_2}{\rho R_0^2}\right) - \sqrt{\left(1+\frac{24\eta\lambda_2}{\rho R_0^2}\right)^2 - \frac{96\eta\lambda_1}{\rho R_0^2}}\right]$$

The solution decays exponentially to a constant rate; that is,

$$\dot{\epsilon}_b(t) = \frac{mg}{6\pi\eta R_0^2} + C_1 \exp(D_1 t) + C_2 \exp(D_2 t) \tag{3.34}$$

where

$$C_1 = \frac{1}{D_1 - D_2}\left(D_2 \frac{mg}{6\pi\eta R_0^2} + \frac{4mg}{\pi\rho R_0^4}\right)$$

$$C_2 = \frac{1}{D_1 - D_2}\left(D_1 \frac{mg}{6\pi\eta R_0^2} + \frac{4mg}{\pi\rho R_0^4}\right)$$

Note that the solution approaches the Newtonian solution as λ_2 approaches to λ_1, and at long times for any λ_1 and λ_2.

Newtonian solution is given by

$$\dot{\epsilon}_b(t) = \frac{mg}{6\pi\eta R_o^2}\left[1 - exp\left(-\frac{24\eta}{\rho R_o^2}t\right)\right]$$

Case II. $$\left(1-\frac{24\eta\lambda_2}{\rho R_o^2}\right)^2 - \frac{96\eta\lambda_1}{\rho R_o^2} = 0 \qquad (3.35)$$

D_1 and D_2 are equal and negative,

$$D_1 = D_2 = -\frac{1}{2\lambda_1}\left(1 + \frac{24\eta\lambda_2}{\rho R_o^2}\right)$$

and

$$\dot{\epsilon}_b(t) = \frac{mg}{6\pi\eta R_o^2} + exp(D_1 t)\cdot(C_3 t + C_4) \qquad (3.36)$$

where

$$C_3 = \frac{4mg}{\pi\rho R_o^4} + D_1\frac{mg}{6\pi\eta R_o^2}$$

$$C_4 = -\frac{mg}{6\pi\eta R_o^2}$$

That is, the fluid is gradually accelerated to a steady state deformation rate.

Case III. $$\left(1+\frac{24\eta\lambda_2}{\rho R_o^2}\right)^2 - \frac{96\eta\lambda_1}{\rho R_o^2} < 0 \qquad (3.37)$$

D_1 and D_2 are complex conjugates, given by

$$D_1 = \frac{1}{2\lambda_1}\left[-\left(1+\frac{24\eta\lambda_2}{\rho R_o^2}\right) + i\sqrt{\frac{96\eta\lambda_1}{\rho R_o^2} - \left(1+\frac{24\eta\lambda_2}{\rho R_o^2}\right)^2}\right]$$

$$D_2 = \frac{1}{2\lambda_1}\left[-\left(1+\frac{24\eta\lambda_2}{\rho R_o^2}\right) - i\sqrt{\frac{96\eta\lambda_1}{\rho R_o^2} - \left(1+\frac{24\eta\lambda_2}{\rho R_o^2}\right)^2}\right]$$

and the solution is an oscillatory one in which we are particularly interested. The following case is of particular interest:

$$\frac{96\eta\lambda_1}{\rho R_o^2} >> \left(1+\frac{24\eta\lambda_2}{\rho R_o^2}\right)^2 \qquad (3.38)$$

$$\dot{\epsilon}_b \approx \frac{mg}{6\pi\eta R_o^2} - \frac{4mg\lambda_1}{\pi\rho R_o^4}\sqrt{\frac{\rho R_o^2}{24\eta\lambda_1}}\exp\left[-\frac{1}{2}\left(1+\frac{24\eta\lambda_2}{\rho R_o^2}\right)\frac{t}{\lambda_1}\right]\sin\sqrt{\frac{24\eta\lambda_1}{\rho R_o^2}}\frac{t}{\lambda_1} \tag{3.39}$$

and, from (3.16)

$$\frac{H}{H_o} = \exp\left[-2\int_o^t \dot{\epsilon}_b\, dt\right]$$

$$= \underbrace{\exp\left[-\frac{mgt}{3\pi\eta R_o^2}\right]}_{(A)} \cdot \underbrace{\exp\left[\frac{mg\lambda_1}{3\pi\eta R_o^2}\left\{\exp\underbrace{\left(-\frac{1}{2}-\frac{12\eta\lambda_2}{\rho R_o^2}\right)\frac{t}{\lambda_1}}_{(C)}\cdot\underbrace{\cos\sqrt{\frac{24\eta\lambda_1}{\rho R_o^2}}\frac{t}{\lambda_1}}_{(D)}-1\right\}\right]}_{(B)} \tag{3.40}$$

Each term in equation (3.40) represents different features of the lubricated compressive flow of linear viscoelastic materials under the condition (3.38). The first term (A) represents Newtonian viscous damping, the second (B) is related to the initial amplitude, and the third (C) represents the damping of the oscillatory term (D), whose oscillation period is $\pi R_o\sqrt{\frac{\rho\lambda_1}{6\eta}}$.

This oscillatory motion originates from the coexistence of the unsteady inertia term ($\rho\frac{\partial V}{\partial t}$) and the unsteady elastic relaxation term ($\lambda\frac{\partial \tau}{\partial t}$). These two time derivatives interact to generate the second order time derivative in equation (3.29).

The condition (3.37) is rather conservative for the oscillatory motion, since the solution (3.40) will behave as the non-oscillatory one if the damping term (C) is fast enough to make the product (C)*(D) very small in a time

which is smaller than the oscillation period. From this fact, we can develop a more useful necessary condition for the oscillatory motion: that is,

time scale of damping > oscillation period

or

$$a\cdot\frac{1}{\frac{1}{2\lambda_1}+\frac{12\eta\lambda_2}{\rho R_0^2\lambda_1}} > \pi R_0\sqrt{\frac{\rho\lambda_1}{6\eta}} \qquad (3.41)$$

Here the choice of the factor a in front of the lefthand side is rather arbitrary, and one may choose a value between 1 and 3. The value 1 gives 63%, 2 gives 86%, and 3 gives 95% of decay in the exponential term. Choosing a=2, equation (3.41) becomes

$$10\frac{\eta\lambda_1}{\rho R_0^2} > \left(1+\frac{24\eta\lambda_2}{\rho R_0^2}\right)^2 \quad : \text{oscillation} \qquad (3.42)$$

and

$$10\frac{\eta\lambda_1}{\rho R_0^2} < \left(1+\frac{24\eta\lambda_2}{\rho R_0^2}\right)^2 \quad : \text{no oscillation} \qquad (3.43)$$

When $\lambda_2=0$, equations (3.42) and (3.43) become

$$10\frac{\eta\lambda_1}{\rho R_0^2} > 1 \quad : \text{oscillation} \qquad (3.42A)$$

and

$$10\frac{\eta\lambda_1}{\rho R_0^2} < 1 \quad : \text{no oscillation} \qquad (3.43A)$$

It is useful to rewrite the condition (3.42) and

(3.43) in terms of the dimensionless groups defined below:

$$10\frac{De}{Re}\left(\frac{H}{R_o}\right)^2 > \left[1+24\frac{R_d}{Re}\left(\frac{H}{R_o}\right)^2\right]^2 \quad : \text{oscillation} \qquad (3.44)$$

$$10\frac{De}{Re}\left(\frac{H}{R_o}\right)^2 < \left[1+24\frac{R_d}{Re}\left(\frac{H}{R_o}\right)^2\right]^2 \quad : \text{no oscillation} \qquad (3.45)$$

where

$$Re = \frac{HV\rho}{\eta} \qquad \text{(Reynolds No.)}$$

$$De = \frac{V\lambda_1}{H} \qquad \text{(Deborah No.)}$$

$$Rd = \frac{V\lambda_2}{H} \qquad \text{(Retardation No.)}$$

Note that De/Re or Rd/Re depends on the material properties and the geometry only, but not on the squeezing speed, even though each group does depend on the squeezing speed. Also note that the dimensionless group De/Re is similar to the first elasticity number given by Astarita and Marrucci(1974), which has been defined by the ratio of the Weissenberg and Reynolds numbers in quasi-viscometric flows. This elasticity number was employed by Denn and Porteous(1971) to identify conditions under which elasticity can be expected to be important in viscoelastic fluid flow. Also it is seen in the paper by Tordella(1958) who used this number to predict the onset of melt fracture, and in the paper by Boger(1977) who tried to correlate pressure losses due to the elasticity in the capillary rheometer to the

elasticity number.

The equation (3.29) and the conditions (3.42-3.45) can be modified to include the load inertia term, which has been neglected in the above by assuming $\frac{16mH}{\pi R^4} << \rho$. First, we define several different densities,

$$\rho^* = \rho + \rho_m \tag{3.46}$$

$$\rho_m = \frac{16mH}{\pi R^4} \tag{3.47}$$

ρ is the fluid density, and ρ_m is a pseudo-fluid density corresponding to the mass of the load (m) in the lubricated compressive flow; ρ^* is the apparent density which represents both effects of the fluid inertia and the load inertia. If we use ρ^* instead of using ρ in the equation (3.29) to include both inertia effects, we have

$$\rho^*\lambda_1 \frac{d^2\dot{\epsilon}_b}{dt^2} + \rho^*\left(1 + \frac{24\eta\lambda_2}{\rho^* R^2}\right)\frac{d\dot{\epsilon}_b}{dt} + \frac{24\eta}{R^2}\dot{\epsilon}_b = \frac{4mg}{\pi R^4} \tag{3.48}$$

Here the constant radius condition also has been relaxed to include the situation of Fig. 3.1(a). Then the conditions (3.42-45) become

$$10\frac{3\lambda_1}{\rho^* R^2} > \left(1 + \frac{24\eta\lambda_2}{\rho^* R^2}\right)^2 \quad : \text{oscillation} \tag{3.49}$$

$$10\frac{3\lambda_1}{\rho^* R^2} < \left(1 + \frac{24\eta\lambda_2}{\rho^* R^2}\right)^2 \quad : \text{no oscillation} \tag{3.50}$$

or

$$10\frac{De}{Re^*}\left(\frac{H}{R}\right)^2 > \left[1+24\frac{Rd}{Re^*}\left(\frac{H}{R}\right)^2\right]^2 \quad : \text{oscillation} \qquad (3.51)$$

$$10\frac{De}{Re^*}\left(\frac{H}{R}\right)^2 < \left[1+24\frac{Rd}{Re^*}\left(\frac{H}{R}\right)^2\right]^2 \quad : \text{no oscillation} \qquad (3.52)$$

where

$$Re = \frac{H V \rho^*}{\eta} \qquad \text{(modified Reynolds No.)}$$

The oscillation period is also modified to $\pi R\sqrt{\frac{\rho^*\lambda_1}{6\eta}}$.

At this point we may note several interesting aspects of the lubricated compressive flow of linear viscoelastic materials :

(1) The compressive motion under a constant amount of load may or may not be oscillatory, depending upon the conditions (the material properties, the amount of the load, and the geometry) as predicted by equations (3.49)-(3.52).

(2) When oscillation occurs, it is due to the combined effects of the inertia, the elasticity, and the viscosity. The oscillation period depends only on geometry, inertia, and the elastic modulus.

(3) The retardation time may play an important role in the damping of the oscillatory motion (see term (C) in equation (3.40)).

(4) As λ_2 approaches λ_1, the response of linear viscoelastic materials approaches the Newtonian one.

In the next section, numerical solutions will be considered with no assumptions made, and this will further support and refine the conclusions noted.

3.2.3 Numerical solution

Equation (3.19), together with (3.16), (3.22), and constitutive equations (3.24) and (3.25), can be solved simultaneously by the Runge-Kutta method or the method of Gear(1970). Many different combinations of material properties and geometrical factors have been considered to investigate the characteristic features of this flow in the case of Fig. 3.1(a), in which the radius varies to keep the total mass of the fluid constant.

In Fig. 3.2, curves of H/H_o vs. time are shown at various values of relaxation times (λ_1 = 0.003, 0.03, 0.1, 0.3) and zero retardation time, and compared to the corresponding Newtonian curve (λ_1 = 0.). When $10\frac{3\lambda_1}{\rho^* R^2}$ is less than the unity, the curve does not oscillate (see curve 4), as expected from the condition (3.50). As $10\frac{3\lambda_1}{\rho^* R^2}$ increases, the oscillatory motion begins and becomes severe as the relaxation time, and hence the value of the group $10\frac{3\lambda_1}{\rho^* R^2}$, increases (see curves 1 to 3). The oscillation period is about the same as the calculated value from equation (3.40), if we consider the change of radius in these calculations [equation (3.40) was derived on the basis

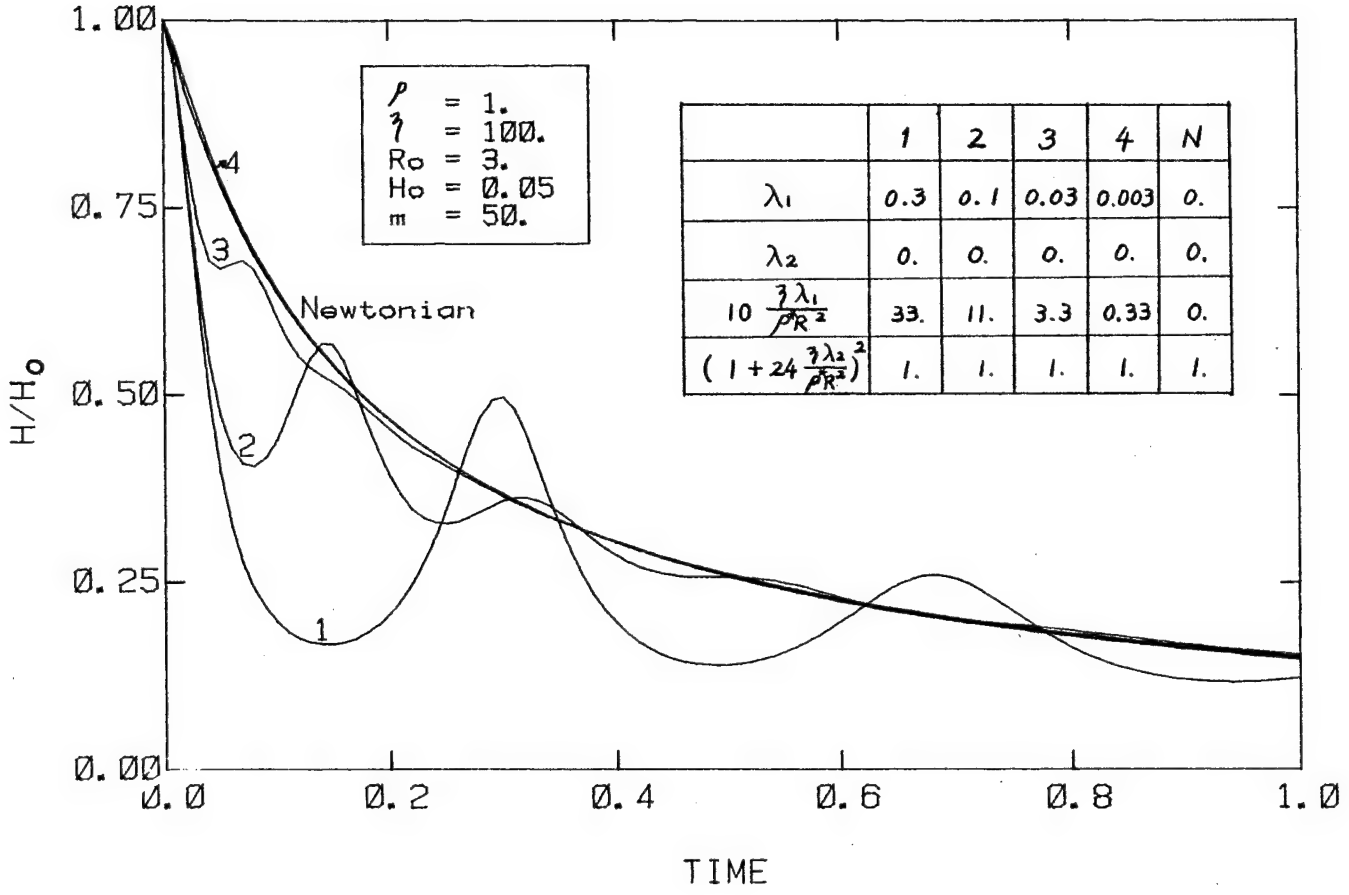

	1	2	3	4	N
λ_1	0.3	0.1	0.03	0.003	0.
λ_2	0.	0.	0.	0.	0.
$10\,\frac{\gamma\lambda_1}{\rho R^2}$	33.	11.	3.3	0.33	0.
$\left(1+24\,\frac{\gamma\lambda_2}{\rho R^2}\right)^2$	1.	1.	1.	1.	1.

Fig. 3.2 H/H_o vs. time in the lubricated compressive flow of linear viscoelastic materials : the effect of the relaxation time.

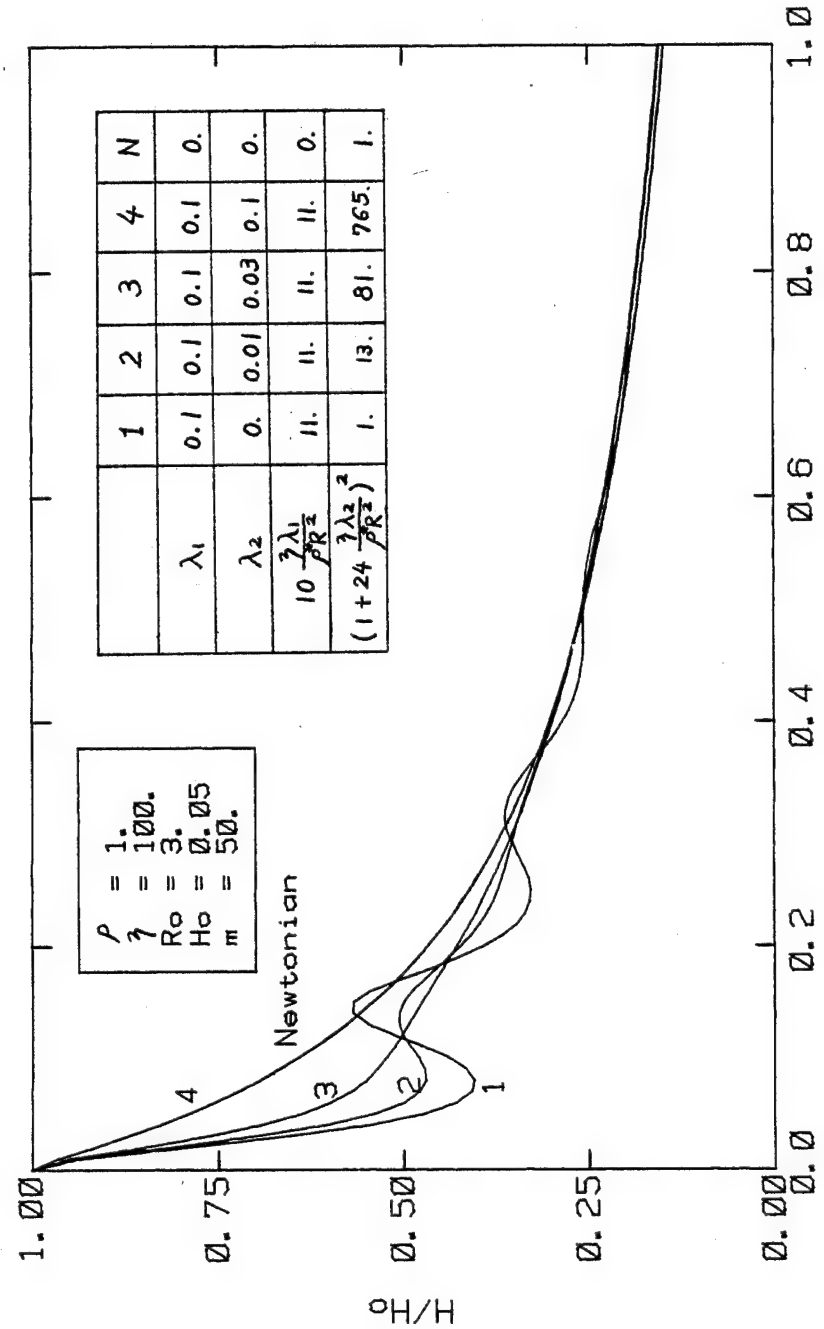

Fig. 3.3 H/H_o vs. time in the lubricated compressive flow of linear viscoelastic materials : the effect of the retardation time.

of a constant radius]. Note that most of the viscoelastic curves remain below the corresponding Newtonian curve, though the difference is minor at large times.

In Fig. 3.3, the effect of the retardation time has been illustrated. All the conditions are the same as before, except that λ_1 is kept constant (at 0.1) in all these calculations, and λ_2 varies (λ_2 = 0., 0.01, 0.05, 0.1). We can recognize that a small increase of the retardation time reduces the oscillation amplitude greatly, and the response approaches the Newtonian curve as λ_2 approaches λ_1. All curves remain below the corresponding Newtonian curve ($\lambda_1=\lambda_2=0.$).

3.3 Non-linear viscoelastic cases

3.3.1 Constitutive equations

Since the linear model does not predict some of the important non-Newtonian behavior of polymeric materials, such as shear thinning, normal stresses in simple shear flows, and high extensional viscosity in extensional flows, various kinds of non-linear models have been proposed. We shall now consider some of the currently popular and promising models.

One of the most successful models is the one proposed by Phan-Thien and Tanner(1977) and

Phan-Thien(1978), which has the following form with a single relaxation time:

$$\underset{\sim}{\tau} \exp\left[\frac{\varepsilon\lambda}{\eta_0}\,\mathrm{tr}\,\underset{\sim}{\tau}\right] + \lambda\left[(1-\tfrac{1}{2}\xi)\overset{\nabla}{\underset{\sim}{\tau}} + \tfrac{1}{2}\xi\overset{\Delta}{\underset{\sim}{\tau}}\right] = 2\eta_0\underset{\sim}{d} \qquad (3.53)$$

Here, $\overset{\nabla}{\underset{\sim}{\tau}}$ and $\overset{\Delta}{\underset{\sim}{\tau}}$ are the contravariant and covariant convected derivatives given by Oldroyd(1950), respectively, and denoted by

$$\overset{\nabla}{\underset{\sim}{\tau}} = \frac{D\underset{\sim}{\tau}}{Dt} - \nabla\underset{\sim}{v}\,\underset{\sim}{\tau} - \underset{\sim}{\tau}\,\nabla\underset{\sim}{v}^{T}$$

$$\overset{\Delta}{\underset{\sim}{\tau}} = \frac{D\underset{\sim}{\tau}}{Dt} + \nabla\underset{\sim}{v}^{T}\underset{\sim}{\tau} + \underset{\sim}{\tau}\,\nabla\underset{\sim}{v}$$

This equation has four material parameters, η_0, λ, ξ, and ε. η_0 is the zero shear viscosity and λ is the relaxation time. The parameter ξ can be determined from normal stress data in simple shear flow, since $\tau\xi/2$ is simply the ratio of the second normal stress difference to the first normal stress difference, or from the deviation of the viscosity from η_0. ε is related to the limiting value of extensional viscosity by $\lim_{\dot{\varepsilon}_E\to\infty}\eta_E = \text{const}\cdot(1/\varepsilon)$

When ε vanishes, (i.e., when the extensional viscosity has no limit), the Phan-Thien-Tanner model reduces to the one by Johnson and Segalman(1977), represented by

$$\underset{\sim}{\tau} + \lambda\left[(1-\tfrac{1}{2}\xi)\overset{\nabla}{\underset{\sim}{\tau}} + \tfrac{1}{2}\xi\overset{\Delta}{\underset{\sim}{\tau}}\right] = 2\eta_0\underset{\sim}{d} \qquad (3.54)$$

By adding a retardation term to the righthand side of (3.54), a modification of the Johnson-Segalman model is obtained as

$$\underset{\sim}{\tau} + \lambda_1\left[(1-\tfrac{1}{2}\mathfrak{z})\,\overset{\nabla}{\underset{\sim}{\tau}} + \tfrac{1}{2}\mathfrak{z}\,\overset{\Delta}{\underset{\sim}{\tau}}\right] = 2\eta_0\left[\underset{\sim}{d} + \lambda_2\left\{(1-\tfrac{1}{2}\mathfrak{z})\,\overset{\nabla}{\underset{\sim}{d}} + \tfrac{1}{2}\mathfrak{z}\,\overset{\Delta}{\underset{\sim}{d}}\right\}\right] \tag{3.55}$$

where λ_2 is the retardation time and $\overset{\nabla}{\underset{\sim}{d}}$ and $\overset{\Delta}{\underset{\sim}{d}}$ are defined in the same way as $\overset{\nabla}{\underset{\sim}{\tau}}$ and $\overset{\Delta}{\underset{\sim}{\tau}}$. The existence of the retardation term can be explained if one considers a polymer solution made up of a Newtonian solvent and a polymeric solute which is described by (3.54). The total stress in the solution would be the sum of the polymeric contribution and Newtonian solvent contribution, that is,

$$\underset{\sim}{\tau} = \underset{\sim}{\tau}_p + \underset{\sim}{\tau}_{sv} \tag{3.56}$$

where

$$\underset{\sim}{\tau}_p + \lambda_1\left[(1-\tfrac{1}{2}\mathfrak{z})\,\overset{\nabla}{\underset{\sim}{\tau}}_p + \tfrac{1}{2}\mathfrak{z}\,\overset{\Delta}{\underset{\sim}{\tau}}_p\right] = 2\eta_p\,\underset{\sim}{d} \tag{3.57}$$

$$\underset{\sim}{\tau}_{sv} = 2\eta_{sv}\,\underset{\sim}{d} \tag{3.58}$$

Here the subscript p stands for the polymer and sv for the solvent.

Differentiating equation (3.58)

$$\overset{\nabla}{\underset{\sim}{\tau}}_{sv} = 2\eta_{sv}\,\overset{\nabla}{\underset{\sim}{d}} \qquad \text{and} \qquad \overset{\Delta}{\underset{\sim}{\tau}}_{sv} = 2\eta_{sv}\,\overset{\Delta}{\underset{\sim}{d}}$$

or

$$(1-\tfrac{1}{2}\mathfrak{z})\,\lambda_1\,\overset{\nabla}{\underset{\sim}{\tau}}_{sv} = 2\eta_{sv}(1-\tfrac{1}{2}\mathfrak{z})\,\lambda_1\,\overset{\nabla}{\underset{\sim}{d}} \tag{3.59}$$

$$\frac{1}{2}\mathfrak{Z}\lambda_1 \overset{\Delta}{\underset{\sim}{\tau}}_{sv} = 2\eta_{sv}\cdot\frac{1}{2}\mathfrak{Z}\lambda_1 \overset{\Delta}{\underset{\sim}{d}} \tag{3.60}$$

By adding (3.57-60) together, we get (3.55) in which

$$\eta_0 = \eta_p + \eta_{sv} \tag{3.61}$$

$$\lambda_2 = \lambda_1 \frac{\eta_{sv}}{\eta_p + \eta_{sv}} \tag{3.62}$$

The Johnson-Segalman model((3.54)) further reduces to the contravariant convected, covariant convected, and corotational Maxwell model as $\mathfrak{Z}$ has the values of 0, 2, 1, respectively.

$$\mathfrak{Z} = 0 \quad : \qquad \underset{\sim}{\tau} + \lambda \overset{\nabla}{\underset{\sim}{\tau}} = 2\eta \underset{\sim}{d} \tag{3.63}$$

$$\mathfrak{Z} = 2 \quad : \qquad \underset{\sim}{\tau} + \lambda \overset{\Delta}{\underset{\sim}{\tau}} = 2\eta \underset{\sim}{d} \tag{3.64}$$

$$\mathfrak{Z} = 1 \quad : \qquad \underset{\sim}{\tau} + \lambda \frac{1}{2}\left[\overset{\nabla}{\underset{\sim}{\tau}} + \overset{\Delta}{\underset{\sim}{\tau}}\right] = 2\eta \underset{\sim}{d} \tag{3.65}^{*}$$

An equation of the form of (3.63) has been modified by White and Metzner(1963) to accomodate a non-Newtonian viscosity function:

$$\underset{\sim}{\tau} + \frac{\eta(\bar{\Pi}_d)}{G} \overset{\nabla}{\underset{\sim}{\tau}} = 2\eta(\bar{\Pi}_d)\underset{\sim}{d} \tag{3.66}$$

---

* $\frac{1}{2}\left[\overset{\nabla}{\underset{\sim}{\tau}} + \overset{\Delta}{\underset{\sim}{\tau}}\right]$ is often denoted by $\overset{\circ}{\underset{\sim}{\tau}}$ and is known as corotational Jaumann derivative (see Zaremba(1903) and Fromm(1947)).

where $\bar{\mathrm{II}}_d$ is the second invariant of the deformation rate tensor and G is the shear modulus. This model is useful in situations in which the non-Newtonian viscosity plays an important role.

The model proposed by Acierno et. al.(1976a), often called the "structural model", is also very promising. The model, with a single relaxation time, is represented by

$$\frac{1}{G}\underset{\sim}{\tau} + \lambda \frac{\delta}{\delta t}\left(\frac{1}{G}\underset{\sim}{\tau}\right) = 2\lambda \underset{\sim}{d} \tag{3.67}$$

$$G = G_0 x \quad , \qquad \lambda = \lambda_0 x^{1.4}$$

$$\frac{dx}{dt} = \frac{1}{\lambda}(1-x) - a x \frac{1}{\lambda}\sqrt{\frac{E}{G}} \qquad (a = 0.25 \sim 0.4)$$

$$E = \frac{1}{2} tr\, \underset{\sim}{\tau}$$

where $\frac{\delta}{\delta t}$ is the contravariant convected time derivative, and the scalar dimensionless quantity x($\leq$1.) is regarded as a structural variable which describes how far the existing structure is from equilibrium. G_0 and λ_0 are the equilibrium values of G and λ (when x=1.).

For comparison, we summarize the responses of each model fluid in simple shear flow in Table 3.1.

The covariant convected Maxwell model predicts too large a value of $\tau_{22} - \tau_{33}$ in comparison to what is found in most polymeric materials. The corotational model exhibits a shear viscosity which depends upon the shear rate too

	τ_{12}	$\tau_{11} - \tau_{22}$	$\tau_{22} - \tau_{33}$	Stress overshoot
Phan-Thien-Tanner	No explcit expression, but very close to Johnson-Segalman			yes
Johnson-Segalman	$\frac{\eta_0 \dot{\gamma}}{1+\lambda^2\dot{\gamma}^2\xi(2-\xi)}$	$\frac{2\eta_0\lambda\dot{\gamma}^2}{1+\lambda^2\dot{\gamma}^2\xi(2-\xi)}$	$\frac{-\xi\eta_0\lambda\dot{\gamma}^2}{1+\lambda^2\dot{\gamma}^2\xi(2-\xi)}$	yes
Johnson-Segalman with retard. time	$\frac{\eta_0\dot{\gamma}[1+\lambda_1\lambda_2\dot{\gamma}^2\xi(2-\xi)]}{1+\lambda_1^2\dot{\gamma}^2\xi(2-\xi)}$	$\frac{2\eta_0(\lambda_1-\lambda_2)\dot{\gamma}^2}{1+\lambda_1^2\dot{\gamma}^2\xi(2-\xi)}$	$\frac{-\xi\eta_0(\lambda_1-\lambda_2)\dot{\gamma}^2}{1+\lambda_1^2\dot{\gamma}^2\xi(2-\xi)}$	yes
Contravariant convected Maxwell	$\eta\dot{\gamma}$	$2\eta\lambda\dot{\gamma}^2$	0	no
Covariant convected Maxwell	$\eta\dot{\gamma}$	$2\eta\lambda\dot{\gamma}^2$	$-2\eta\lambda\dot{\gamma}^2$	no
Corotational Maxwell	$\frac{\eta_0\dot{\gamma}}{1+\lambda^2\dot{\gamma}^2}$	$\frac{2\eta_0\lambda\dot{\gamma}^2}{1+\lambda^2\dot{\gamma}^2}$	$\frac{-\eta_0\lambda\dot{\gamma}^2}{1+\lambda^2\dot{\gamma}^2}$	yes
White-Metzner	$\eta(\dot{\gamma})\dot{\gamma}$	$2\frac{\eta(\dot{\gamma})^2}{G}\dot{\gamma}^2$	0	no
Marrucci structural*	$G_0\lambda_0 x^{2.4}\dot{\gamma}$	$2G_0\lambda_0^2 x^{3.8}\dot{\gamma}^2$	0	yes

* Structural variable x satisfies $\frac{1-x}{x^{2.4}} = a\lambda_0\dot{\gamma}$ where $a = 0.25 \sim 0.4$.

Table 3.1 Comparison of non-linear models in simple shear flow.

strongly; it also predicts spurious oscillations after stress overshoot and much too large a value of $\tau_{22} - \tau_{33}$. Therefore, we shall disregard these two models in our numerical calculations.

The contravariant convected Maxwell model and its modification, the White-Metzner model, predict zero $\tau_{22} - \tau_{33}$ and no stress overshoot during startup. The Phan-Thien-Tanner model and its simplified form, the Johnson-Segalman model, predict non-zero values of $\tau_{22} - \tau_{33}$ and also a stress overshoot. The structural model predicts zero $\tau_{22} - \tau_{33}$ but it does predict a stress overshoot.

3.3.2 Numerical calculations

Lubricated compressive flows of the viscoelastic model fluids mentioned above, including the contravariant convected Maxwell model, the White-Metzner model, the Johnson-Segalman model (with and without retardation term), and the structural model, are solved numerically in this section. Since the equations to be solved in each case, which are given in appendix B, consist of first order ordinary differential equations, the Runge-Kutta or Gear method can be used. Here, we consider the situation given in Fig. 3.1(a), and the initial conditions are given by

$$\left.\begin{aligned} \dot{\epsilon}_b = \tau_{rr} = \tau_{zz} = 0 \\ H = H_o \quad , \quad R = R_o \end{aligned}\right\} \quad at \quad t = 0.$$

The results are shown in Figs. 3.4 through 3.10, in which H/H_o is plotted against time in each case. The curves for the contravariant convected Maxwell fluid are given in Fig. 3.4 and 3.5, those for the White-Metzner model in Fig. 3.6, the Johnson-Segalman model in Figs. 3.7-3.9, and the structural model in Fig. 3.10.

When $\frac{\eta\lambda}{\rho^* R^2}$ is small enough, the oscillation does not occur, as shown in Fig. 3.4. But if $\frac{\eta\lambda}{\rho^* R^2}$ is not small, oscillation does occur. When the squeezing rate is slow or moderate, the oscillatory curves stay below the corresponding inelastic ones in all cases (see Fig. 3.5, 3.6, 3.7, 3.10). In fast squeezing, each model behavior is distinct.

The Maxwell model results in oscillation and stays below the Newtonian curve (Fig. 3.5). In contrast, the White-Metzner model does not give oscillation at all for the power-law index of 0.5 and stays below the corresponding power-law curve (Fig. 3.6). The absence of oscillation in the White-Metzner model in fast squeezing seems to be due to the large decrease of the viscosity and the relaxation time at high deformation rates. These effects, plus the increases in R as time progresses, combine to make $\frac{\eta\lambda}{\rho^* R^2}$ very small, under which condition no oscillation would be expected.

The faster squeezing of the Maxwell model may look unusual to those who consider that the Maxwell model predicts very large elongational viscosities. But, if one remembers correctly, the large elongational viscosities of Maxwell fluids are obtained at large values of $\dot{\epsilon}_b\lambda$ after a long time. In other words, in a short time or at small values of $\dot{\epsilon}_b\lambda$ the elongational viscosity is even smaller than in the Newtonian case (6$\frac{1}{2}$). In the squeezing flow, $\dot{\epsilon}_b$ is large initially, but this large $\dot{\epsilon}_b$ can not be maintained for a long time since the film thickness is getting thinner very quickly. Thus, it is very difficult to build up a large elongational viscosity in this geometry. This is why the Maxwell fluid is squeezed faster than the Newtonian fluid even with the high initial value of $\dot{\epsilon}_b\lambda$. But, under the extraordinarily high loading conditions, the Maxwell curves are crossing over the corresponding Newtonian ones at very small values of H/H_o (see Appendix C for the detail). Even though the absolute differences between $(H/H_o)_{Maxwell}$ and $(H/H_o)_{Newtonian}$ are very small (in the order of 10^{-3} or less), the relative differences between them are around 2 in the cases of Appendix C. This fact may be important in the field of lubrication technology.

The rapid squeezing of the Johnson-Segalman model (Fig. 3.7-3.9) and the structural model (Fig. 3.10) are particularly interesting, because those curves move above

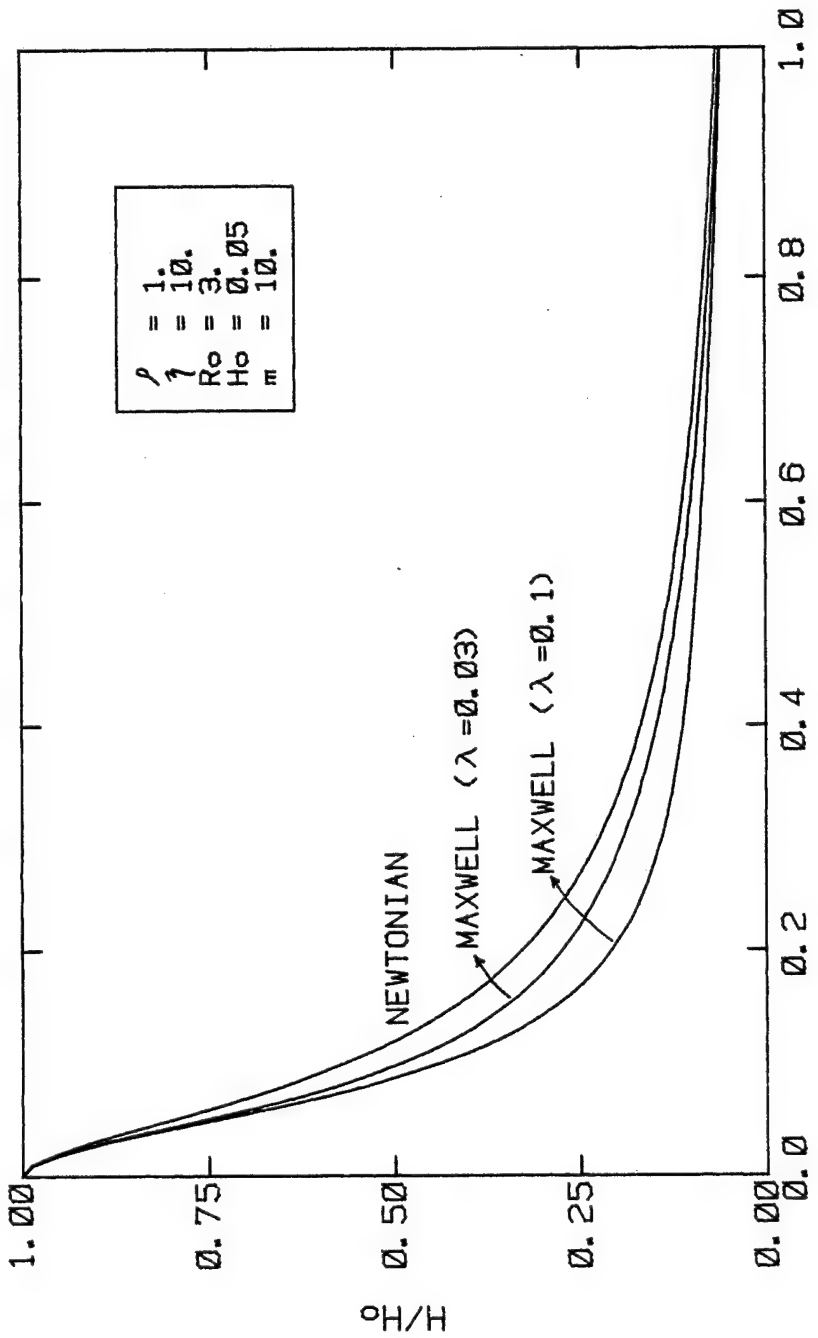

Fig. 3.4 H/H_o vs. time in the lubricated compressive flow of contravariant convected Maxwell model, compared to Newtonian fluid : no oscillation at small value of $\eta\lambda/\rho^* R^2$.

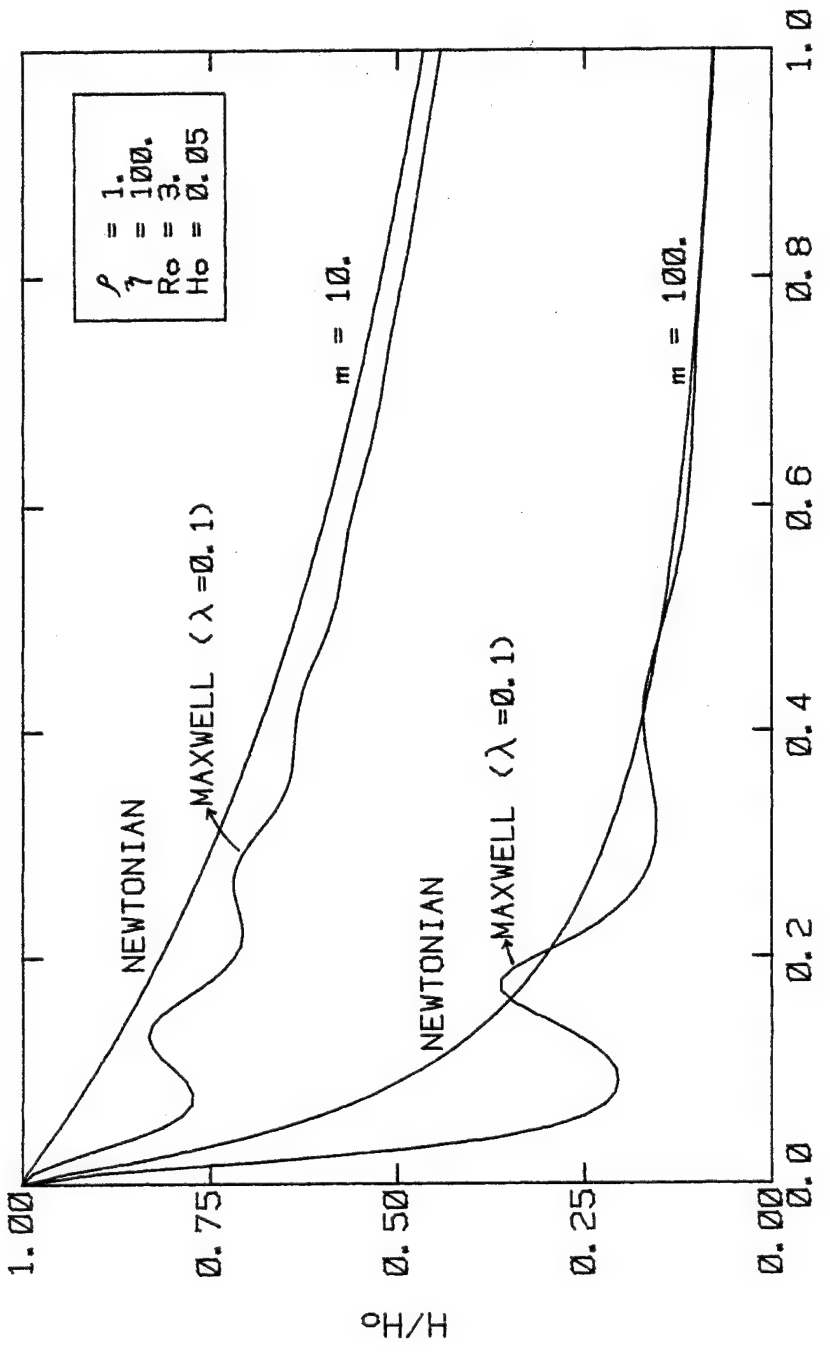

Fig. 3.5 H/H_o vs. time in the lubricated compressive flow of contravariant convected Maxwell model, compared to Newtonian fluid.

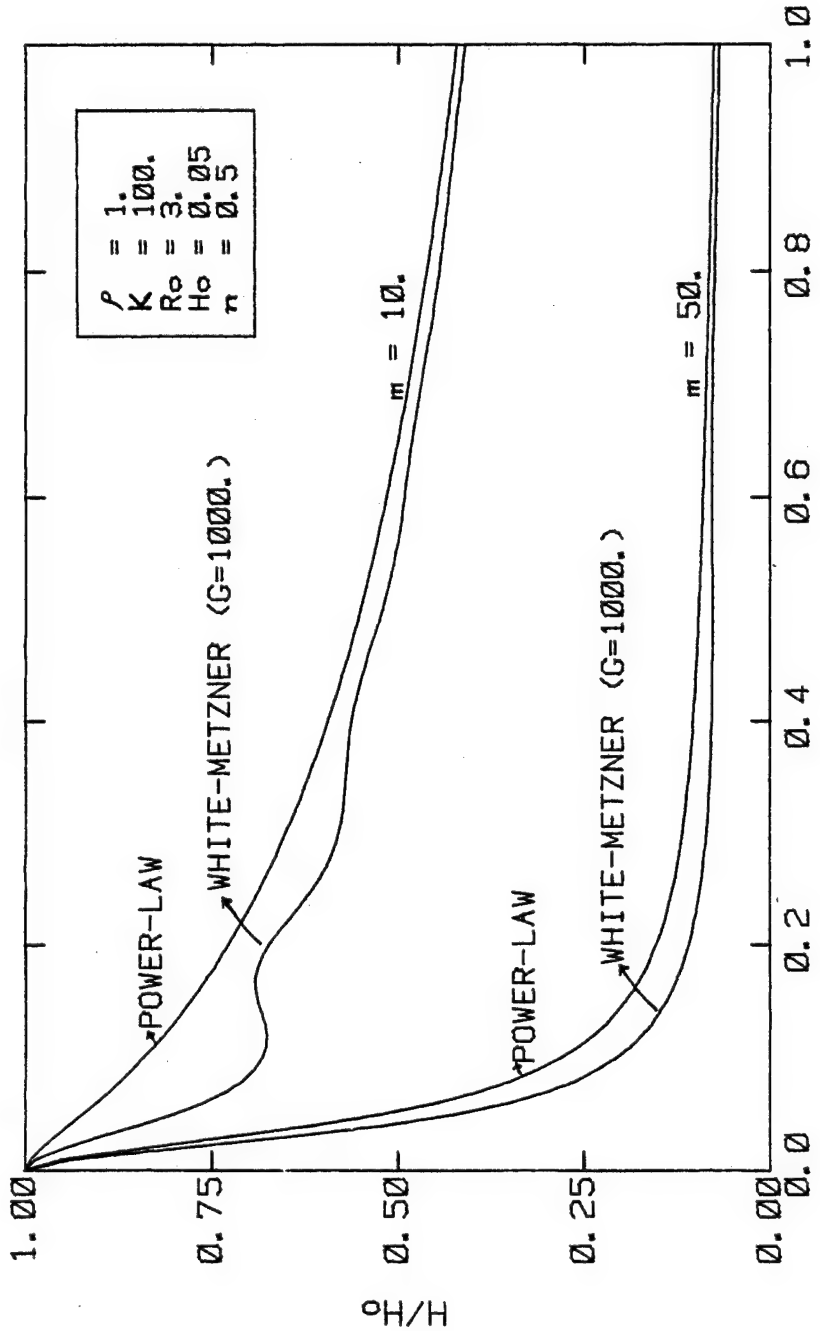

Fig. 3.6 H/H_o vs. time in the lubricated compressive flow of White-Metzner model with power-law viscosity, n=0.5, compared to the power-law case.

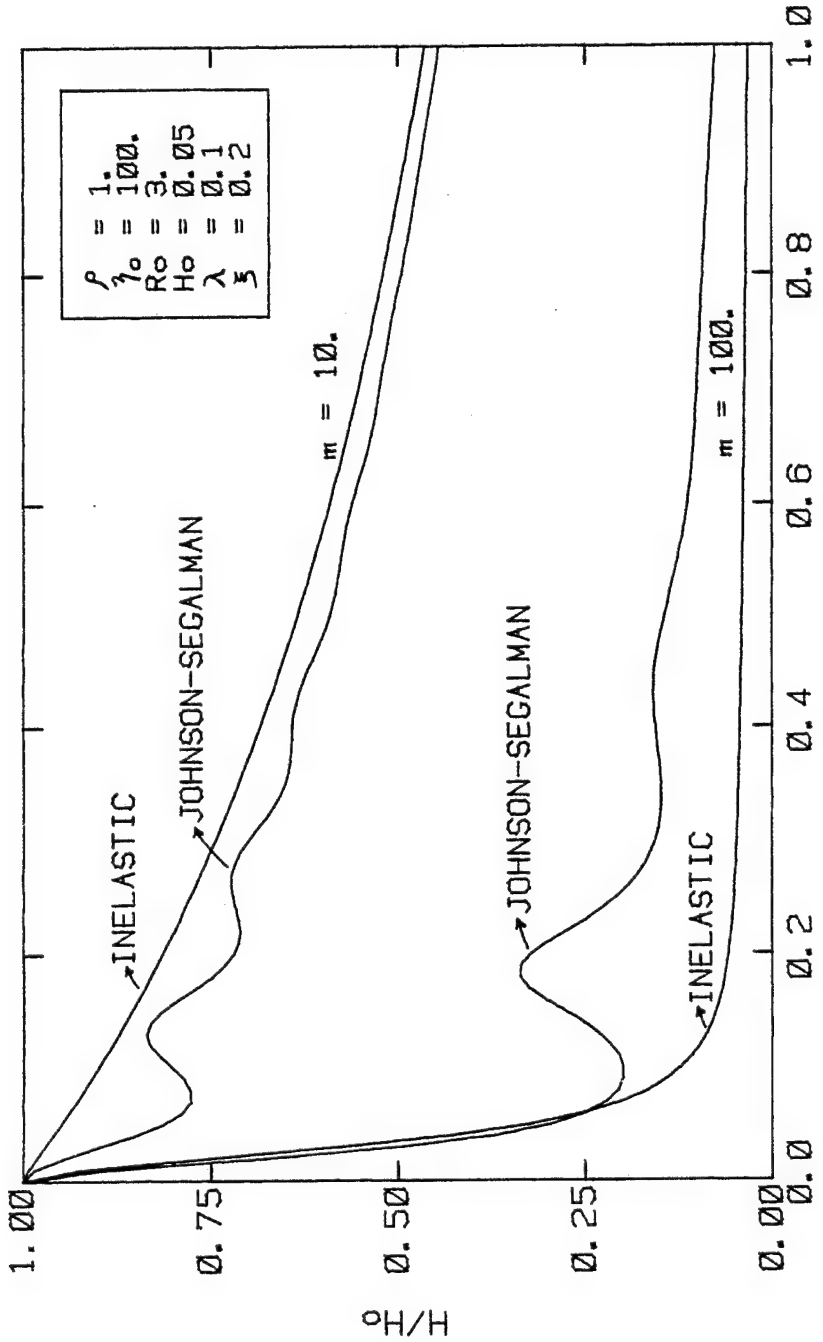

Fig. 3.7 H/H_o vs. time in the lubricated compressive flow of Johnson-Segalman model, compared to the corresponding shear thinning case.

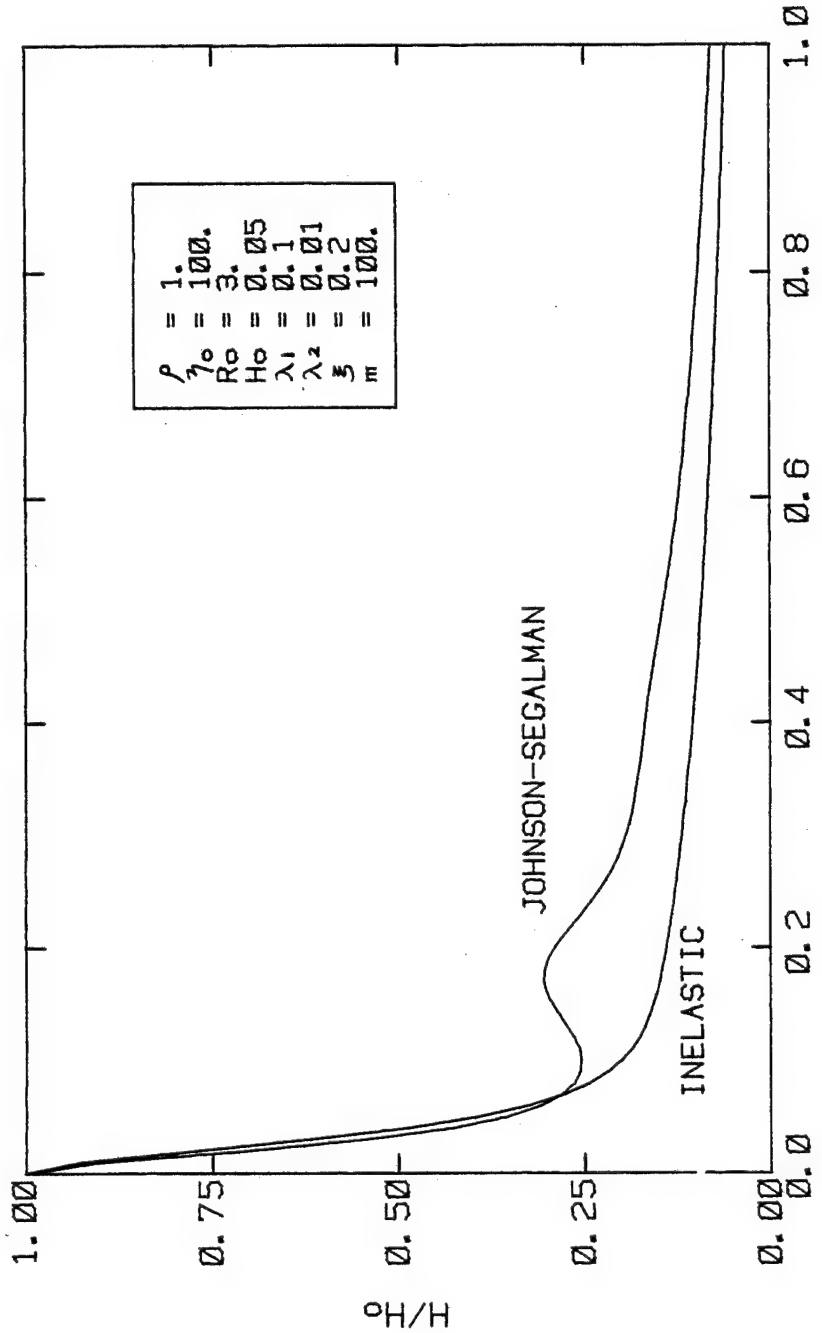

Fig. 3.8 H/H_o vs. time in the lubricated compressive flow of Johnson-Segalman model with non-zero retardation time, compared to the corresponding inelastic case.

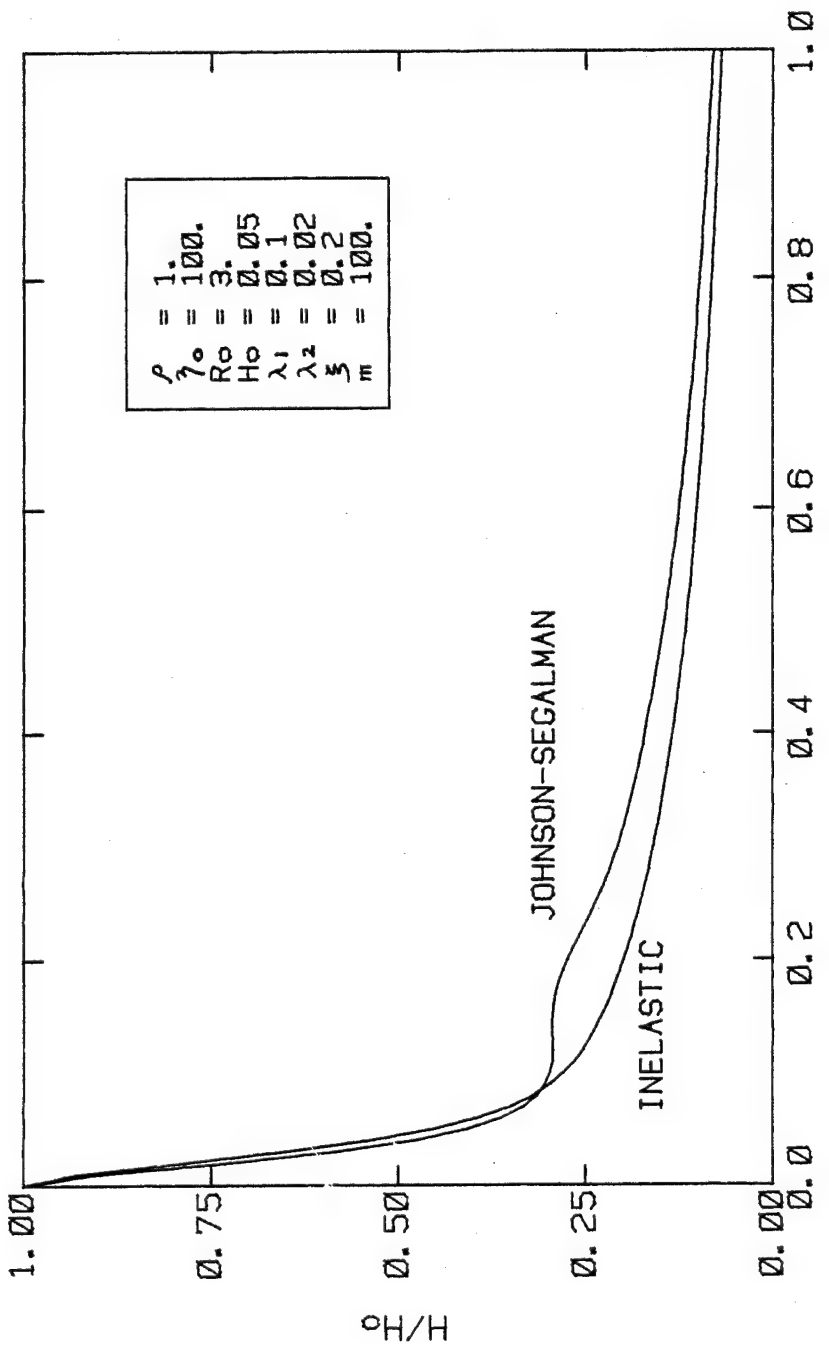

Fig. 3.9 H/H_o vs. time in the lubricated compressive flow of Johnson-Segalman model with non-zero retardation time, compared to the corresponding inelastic case.

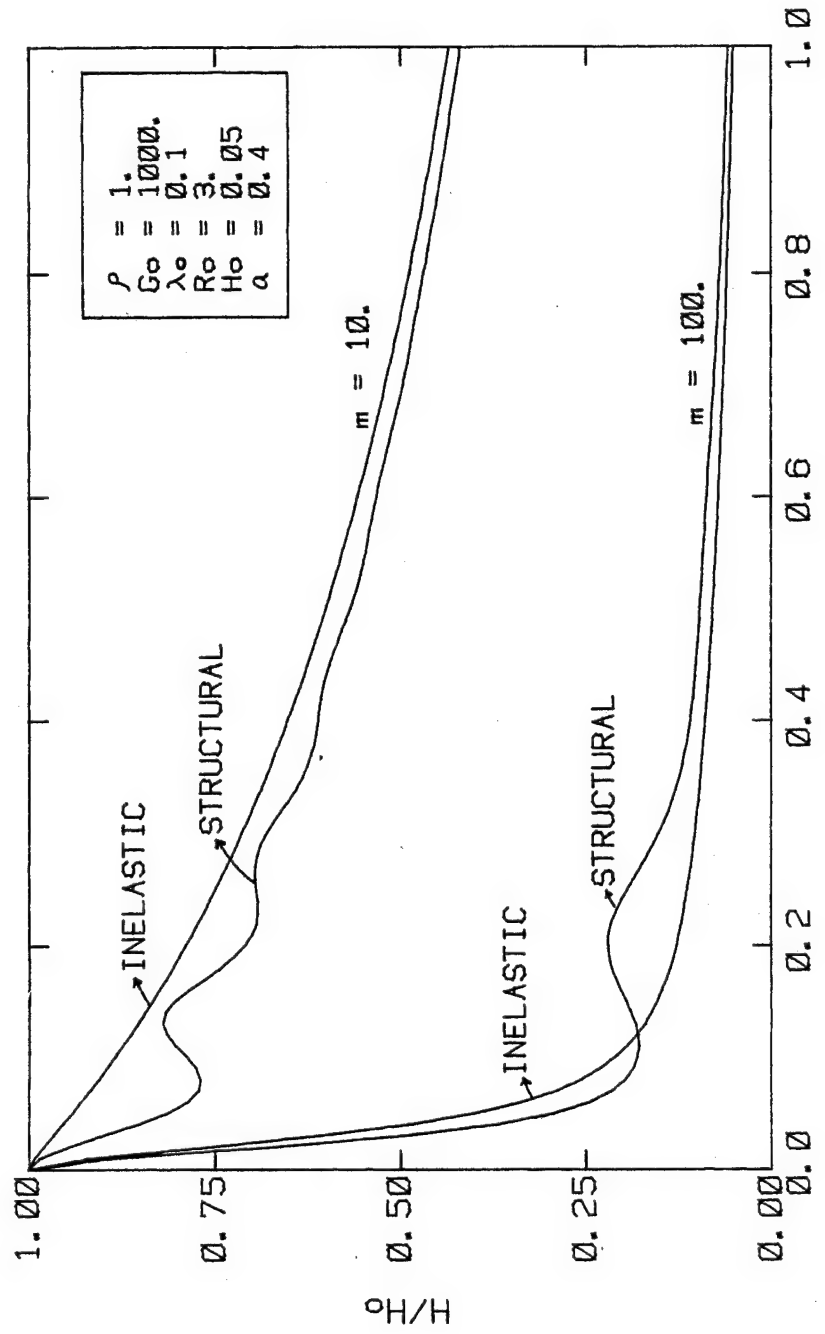

Fig. 3.10 H/H_o vs. time in the lubricated compressive flow of structural model, compared to the corresponding inelastic case.

the corresponding inelastic ones after some amount of initial faster squeezing. The effect is more prominent in the Johnson-Segalman model. The slower squeezing of these models must be due to the specific features which are not found in other models: that is, the predictions of the stress overshoot phenomenon and non-zero $\tau_{22} - \tau_{33}$ in simple shear flow of the Johnson-Segalman model, and the stress overshoot in the structural model. Figs. 3.8 and 3.9 show the effect of non-zero retardation time in the Johnson-Segalman model, which damps the oscillation.

3.4 Finite element simulation (Maxwell)

The main purpose of this section is to develop and test a finite element numerical scheme, to be used in solving the unlubricated problem in chapter 4. In particular, we will consider the contravariant convected Maxwell model. The problem has been already solved in the lubricated case in Section 3.3.2. Thus, the numerical scheme is tested by solving that same problem and comparing the result to the one obtained in Section 3.3.2.

The problem becomes complicated since we wish to include the unsteady inertia and the unsteady elasticity terms in the equations of motion and the constitutive equations, respectively. Numerically, it becomes more complicated because the domain changes as time goes on and

unsteady transient equations have to be solved between time steps. Thus, we will pose the problem in a more natural way, following the pathlines of each material point in Lagrangian coordinates. In other words, each nodal point in the initial grid moves along its own pathline as time goes on, and we use material time derivatives instead of using the partial time derivatives in the equations.

The equations to be solved are

$$\nabla \cdot \underset{\sim}{V} = 0 \tag{3.68}$$

$$\rho \frac{D\underset{\sim}{V}}{Dt} = -\nabla p + \nabla \cdot \underset{\sim}{\tau} \tag{3.69}$$

$$\underset{\sim}{\tau} + \lambda \left[\frac{D\underset{\sim}{\tau}}{Dt} - \nabla \underset{\sim}{V}\, \underset{\sim}{\tau} - \underset{\sim}{\tau}\, \nabla \underset{\sim}{V}^{T} \right] = \eta \left[\nabla \underset{\sim}{V} + \nabla \underset{\sim}{V}^{T} \right] \tag{3.70}$$

Initial conditions have to be specified (since we have time derivatives). These initial conditions are given by

$$\underset{\sim}{\tau} = \underset{\sim}{V} = 0 \qquad \text{at} \quad t = 0. \tag{3.71}$$

The time derivatives are treated by a finite difference scheme in the time coordinate. We use the implicit three point recurrence scheme with variable time steps, which requires at least two previous solutions. To solve for the solution at $t=t_{n+1}$ based on two previous solutions (at t_n and t_{n-1}), the material time derivative is discretized (on the time axis) by

$$\left(\frac{DA}{Dt}\right)_{n+1} = \frac{1}{\Delta t_n\, \Delta t_{n-1}\,(\Delta t_n+\Delta t_{n-1})}\Big[\, \Delta t_{n-1}(2\Delta t_n + \Delta t_{n-1})A_{n+1} - (\Delta t_n + \Delta t_{n-1})^2 A_n + (\Delta t_n) A_{n-1}\Big] \tag{3.72}$$

where $\Delta t_{n-1} = t_n - t_{n-1}$

$\Delta t_n = t_{n+1} - t_n$

$A_i = A \quad \text{at} \quad t = t_i$

All other terms in the equations involve the unknown variables at $t=t_{n+1}$. The discretized (in time) forms of equations (3.68)-(3.70) are given by

$$\nabla \cdot \underset{\sim}{V}_{n+1} = 0 \tag{3.73}$$

$$\rho\left(\frac{D\underset{\sim}{V}}{Dt}\right)_{n+1} = -\nabla P_{n+1} - \nabla \cdot \underset{\sim}{\tau}_{n+1} \tag{3.74}$$

$$\underset{\sim}{\tau}_{n+1} + \lambda\left[\left(\frac{D\underset{\sim}{\tau}}{Dt}\right)_{n+1} - \nabla \underset{\sim}{V}_{n+1}\,\underset{\sim}{\tau}_{n+1} - \underset{\sim}{\tau}_{n+1}\,\nabla \underset{\sim}{V}_{n+1}^{T}\right] = \eta\left[\nabla \underset{\sim}{V}_{n+1} + \nabla \underset{\sim}{V}_{n+1}^{T}\right] \tag{3.75}$$

The whole system has to be solved simultaneously on the given domain. The Newton-Raphson method is used to treat the nonlinear terms, and the predictor-corrector method is used to improve the shape of the grid in each time step.

The mixed finite element method, which was first introduced by Kawahara and Takeuchi(1977) and further

studied by Crochet and Bezy(1979), and Crochet and Keunings(1980), has been adopted to solve the system (3.73)-(3.75). This method differs from the displacement method used by Chang et. al.(1979a,b) in terms of the unknown fields. In the mixed method, the pressure, the velocity components, and the stress components are the unknown fields, while in the displacement method, the pressure and the velocity components are the unknown fields and the stress components are calculated by means of an iterative technique. In particular, we have chosen the triangular elements and the same shape functions as those of Crochet and Keunings; that is, the linear shape function in the pressure and the quadratic shape function in the velocity and the stress components (see Fig. 3.11). The Galerkin finite element formulation of system (3.59)-(3.61) is straightforward and is given in Appendix D. The resulting simultaneous linear algebraic system is solved by the frontal elimination technique proposed by Irons(1970) to reduce the use of the central core memory. The numerical algorithm to solve the lubricated compressive flow of the contravariant convected Maxwell fluid under a constant load is given in Fig. 3.12.

The initial grid used in the calculation and the deformed grids at later times are shown in Fig. 3.13, in which one can easily see that the deformation of the

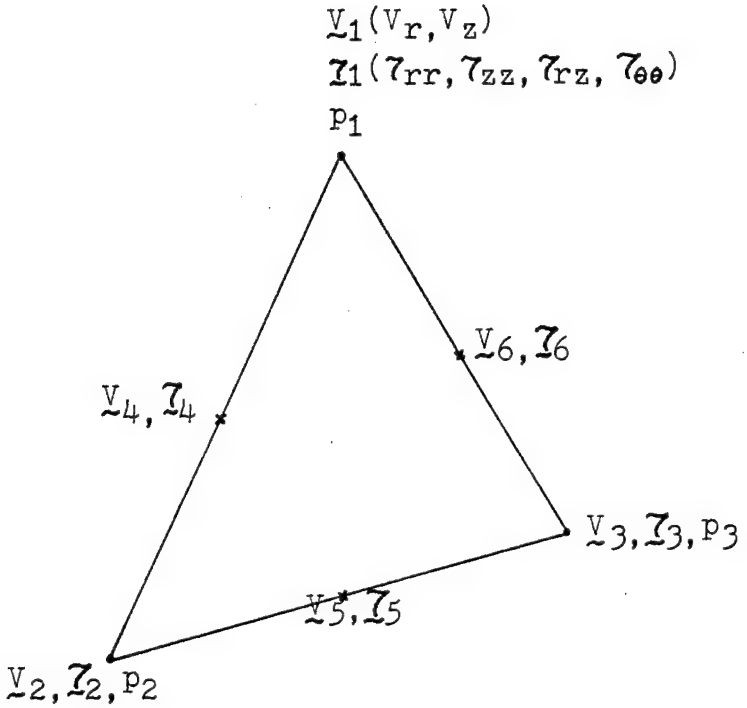

$$\underset{\sim}{V} = \sum_{i=1}^{6} \psi_i \underset{\sim}{V}_i$$

$$\mathcal{T} = \sum_{i=1}^{6} \psi_i \mathcal{T}_i$$

$$p = \sum_{i=1}^{3} \phi_i p_i$$

ψ_i : quadratic

ϕ_i : linear

Fig. 3.11 A triangular element and nodal variables.

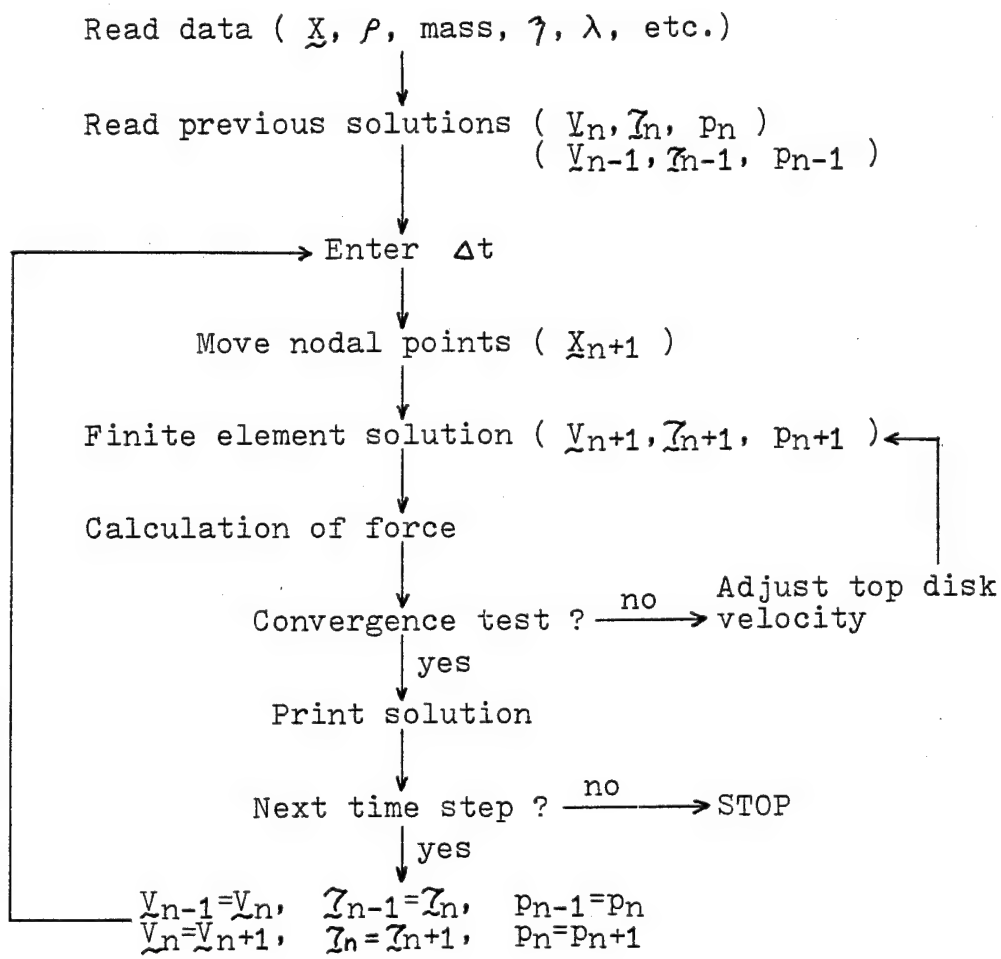

Fig. 3.12 Numerical algorithm to solve the lubricated compressive flow of Maxwell fluid.

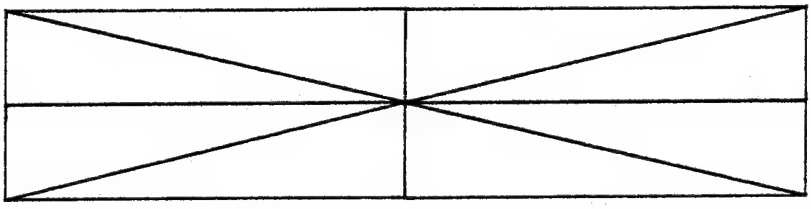

H/Ho = 1.0

Time = 0.0

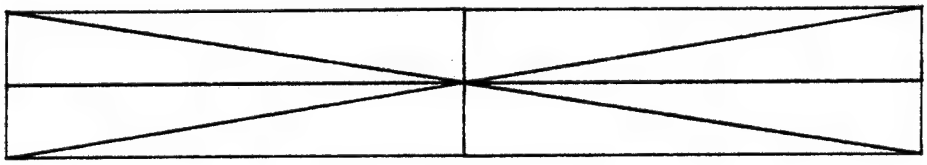

H/Ho = 0.7641

Time = 0.075

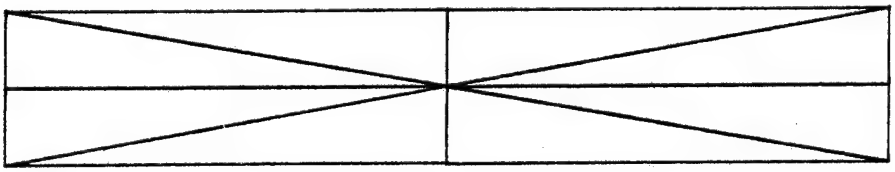

H/Ho = 0.8198

Time = 0.120

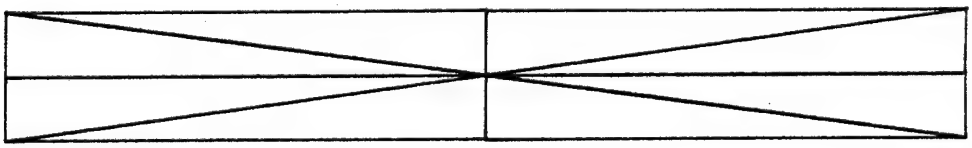

H/Ho = 0.6938

Time = 0.230

Fig. 3.13 The initial grid and the deformed grids (at later times) in the lubricated compressive flow of contravariant convected Maxwell fluid.

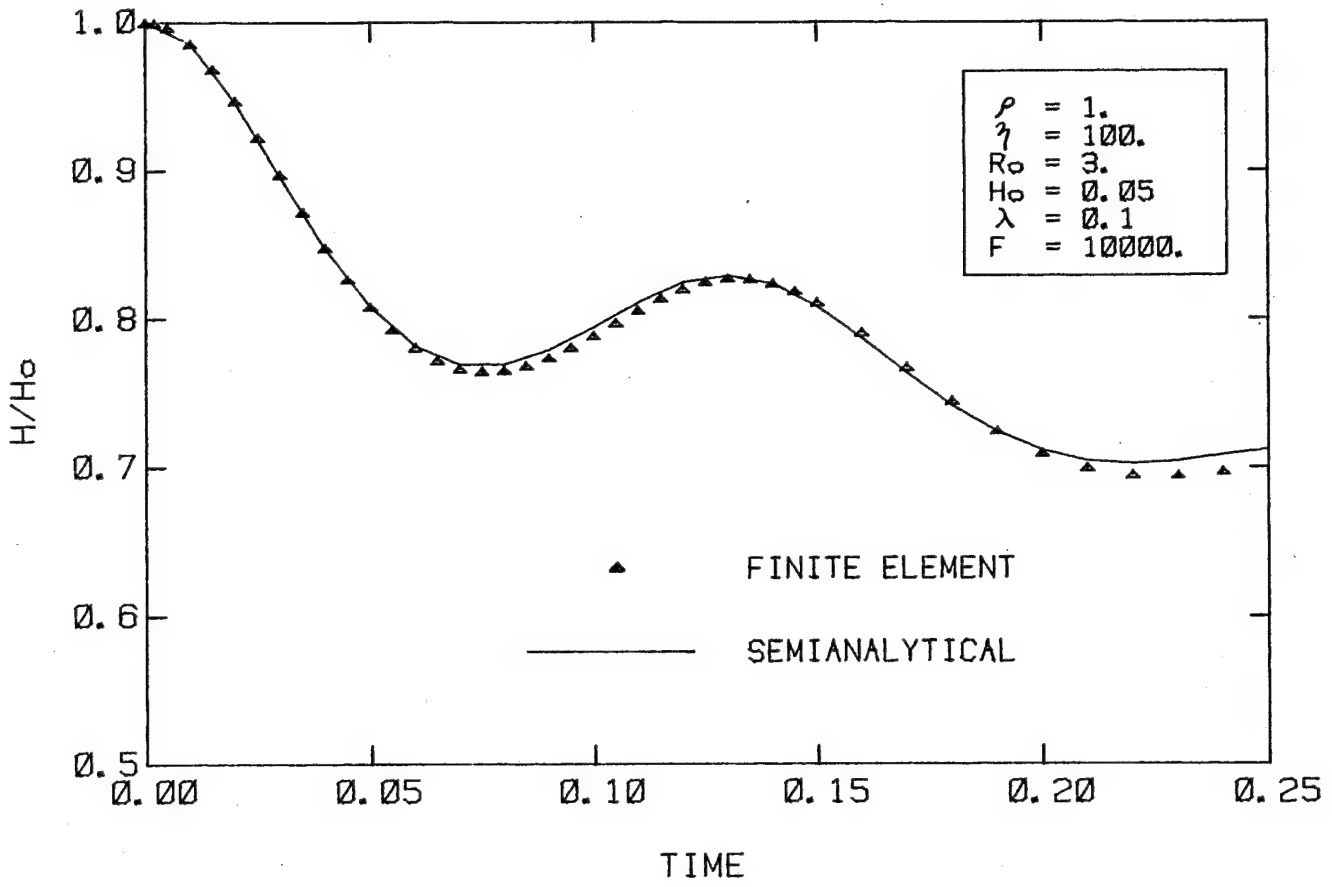

Fig. 3.14 Finite element numerical result (▲) compared to the semianalytical result obtained in the section 3.3.2 : contravariant convected Maxwell model.

material is indeed biaxial extension. Small numbers of elements have been used in this calculation because the stress field is uniform throughout the domain, and there is no stress singularity in this problem. Fig. 3.14 shows the oscillatory finite element result (H/H_o vs. time curve) compared to the semianalytical solution obtained in Section 3.3.2. The agreement between them is very good. Now, we can proceed to the next, more complicated problem, which is the unlubricated compressive flow of the contravariant convected Maxwell fluid.

3.5 Viscosity range of the lubricant to produce the biaxial extensional flow

If the viscosity of the lubricant is too low, the lubricant layer will be expelled quickly during the early time of the squeezing. On the other hand, if the viscosity is too high, then the flow in the viscous testing fluid will no longer be extensional flow. Therefore, to generate a lubricated compressive flow, or a biaxial extensional flow, a lubricant with the proper range of viscosity has to be used.

We know from Section 2.2 that the less viscous fluid near the wall is expelled preferentially when the extensional stress in the central viscous fluid is greater than the shear stress in the less viscous fluid near the

wall. In other words, in order to ensure that the lubricant layer is not preferentially expelled during the early time of the squeezing, we require the following condition:

$$\frac{\text{extensional stress in the viscous fluid}}{\text{shear stress in the lubricant}} < 1$$

or, for Newtonian fluids,

$$4\frac{\eta_2}{\eta_1}\left(\frac{H}{R}\right)^2\left(\frac{\delta}{H}\right)^3 < 1 \tag{3.76}$$

where η_1 is the viscosity of the lubricant, η_2 is the viscosity of the central viscous material, and δ is the thickness of the lubricant layer. From this we have

$$\boxed{\frac{\eta_1}{\eta_2} > 4\left(\frac{H}{R}\right)^2\left(\frac{\delta}{H}\right)^3} \tag{3.77}$$

which gives us the lower limit of the lubricant viscosity.

If the condition (3.77) is satisfied, parallel squeezing would be expected and hence the radial velocity profile is given by

$$V_r = -r\frac{C_1}{2}\int_H^z \frac{\xi\, d\xi}{\eta(\xi)} \tag{3.78}$$

where

$$C_1 = V\left[\int_H^0 du \int_H^u \frac{\xi\, d\xi}{\eta(\xi)}\right]^{-1} \tag{3.79}$$

See Appendix A for the details of deriving the above velocity profile.

In order to have nearly extensional flow in the central viscous fluid, the radial velocity at the interface between two fluids (at $z=H-\delta$) should be very close to the one at the centerplane (at $z=0$). Thus we can set a criterion for this purpose to be

$$\frac{(V_r)_{z=H-\delta}}{(V_r)_{z=0}} > 0.95 \tag{3.80}$$

Since

$$(V_r)_{z=H-\delta} = \frac{1}{2}\frac{r}{2} C_1 \frac{1}{2\eta_1}(\delta^2 - 2H\delta)$$

and

$$(V_r)_{z=0} = -\frac{r}{2} C_1 \left[\frac{1}{2\eta_1}(\delta^2 - 2H\delta) - \frac{1}{2\eta_2}(H-\delta)^2\right]$$

Equation (3.80) becomes

$$\frac{\frac{1}{2\eta_1}(\delta^2 - 2H\delta)}{\frac{1}{2\eta_1}(\delta^2 - 2H\delta) - \frac{1}{2\eta_2}(H-\delta)^2} > 0.95$$

or

$$\boxed{\frac{\eta_1}{\eta_2} < \frac{1-0.95}{0.95}\left[\left(1-\frac{\delta}{H}\right)^{-2} - 1\right]} \tag{3.81}$$

which represents the upper limit of the lubricant viscosity.

Therefore, the conditions (3.77) and (3.81) together determine the range of the viscosity of the lubricant which should be used to produce a nearly biaxial extensional flow in the central viscous fluid, to the extent that the rheology of both fluids can be taken to be Newtonian.

CHAPTER 4

UNLUBRICATED COMPRESSIVE FLOW OF VISCOELASTIC MATERIALS

We consider the unlubricated compressive flow, in which the no-slip boundary condition is satisfied by the viscoelastic materials. First, we consider a linearized viscoelastic case, in which an approximate solution can be obtained, which gives us much useful information. The contravariant convected Maxwell fluid will then be examined, since this model is on the side of convenience with a modest approach toward realism, even though it cannot predict the stress overshoot and the second normal stress difference in shear flow. In this case a numerical solution of the partial differential equations is inevitable. A finite element method, which has been tested in Section 3.3, will be used.

4.1 A linearized viscoelastic case

4.1.1 Assumptions and governing equations

First it will be assumed that the velocity profiles are the same as those of a Newtonian fluid; that is,

$$V_z = f(z,t) \tag{4.1}$$

$$V_r = -\frac{1}{2} r f'(z,t) \tag{4.2}$$

where $$f(z,t) = \frac{V}{4}\left[\left(\frac{z}{H}\right)^3 - 3\left(\frac{z}{H}\right)^2\right] \tag{4.3}$$

The prime in equation (4.2) implies partial differentiation with respect to z. The term V in (4.3) is the downward velocity of the top plate. The coordinate system used here is given in Fig. 4.1.

We will also assume that the fluid inertia is much less important than the load inertia. This will be shown later to be observed in most of the experimental conditions.

From equations (4.1) and (4.2), the deformation rate tensor is given by

$$\underset{\sim}{d} = \begin{pmatrix} -\frac{1}{2}f' & -\frac{1}{4}rf'' & 0 \\ -\frac{1}{4}rf'' & -\frac{1}{2}f' & 0 \\ 0 & 0 & f' \end{pmatrix} \tag{4.4}$$

Using the constitutive equation (3.23), the non-zero components of the stress are:

$$\tau_{rr} + \lambda_1 \frac{\partial \tau_{rr}}{\partial t} = -\eta\left(f' + \lambda_2 \frac{\partial f'}{\partial t}\right) \tag{4.5}$$

$$\tau_{\theta\theta} + \lambda_2 \frac{\partial \tau_{\theta\theta}}{\partial t} = -\eta\left(f' + \lambda_2 \frac{\partial f'}{\partial t}\right) \tag{4.6}$$

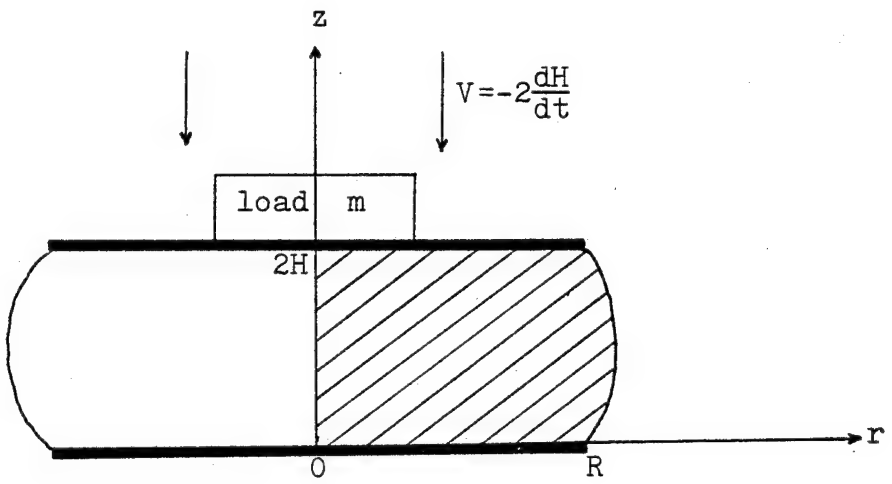

Fig. 4.1 The domain used in the unlubricated compressive flow of viscoelastic materials.

$$\tau_{zz} + \lambda_1 \frac{\partial \tau_{zz}}{\partial t} = 2\eta \left(f' + \lambda_2 \frac{\partial f'}{\partial t}\right) \tag{4.7}$$

$$\tau_{rz} + \lambda_1 \frac{\partial \tau_{rz}}{\partial t} = -\frac{1}{2}\eta r \left(f'' + \lambda_2 \frac{\partial f''}{\partial t}\right) \tag{4.8}$$

from which each component of the extra stress tensor $\underset{\sim}{\tau}$ is obtained as

$$\tau_{rr} = \tau_{\theta\theta} = -\frac{\eta}{\lambda_1} \exp\left(-\frac{t}{\lambda_1}\right) \int_0^t \left(f' + \lambda_2 \frac{\partial f'}{\partial t}\right) \exp\left(\frac{t}{\lambda_1}\right) dt \tag{4.9}$$

$$\tau_{zz} = -2\,\tau_{rr} \tag{4.10}$$

$$\tau_{rz} = -\frac{1}{2} \frac{\eta}{\lambda_1} r \exp\left(-\frac{t}{\lambda_1}\right) \int_0^t \left(f'' + \lambda_2 \frac{\partial f''}{\partial t}\right) \exp\left(\frac{t}{\lambda_1}\right) dt \tag{4.11}$$

From equation (4.9) $\frac{\partial \tau_{rr}}{\partial r} = 0$ and $\tau_{rr} - \tau_{\theta\theta} = 0$. Therefore, the equations of motion become (neglecting fluid inertia):

$$\frac{\partial p}{\partial r} = \frac{\partial \tau_{rz}}{\partial z} \tag{4.12}$$

$$\frac{\partial p}{\partial z} = \frac{1}{r} \frac{\partial}{\partial r}(r \tau_{rz}) + \frac{\partial \tau_{zz}}{\partial z} \tag{4.13}$$

or

$$\frac{\partial p}{\partial r} = -\frac{1}{2} \frac{\eta}{\lambda_1} r \exp\left(-\frac{t}{\lambda_1}\right) \int_0^t \left(f''' + \lambda_2 \frac{\partial f'''}{\partial t}\right) \exp\left(\frac{t}{\lambda_1}\right) dt \tag{4.14}$$

$$\frac{\partial p}{\partial z} = \frac{\eta}{\lambda_1} \exp\left(-\frac{t}{\lambda_1}\right) \int_0^t \left(f'' + \lambda_2 \frac{\partial f''}{\partial t}\right) \exp\left(\frac{t}{\lambda_1}\right) dt \tag{4.15}$$

Integrating equations (4.14) and (4.15), the pressure is obtained as

$$p(r,z,t) = -\frac{1}{4} \frac{\eta}{\lambda_1} r^2 \exp\left(-\frac{t}{\lambda_1}\right) \int_0^t \left(f''' + \lambda_2 \frac{\partial f'''}{\partial t}\right) \exp\left(\frac{t}{\lambda_1}\right) dt + \frac{\eta}{\lambda_1} \exp\left(-\frac{t}{\lambda_1}\right) \int_0^t \left(f' + \lambda_2 \frac{\partial f'}{\partial t}\right) \exp\left(\frac{t}{\lambda_1}\right) dt + p_0(t) \tag{4.16}$$

To determine $p_o(t)$, the boundary condition at the free surface (at r=R) is applied as

$$\int_o^{2H} (\sigma_{rr})_{r=R}\, dz = 0 \tag{4.17}$$

We thus have

$$p_o(t) = \frac{3}{8}\frac{\eta}{\lambda_1} R^2 \exp(-\tfrac{t}{\lambda_1}) \int_o^t \left(\frac{V}{H^3} + \lambda_2 \frac{\partial}{\partial t}\left(\frac{V}{H^3}\right)\right) \exp(\tfrac{t}{\lambda_1})\, dt + 2\frac{\eta}{\lambda_1} \exp(-\tfrac{t}{\lambda_1}) \int_o^t \left(V + \lambda_2 \frac{\partial V}{\partial t}\right) \exp(\tfrac{t}{\lambda_1})\, dt \tag{4.18}$$

The total force exerted by the fluid on the top plate is given by the following integration.

$$F = \int_o^R (-\sigma_{zz})_{z=2H} 2\pi r\, dr = \int_o^R (p - \tau_{zz})_{z=2H} 2\pi r\, dr \tag{4.19}$$

Substituting equations (4.10), (4.16), and (4.18) into (4.19) and performing the integration one obtains

$$F = \frac{3}{16}\frac{\eta}{\lambda_1} \pi R^4 \exp(-\tfrac{t}{\lambda_1}) \int_o^t \left[\frac{V}{H^3} + \lambda_2 \frac{\partial}{\partial t}\left(\frac{V}{H^3}\right)\right] \exp(\tfrac{t}{\lambda_1})\, dt + \frac{\eta}{\lambda_1} \pi \frac{R^2}{H} \exp(-\tfrac{t}{\lambda_1}) \int_o^t \left[V + \lambda_2 \frac{\partial V}{\partial t}\right] \exp(\tfrac{t}{\lambda_1})\, dt \tag{4.20}$$

This force is balanced by the one exerted by the load,

$$F = m\left(g - \frac{dV}{dt}\right) \tag{4.21}$$

Equating equations (4.20) and (4.21) we have

$$m\left(g - \frac{dV}{dt}\right) = \frac{3}{16}\frac{\eta}{\lambda_1} \pi R^4 \exp(-\tfrac{t}{\lambda_1}) \int_o^t \left[\frac{V}{H^3} + \lambda_2 \frac{\partial}{\partial t}\left(\frac{V}{H^3}\right)\right] \exp(\tfrac{t}{\lambda_1})\, dt + \frac{\eta}{\lambda_1} \pi \frac{R^2}{H} \exp(-\tfrac{t}{\lambda_1}) \int_o^t \left[V + \lambda_2 \frac{\partial V}{\partial t}\right] \exp(\tfrac{t}{\lambda_1})\, dt \tag{4.22}$$

Multiplying this equation by $\exp(\frac{t}{\lambda_1})$ and differentiating with respect to time gives the following second order dynamical equation:

$$m\lambda_1 \frac{d^2V}{dt^2} + m\left[1 + \lambda_2 \frac{3\pi\eta R^4}{16mH^3}\left(1 + \frac{16}{3}\left(\frac{H}{R}\right)^2\right)\right]\frac{dV}{dt} + \frac{3\pi\eta R^4}{16H^3}\left[1 + \frac{16}{3}\left(\frac{H}{R}\right)^2\right]V = mg \qquad (4.23)$$

When R/H>>1, equation (4.23) reduces to

$$m\lambda_1 \frac{d^2V}{dt^2} + m\left[1 + \lambda_2 \frac{3\pi\eta R^4}{16mH^3}\right]\frac{dV}{dt} + \frac{3\pi\eta R^4}{16H^3}V = mg$$

or

$$\rho_m \lambda_1 \frac{d^2V}{dt^2} + \rho_m\left[1 + \frac{3}{2}\frac{\eta\lambda_2}{\rho_m H^2}\right]\frac{dV}{dt} + \frac{3}{2}\frac{\eta}{H^2}V = \rho_m g \qquad (4.24)$$

where $\rho_m (= \frac{8mH}{\pi R^4})$ is a pseudo-fluid density corresponding to the amount of the load in the unlubricated compressive flow. The group ρ_m arises when we compare the load inertia to the fluid inertia, that is,

$$\text{load inertia} = m\frac{dV}{dt}$$

$$\text{fluid inertia} = (\pi R^2)\frac{1}{2H}\int_0^{2H}\left[\int_0^r \rho \frac{\partial V_r}{\partial t}\,dr\right]_{r=R} dz$$

$$= \frac{1}{8}\pi\rho\frac{R^4}{H}\frac{dV}{dt}$$

When $\lambda_2 = 0$, equation (4.24) reduces further to

$$\rho_m \lambda_1 \frac{d^2V}{dt^2} + \rho_m \frac{dV}{dt} + \frac{3}{2}\frac{\eta}{H^2} V = \rho_m g \qquad (4.25)$$

This equation is to be compared to the counterpart for lubricated flow, equation (3.29),

$$\rho \lambda_1 \frac{d^2\dot{\epsilon}_b}{dt^2} + \rho \frac{d\dot{\epsilon}_b}{dt} + 24 \frac{\eta}{R^2} \dot{\epsilon}_b = \frac{4 m g}{\pi R^4}$$

or since $V=4H\dot{\epsilon}_b$ from equation (3.2)

$$\rho \lambda_1 \frac{d^2V}{dt^2} + \rho \frac{dV}{dt} + 24 \frac{\eta}{R^2} V = \frac{16 mH}{\pi R^4} g = \rho_m g \qquad (3.29A)$$

It is to be noted that ρ_m is equal to $\frac{16 mH}{\pi R^4}$ in the lubricated case.

Equations (4.25) and (3.29A) have very similar forms except for the coefficients of the third terms. Equation (4.25) has η/H^2, while (3.29A) has η/R^2. This difference comes from the different origin of this third term in each equation; the term in equation (4.25) is from the shear stress, and the term in equation (3.29A) is from the normal stresses.

The condition under which equation (4.24) predicts the occurrence of oscillatory motion is given by:

$$\rho_m^2 \left(1 + \frac{3}{2}\frac{\eta \lambda_2}{\rho_m H^2}\right)^2 - 4 \rho_m \lambda_1 \frac{3}{2}\frac{\eta}{H^2} < 0$$

If the fluid inertia is included in the more general

development, this becomes

$$\rho^{*2}\left(1+\frac{3}{2}\frac{3\lambda_2}{\rho^* H^2}\right)^2 - 6\rho^*\frac{3\lambda_1}{H^2} < 0$$

or

$$6\frac{3\lambda_1}{\rho^* H^2} > \left(1+\frac{3}{2}\frac{3\lambda_2}{\rho^* H^2}\right)^2 \tag{4.26}$$

$$6\frac{De}{Re^*} > \left(1+\frac{3}{2}\frac{Rd}{Re^*}\right)^2 \tag{4.27}$$

Here $\rho^* = \rho + \rho_m$

$Re = \frac{HV\rho^*}{3}$ (modified Reynolds No.)

$Rd = \frac{V\lambda_2}{H}$ (Retardation No.)

$De = \frac{V\lambda_1}{H}$ (Deborah No.)

When $6\frac{3\lambda_1}{\rho_m H^2} >> \left(1+\frac{3}{2}\frac{3\lambda_2}{\rho_m H^2}\right)^2$, equation (4.24) has the following approximate oscillatory solution.

$$V \approx \frac{2\rho_m g H^2}{3\eta} + \exp\left[-\frac{t}{2\lambda_1}\left(1+\frac{3}{2}\frac{3\lambda_2}{\rho_m H^2}\right)\right]\cdot\left[C_1 \sin\sqrt{\frac{3}{2}\frac{3\lambda_1}{\rho_m H^2}}\frac{t}{\lambda_1} + C_2 \cos\sqrt{\frac{3}{2}\frac{3\lambda_1}{\rho_m H^2}}\frac{t}{\lambda_1}\right]$$

The oscillation period is obtained as $4\pi H\sqrt{\frac{\rho_m\lambda_1}{6\eta}}$ or, in general, as $4\pi H\sqrt{\frac{\rho^*\lambda_1}{6\eta}}$. This again has a different dependence of the length scale from the period in the lubricated case, $\pi R\sqrt{\frac{\rho^*\lambda_1}{6\eta}}$.

The condition (4.27) is conservative for the reason that has been discussed in Section 3.2.2; that is, the time

scale of the damping needs to be larger than the time scale of the oscillation for the oscillation to be observed. The more useful condition is obtained by

$$2 \cdot \frac{1}{\frac{1}{2\lambda_1}\left(1+\frac{3}{2}\frac{3\lambda_2}{\rho^* H^2}\right)} > 4\pi H\sqrt{\frac{\rho^*\lambda_1}{6\eta}} \qquad (4.28)$$

or

$$0.6\,\frac{3\lambda_1}{\rho^* H^2} > \left(1+\frac{3}{2}\frac{3\lambda_2}{\rho^* H^2}\right)^2 \qquad (4.29)$$

$$0.6\,\frac{De}{Re^*} > \left(1+\frac{3}{2}\frac{Rd}{Re^*}\right)^2 \qquad (4.30)$$

Here we have again chosen the factor 2 in front of the lefthand side of equation (4.28), which has resulted in a coefficient of 0.6 in equation (4.30). If one chooses 1 or 3 instead 2 in equation (4.28), we will have 0.15 or 1.4, respectively, instead 0.6 in (4.30).

4.1.2 Numerical solution

Numerical solutions of equation (4.24) are given in this section. H/H_o vs. time curves are shown in Fig. 4.2 at various values of relaxation times (λ_1 = 0.003, 0.01, 0.03) and zero retardation time, and compared to the corresponding Newtonian curve. When $0.6\frac{3\lambda_1}{\rho^* H^2}$ is less than unity, the curve does not oscillate, as expected from the condition (4.29). As $0.6\frac{3\lambda_1}{\rho^* H^2}$ increases, the oscillation begins and becomes severe. The oscillation period is about the same as the calculated value of $T=4\pi H\sqrt{\frac{\rho^*\lambda_1}{6\eta}}$. Most of the viscoelastic

curves remain below the corresponding Newtonian curve.

The effect of the retardation time is shown in Fig. 4.3. Here, the relaxation time (λ_1) is kept constant and the retardation time (λ_2) varies ($\lambda_2 = 0.$, 0.001, 0.003, 0.01). A small increase of the retardation time reduces the oscillation amplitude greatly, as expected from the condition (4.30), and the response approaches the Newtonian curve as λ_2 approaches λ_1.

4.2 Contravariant convected Maxwell fluid

4.2.1 Governing equations

With the following kinematics,

$$V_r = V_r(r,z,t) \ , \quad V_z = V_z(r,z,t) \ , \quad V_\theta = 0 \qquad (4.31)$$

the non-zero components of the deformation rate tensor $\underset{\sim}{d}$ are d_{rr}, $d_{\theta\theta}$, d_{zz}, and d_{rz}, from which we also assume that the non-zero components of the extra stress tensor $\underset{\sim}{\tau}$ are τ_{rr}, $\tau_{\theta\theta}$, τ_{zz}, and τ_{rz}. The unlubricated compressive flow of a contravariant convected Maxwell fluid is then governed by the following equations and the boundary conditions:

Continuity:

$$\frac{1}{r}\frac{\partial}{\partial r}(rV_r) + \frac{\partial V_z}{\partial z} = 0 \qquad (4.32)$$

Momentum:

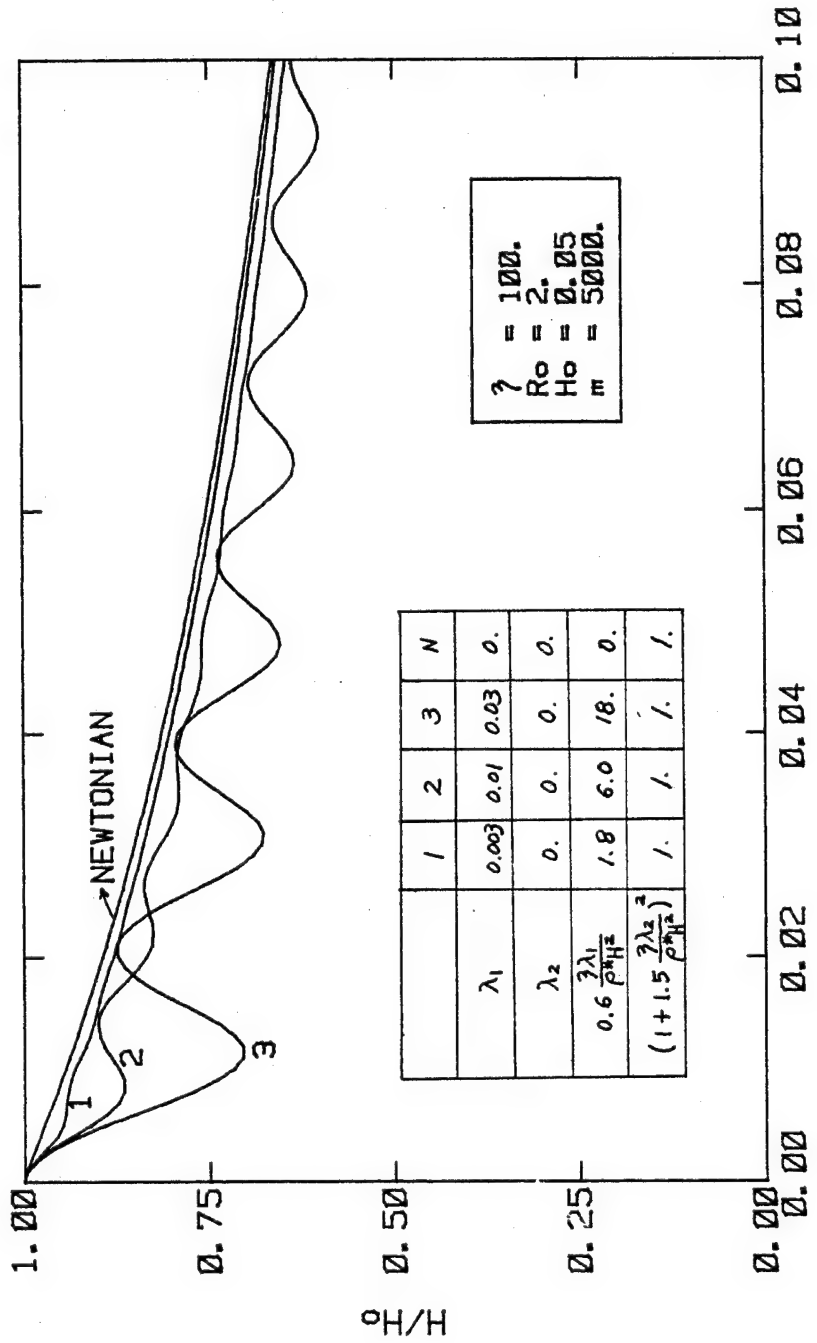

Fig. 4.2 H/H_o vs. time in the unlubricated compressive flow of linear viscoelastic materials : the effect of the relaxation time.

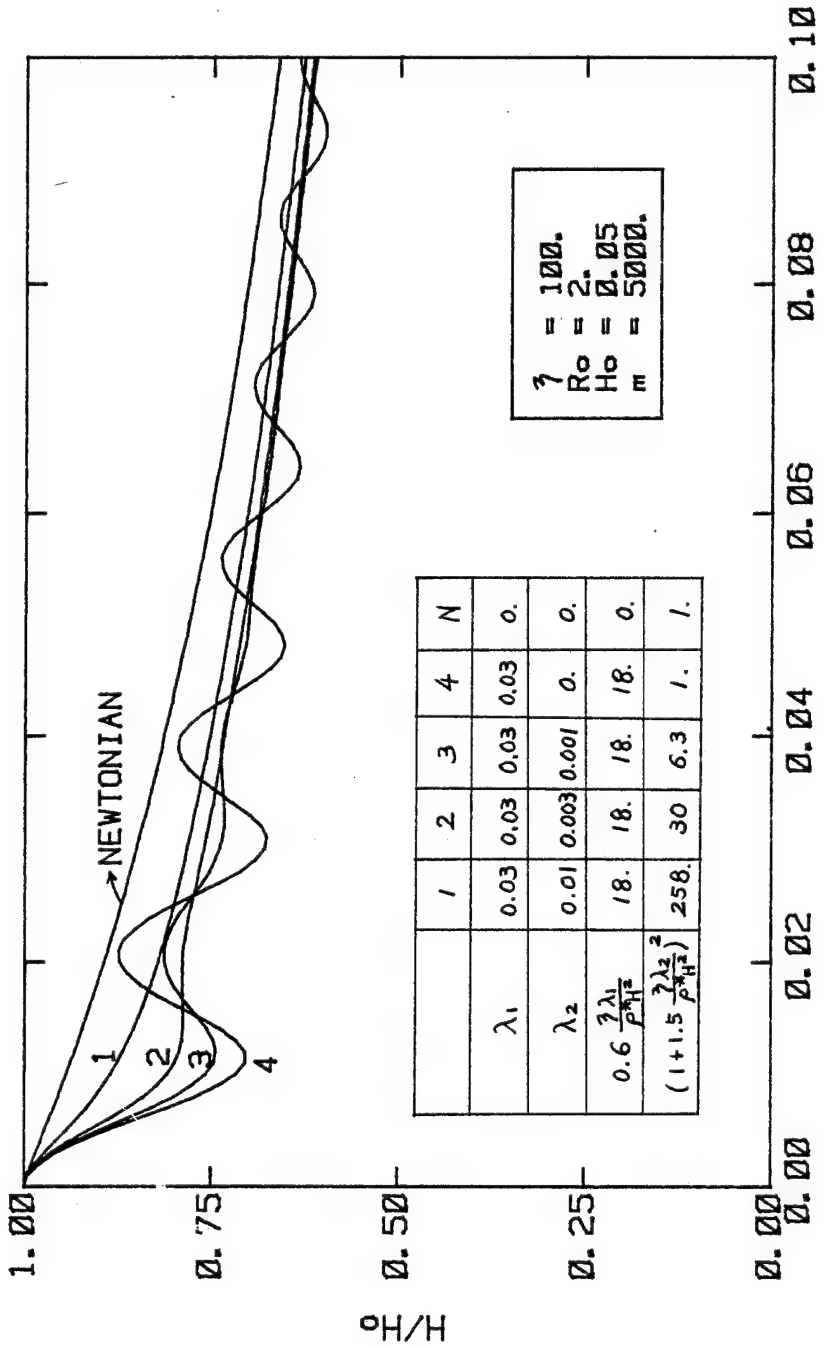

Fig. 4.3 H/H_o vs. time in the unlubricated compressive flow of linear viscoelastic materials : the effect of the retardation time.

$$\rho \frac{DV_r}{Dt} = -\frac{\partial p}{\partial r} + \frac{1}{r}\frac{\partial}{\partial r}(r\tau_{rr}) - \frac{\tau_{\theta\theta}}{r} + \frac{\partial \tau_{rz}}{\partial z} \tag{4.33}$$

$$\rho \frac{DV_z}{Dt} = -\frac{\partial p}{\partial z} + \frac{1}{r}\frac{\partial}{\partial r}(r\tau_{rz}) + \frac{\partial \tau_{zz}}{\partial z} \tag{4.34}$$

Constitutive:

$$\tau_{rr} + \lambda\left[\frac{D\tau_{rr}}{Dt} - 2\tau_{rr}\frac{\partial V_r}{\partial r} - 2\tau_{rz}\frac{\partial V_r}{\partial z}\right] = 2\eta\frac{\partial V_r}{\partial r} \tag{4.35}$$

$$\tau_{\theta\theta} + \lambda\left[\frac{D\tau_{\theta\theta}}{Dt} - 2\tau_{\theta\theta}\frac{V_r}{r}\right] = 2\eta\frac{V_r}{r} \tag{4.36}$$

$$\tau_{zz} + \lambda\left[\frac{D\tau_{zz}}{Dt} - 2\tau_{zz}\frac{\partial V_z}{\partial z} - 2\tau_{rz}\frac{\partial V_z}{\partial r}\right] = 2\eta\frac{\partial V_z}{\partial z} \tag{4.37}$$

$$\tau_{rz} + \lambda\left[\frac{D\tau_{rz}}{Dt} - \tau_{rr}\frac{\partial V_z}{\partial r} - \tau_{zz}\frac{\partial V_r}{\partial z} - \tau_{rz}\left(\frac{\partial V_r}{\partial r} + \frac{\partial V_z}{\partial z}\right)\right] = \eta\left(\frac{\partial V_r}{\partial z} + \frac{\partial V_z}{\partial r}\right) \tag{4.38}$$

in which $\frac{D}{Dt}$ is the material time derivative.

Boundary conditions:

$$\left.\begin{aligned} V_r &= 0 \quad \text{at } z = 0,\ 2H \\ V_z &= 0 \quad \text{at } z = 0 \\ V_z &= -V \quad \text{at } z = 2H \\ V_r &= 0 \quad \text{at } r = 0 \\ \frac{\partial V_z}{\partial r} &= 0 \quad \text{at } r = 0 \\ &\text{All the stresses vanish at} \\ &\qquad \text{the free surface.} \end{aligned}\right\} \tag{4.39}$$

Here we consider the region $(0,R)\times(0,2H)$ (the shaded portion in Fig. 4.1). Note that we do not have flow symmetry with respect to z=H (the center plane) because we wish to include the fluid inertia and the load inertia, while the top plate is moving down and the bottom plate is stationary.

In the linear viscoelastic case, it was possible to solve for the stress components explicitly, assuming that the velocity profiles are the same as for a Newtonian fluid. Then, substituting into the momentum equation, we were able to compute the closing rate. In the present problem we cannot obtain the stress components explicitly because of the nonlinearity of the constitutive equations. Therefore, we have to solve seven partial differential equations (4.32-4.38) simultaneously under the given condition (4.39). The finite element numerical technique, which has been tested in Section 3.4, will be applied to solve this problem.

4.2.2 Finite element simulation

In section 3.4, we were able to solve the lubricated compressive flow of a contravariant convected Maxwell fluid using a finite element numerical technique. We now wish to solve the unlubricated compressive flow problem using the same finite element routine but with different boundary

conditions. The no-slip boundary conditions along the solid wall (see (4.39)) are imposed in the present problem, while the slip boundary conditions were used in the lubricated case. Since the no-slip boundary conditions cause the stress singularity at the edge of the disk, we use small elements around the edge of the disk to relax the singularity within a small neighborhood of the edge.

The initial grid used in the calculation and the shapes of the boundaries at later times are shown in Fig. 4.4 and the calculated results are given in Fig. 4.5, in which H/H_0 is plotted against time. This is compared to the linear viscoelastic case. It is seen from this figure that the overall behavior of the Maxwell fluid is about the same as in the linear viscoelastic case, except that the Maxwell case shows a somewhat smaller amplitude of the oscillation, which may be due to the non-linear behavior of the Maxwell fluid. Both viscoelastic curves remain below the corresponding Newtonian curve.

The shear rate in this flow depends upon the position and the time. The maximum shear rate occurs at the edge of the disk and at the time when the closing speed reaches the highest value. In the calculation presented in Fig. 4.4 and 4.5, this maximum value of shear rate, $\dot{\gamma}_{max}$, is 210 sec^{-1} at time t=0.22. Since the relaxation time(λ) used in this calculation is 0.1 sec, $\dot{\gamma}_{max}\lambda$ turns out to be

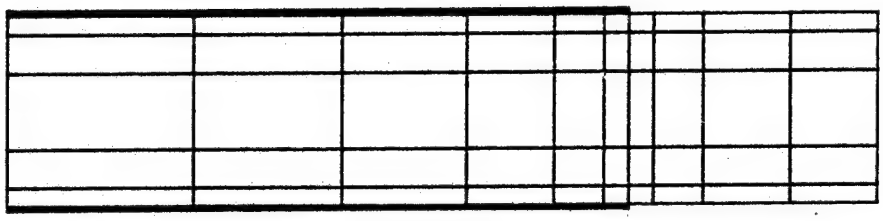

t = 0.
H/H_o = 1.

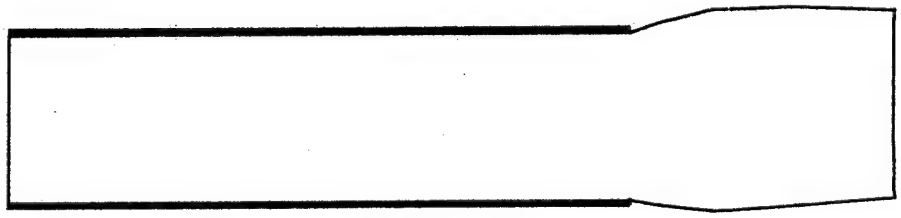

t = 0.018
H/H_o = 0.885

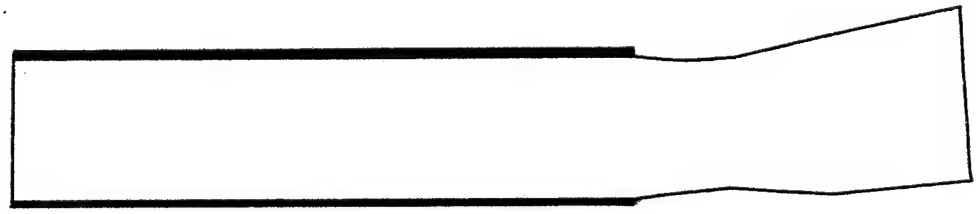

t = 0.038
H/H_o = 0.756

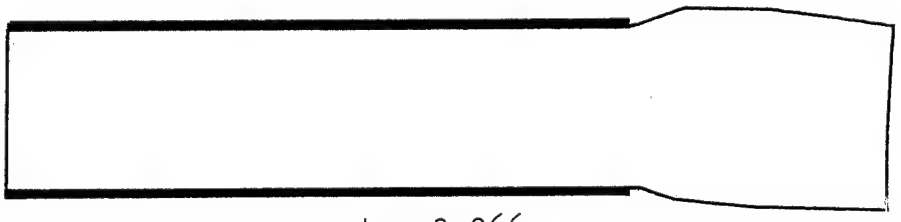

t = 0.066
H/H_o = 0.866

Fig. 4.4 The initial grid and the shapes of the boundaries at later times in the unlubricated compressive flow of a contravariant convected Maxwell fluid.

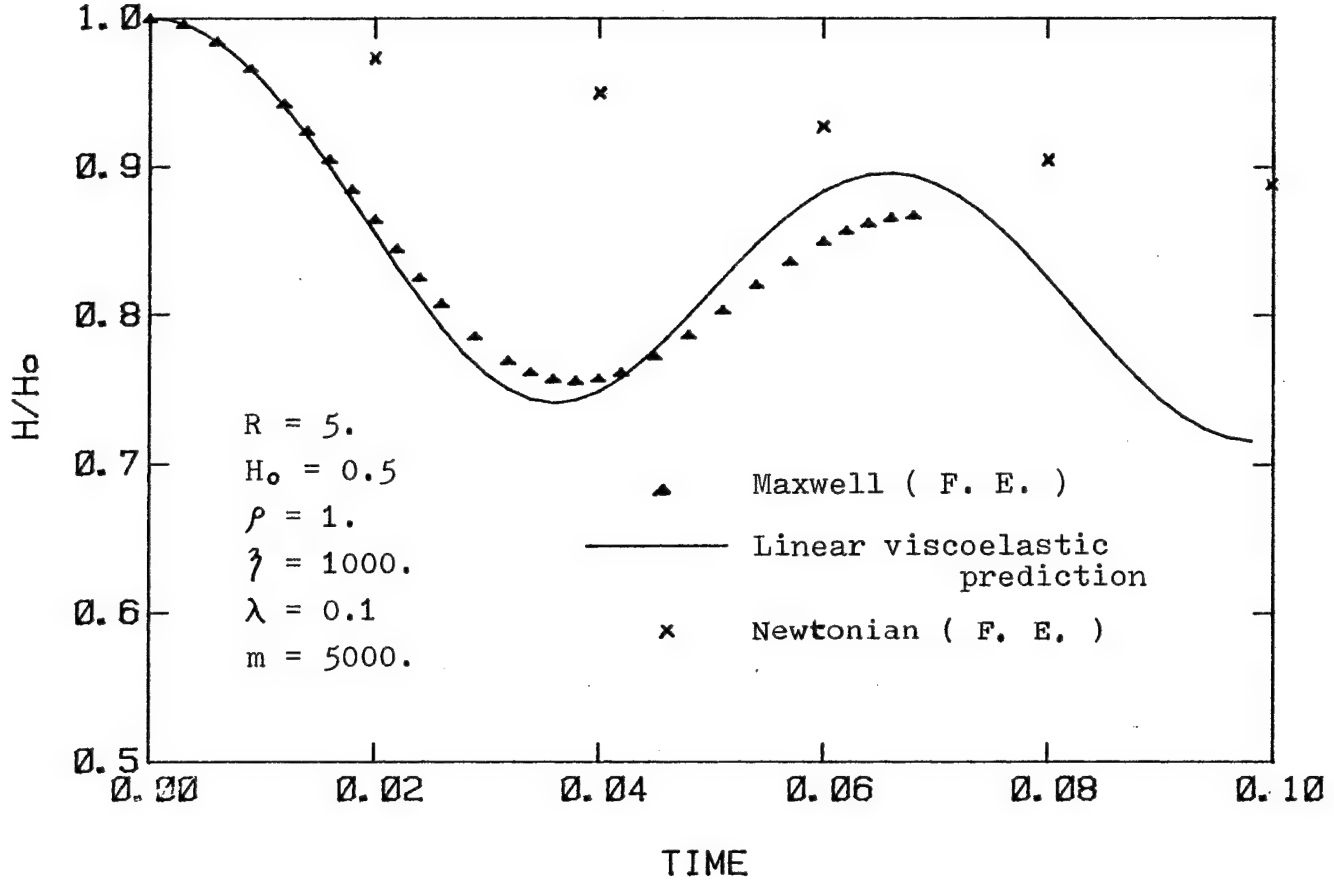

Fig. 4.5 H/H_o vs. time in the unlubricated squeezing of contravariant convected Maxwell fluid, compared to the linear viscoelastic case.

21. This high value of $\dot{\gamma}_{max}\lambda$, under which the solution converges, is not surprising if one considers that this flow is an oscillatory transient flow. The value of $\dot{\gamma}_{max}\lambda$ is zero at t=0, it increases as the squeezing goes on, and it reaches the maximum, then it decreases, etc. Higher values of $\dot{\gamma}_{max}\lambda$ were tried, but the solution didn't converge after several time step when $\dot{\gamma}_{max}\lambda$ reaches 36. In the steady state calculation of Maxwell fluid, the highest value of $\dot{\gamma}\lambda$, under which the solution converges, has been known as around 1 to 2 depending upon the type of the flow (see Crochet and Keunings, 1982; Mendelson et. al., 1982; Viriyayuthakorn and Caswell,1980). It is desirable to do the computation with higher $\dot{\gamma}_{max}\lambda$ in the future, when the convergence problem at high $\dot{\gamma}\lambda$, which is one of the major problem in the numerical calculation of viscoelastic materials, is resolved.

At this point, one can conclude that approximating the overall behavior (H/H_o vs. time) of the Maxwell fluid by the linear viscoelastic prediction is favorable at the values of $\dot{\gamma}_{max}\lambda$ at least up to 21, since the finite element calculation of Maxwell fluid is several orders of magnitude more expensive than the linear viscoelastic case.

CHAPTER 5

EXPERIMENTS

Experiments on the unlubricated compressive flow of Newtonian and viscoelastic materials under a constant load have been carried out to obtain the film thickness as a function of time. The apparatus and the materials used are described in Sections 5.1 and 5.2, respectively. The experimental results are shown and compared to the theoretical predictions in Section 5.3.

Experiments on the lubricated compressive flow were attempted; these were unsuccessful, since the lubricant along the wall surface was expelled quickly during the early moments of squeezing, after which the central test material began to stick to the wall. To perform this type of experiment successfully, the viscosity ratio of the lubricant and the test material must be chosen very carefully (see Section 3.5), or a sophisticated device which can supply the lubricant to maintain almost constant thickness of the lubricant layer through the squeezings needs to be designed.

5.1 Apparatus

The apparatus used in the experiments is shown in the picture (Fig. 5.1). There are three parts: the squeezing equipment (A), the thickness measuring device (B), and the recording equipment (C).

5.1.1 Squeezing equipment (see Fig. 5.2)

The squeezing equipment is composed of a rigid stationary part and a moving part. The central cylindrical rod (A1), at the bottom of which a flat circular disk (A2) is attached, moves through two linear ball bushings (A3,A4) which provide the straight movement of the moving rod. The test material is placed between the bottom plate (A5) and the circular disk. At the instant t=0, the load (all the moving parts) on the material is released. The upper plate falls down under the influence of the gravitational acceleration, with the test material being squeezed out.

5.1.2 Thickness measuring device (LVDT, see Fig. 5.3)

Continuous measurement of the film thickness during squeezing is accomplished with the LVDT (linear variable differential transducer), which is manufactured by Schaevitz Eng. Co. The specifications of the LVDT used are given in Table 5.1. The LVDT is composed of two parts, the body (B1) and the core (B2). The body is fixed on the stationary part of the squeezing equipment and the core is attached to the

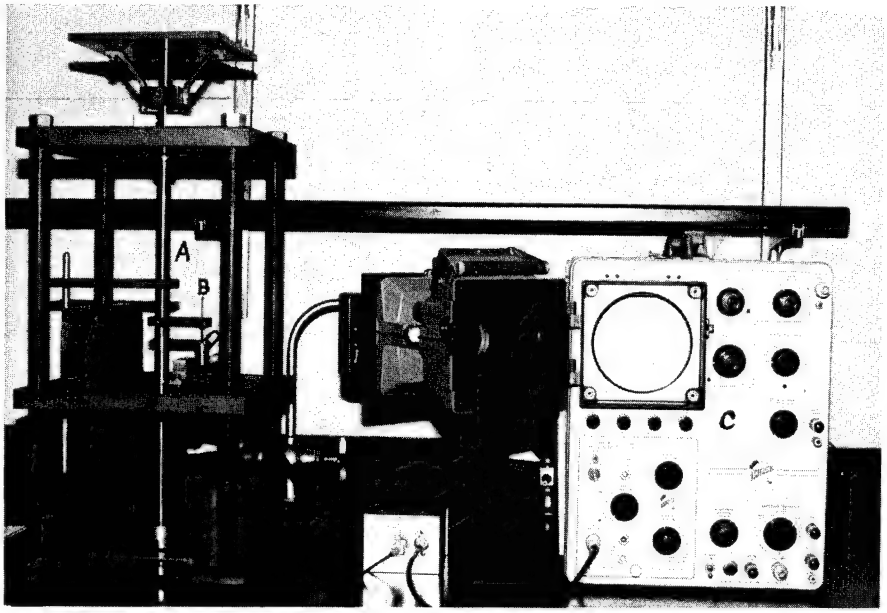

Fig. 5.1 The apparatus used in the squeezing experiments: (A)squeezing equipment, (B)thickness measuring device, (C)recording equipment.

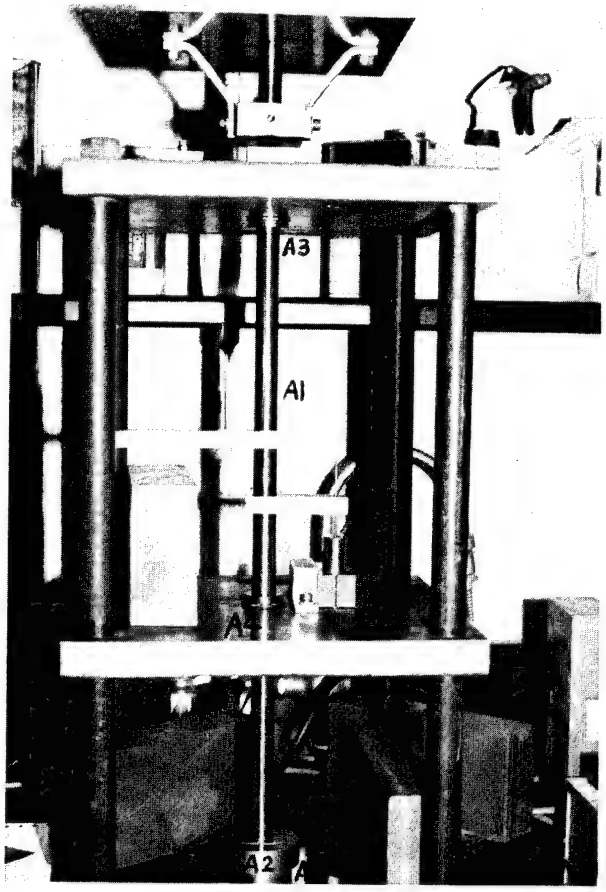

Fig. 5.2 The squeezing equipment: (A1)cylindrical moving rod, (A2)circular disk, (A3,A4)linear ball bushings, (A5)bottom plate.

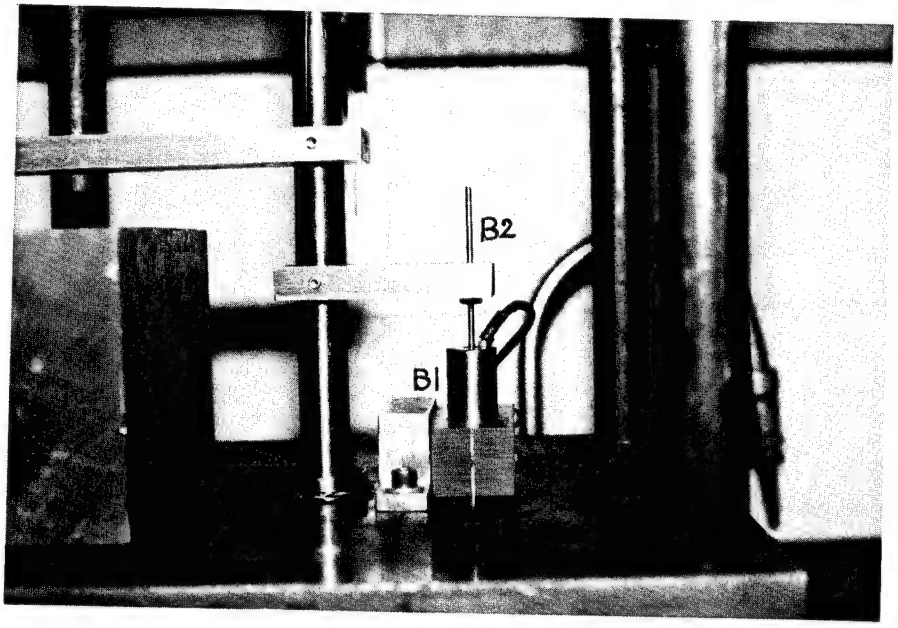

Fig. 5.3 The thickness measuring device (LVDT): (B1)body, (B2)core.

Manufacturer : Schaevitz Engineering Co.

Model no. : 200 DC-D

Calibration data by manufacturer

Linear range : ±0.200 in.
Sensitivity : 51.500 V/in.
Linearity : <0.25% of full range
AC ripple : <10 mV (max.)

Dimensions

Body : 0.75 in. d * 3.80 in. l
Core : 0.187 in. d * 1.80 in. l

Weight

Body : 73 g
Core : 5 g

Operated by ±15 V DC

Table 5.1 The specifications of LVDT used

moving cylindrical rod, so that the core moves with the rod.

5.1.3 Recording equipment

The continuous measurement from the LVDT is sent to the oscilloscope (Textronix 531A) and appears as a moving spot on the screen. The picture of the trace of the moving spot is taken with the Tektronix C-13 camera and a Polaroid Land pack film camera back.

5.2 Materials

Two Newtonian fluids have been used as the standards to test the apparatus. Three different viscoelastic materials have been used in the experiments to investigate viscoelastic effects in the compressive flow.

5.2.1 Newtonian materials

Viscasil 60000 : This is a viscous silicone fluid manufactured by General Electric Co., whose viscosity is constant and known as 60000 cs (at 25°C) and density is 0.97 g/cm^3.

Dow Corning 200 fluid, 12500 : manufactured by Dow Corning Co. Its viscosity is 12500 cs (at 25°C) and density is 0.975 g/cm^3.

5.2.2 Viscoelastic materials

Silicone Polymer : This is a three phase material (silicone resin, plasticizer, and filler) manufactured by ICI, England. This material is known to have rheological properties close to those of linear Maxwell fluid, based upon the oscillatory shear measurements (see also Fig. 19-2 of Denn(1980)).

The oscillatory shear data have been obtained through the courtesy of Dr. K. F. Wissbrun of the Celanese Research Corporation. Appendix F.1 contains a tabulation of the storage modulus(G'), the loss modulus(G") and the absolute value of the complex viscosity(η^*) as a function of the circular frequency(ω) at three different temperatures. By taking 23°C as a reference temperature, $|\eta^*|\omega$ could be superposed on to one mastercurve with the help of the horizontal shift factors(a_T) (see Gupta(1980)), which is shown in Fig. 5.4. And furthermore we know from the linear viscoelastic theory that

$$|\eta^*|\omega = \frac{\eta\omega}{(1+\omega^2\lambda^2)^{1/2}} \qquad (5.1)$$

or

$$\eta\omega = |\eta^*|\omega\,(1+\omega^2\lambda^2)^{1/2} \qquad (5.2)$$

Using (5.2), $\eta\omega$ vs. ωa_T is plotted in Fig. 5.5, from which one can see that the viscosity is nearly constant in the given range of the circular frequency. We will use this constant viscosity to analyze the squeeze film data later.

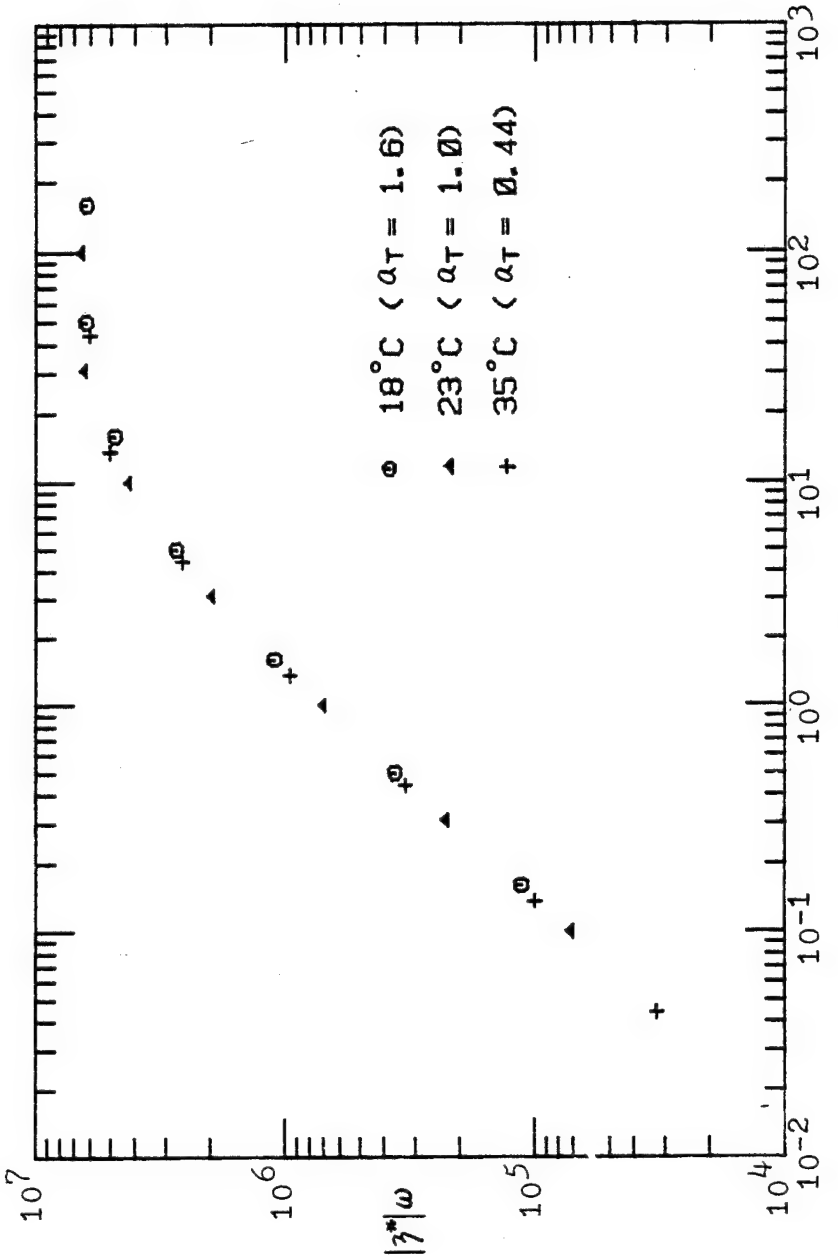

Fig. 5.4 $|\eta^*|\omega$ vs. ωa_T of silicone polymer (from oscillatory shear measurements).

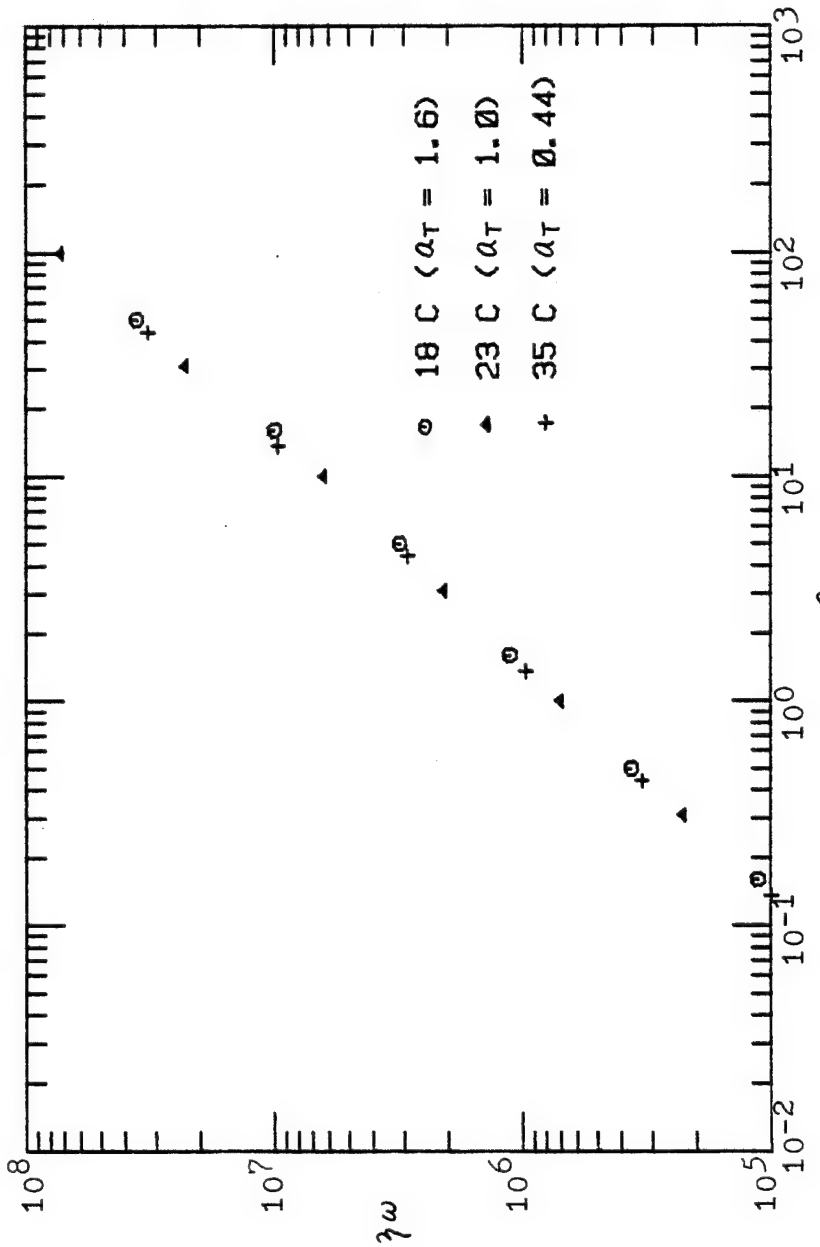

Fig. 5.5 $\eta'\omega$ vs. ωa_T of silicone polymer (from oscillatory shear measurements).

TLA-227 : A concentrate of a methacrylate copolymer in petroleum oil, manufactured by Texaco, Inc. The steady shear measurements at low shear rate range were made on the Rheometrics Mechanical Spectrometer (of Celanese) and the capillary measurements were made at high shear rates. The shear stress and the normal stress data are tabulated as a function of the shear rate in Appendix F.2. The end correction (see Bagley, 1957) in the capillary measurement was unnecessary since the capillary tubes used were long enough (L/R=160, 268). The results are shown in Fig. 5.6 at various temperatures. At 27°C, the spectrometer data and the capillary data agree well, which illustrates the correctness of both data. The material shows slightly shear thinning behavior(n=0.86) at high shear rates.

PAA-water solution : 3.3 wt. % Separan AP-30 (a partially hydrolyzed polyacrylamide manufactured by Dow Chemical Company) in water solution was made and characterized with a Weissenberg Rheogoniometer. The shear stress and the first normal stress data are given in Appendix F.3 and shown in Fig. 5.7. This material is highly shear thinning(n=0.267) and highly elastic.

5.3 Experimental results and discussion

Experimental results on Newtonian fluids are tabulated in Appendix G.1 and shown in Fig. 5.8, in which

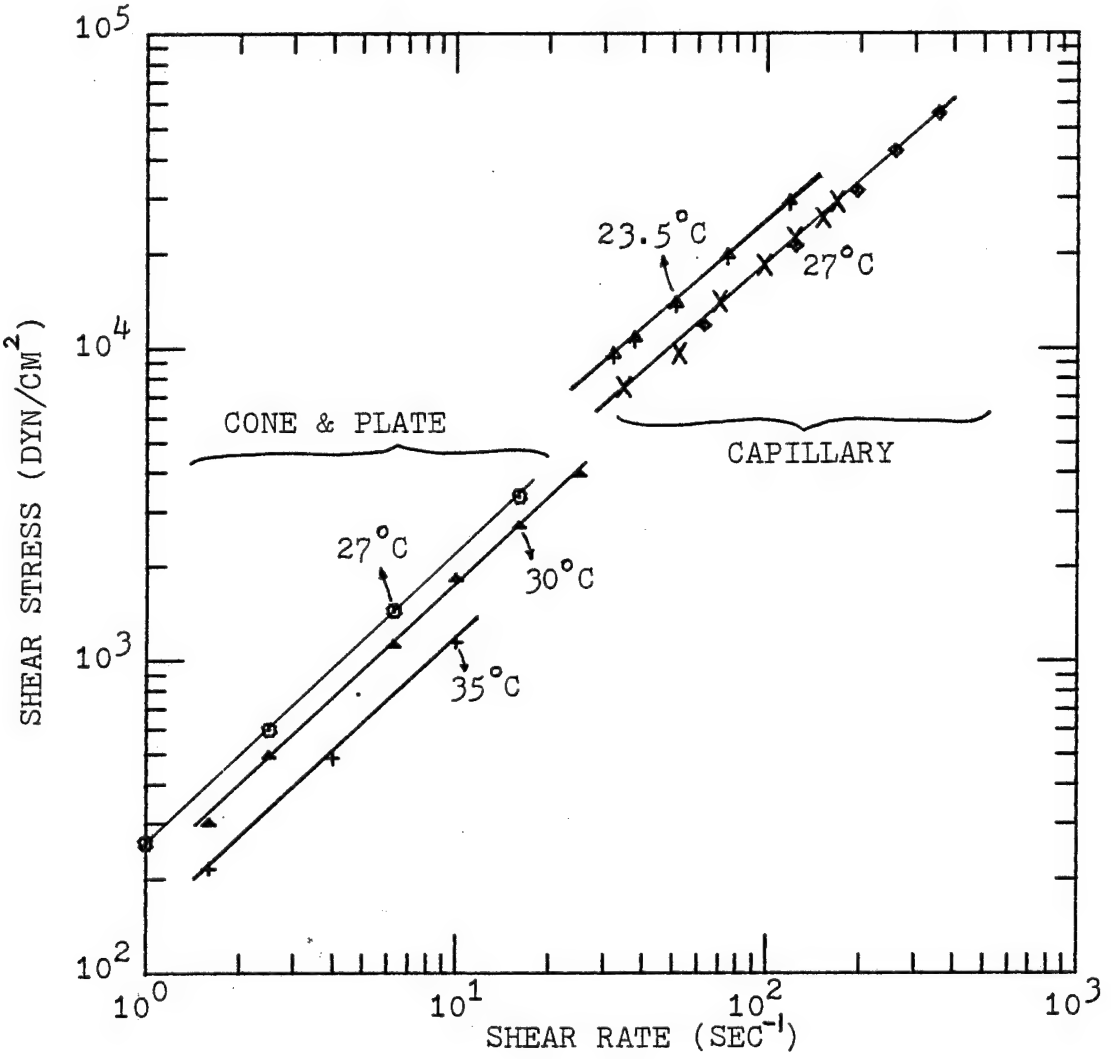

Fig. 5.6 Shear stress vs. shear rate of TLA-227.

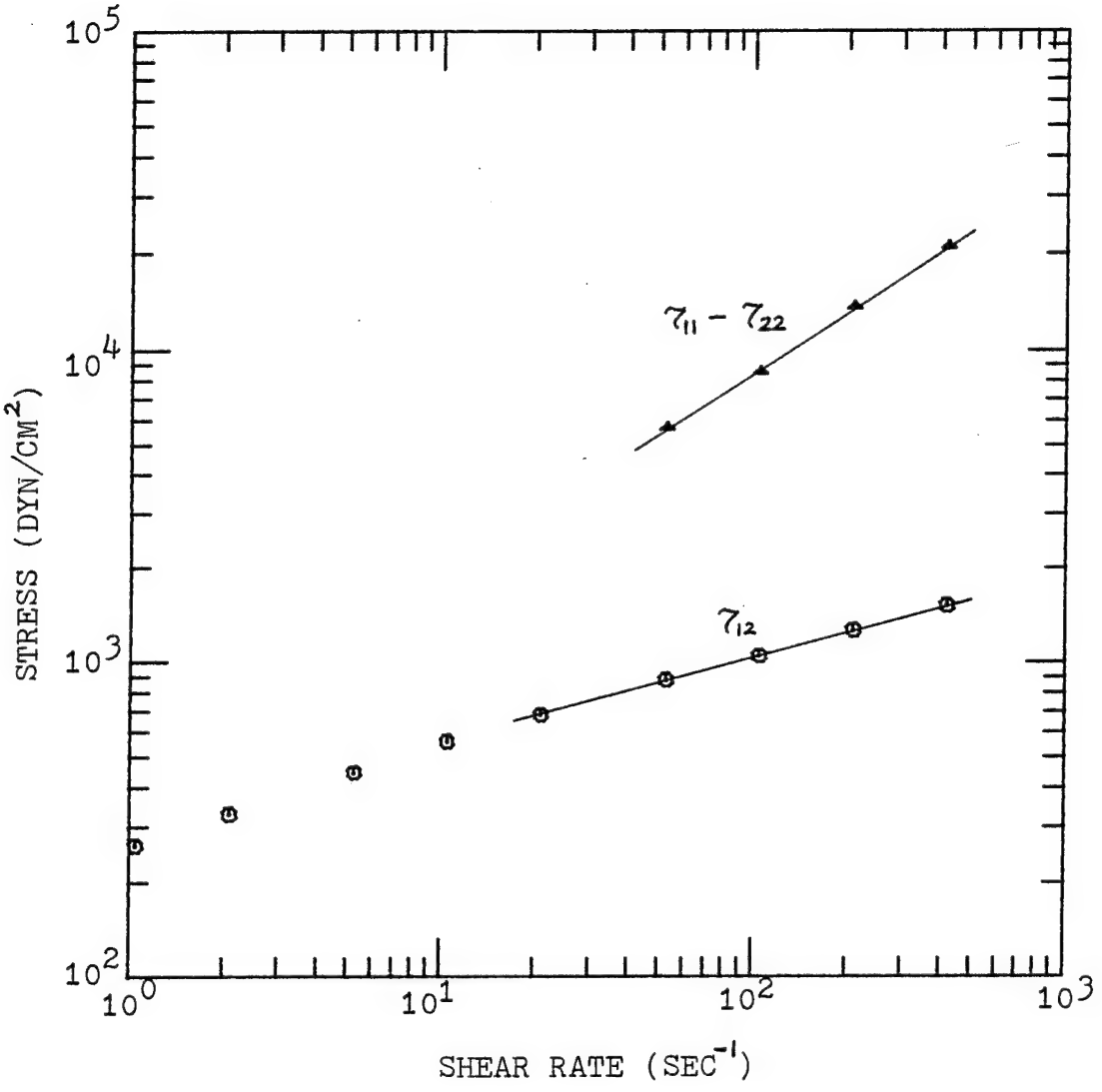

Fig. 5.7 The shear stress and the first normal stress difference of 3.3 wt. % PAA in water solution.

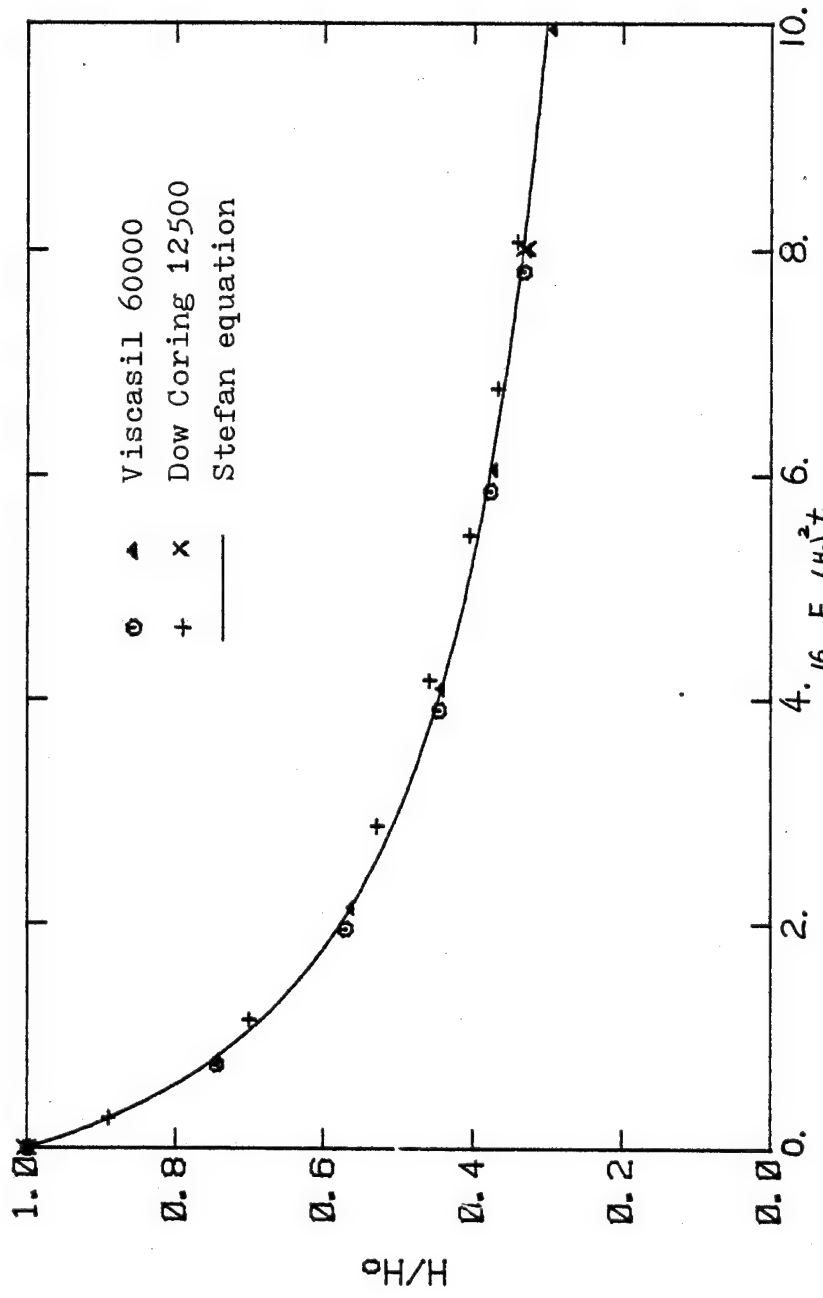

Fig.5.8 Dimensionless spacing(H/H_o) vs. dimensionless time($\frac{16}{3}\frac{F}{\pi R^2}\left(\frac{H_o}{R}\right)^2\frac{t}{\eta}$) in the unlubricated squeezing of Newtonian fluids, compared to Stefan equation.

H/H_o is plotted against dimensionless time, $\bar{t}$ $(=\frac{16}{3}\frac{F}{\pi R^2}\left(\frac{H_o}{R}\right)^2\frac{t}{\eta})$. They agree well with the Stefan equation, which illustrates the quality of the apparatus and technique used.

Experimental results on viscoelastic materials are given in Appendix G.2 and shown in Figs. 5.9-5.13. The corresponding inelastic curves (analytical or numerical) are also shown in each figure for comparison purposes. The values of $\dot{\gamma}_{max}\lambda$ for each run are also given in Appendix G.2.

Figs. 5.9 and 5.10 show the squeezing of Silicone polymer. It is seen from Fig. 5.9 that the material seems to be squeezed instantaneously at t=0. The details of this initial movement have been obtained by expanding the time axis and are shown in Fig. 5.10, in which the linear viscoelastic prediction is also shown for comparison purposes. Since $\dot{\gamma}_{max}\lambda$ in this experiment is 9, we expect that the Maxwell prediction would be close to the linear viscoelastic one based upon the conclusion drawn in Section 4.2.2. It shows that the initial movement is not the instantaneous squeezing, but the oscillatory squeezing, and that the linear viscoelastic theory predicts the correct oscillation period, but a larger oscillation amplitude than the experimental result. Both experimental results on silicone polymers stay below the corresponding Newtonian curve and it is likely that this material is close to a Maxwell type of fluid, as expected from the oscillatory

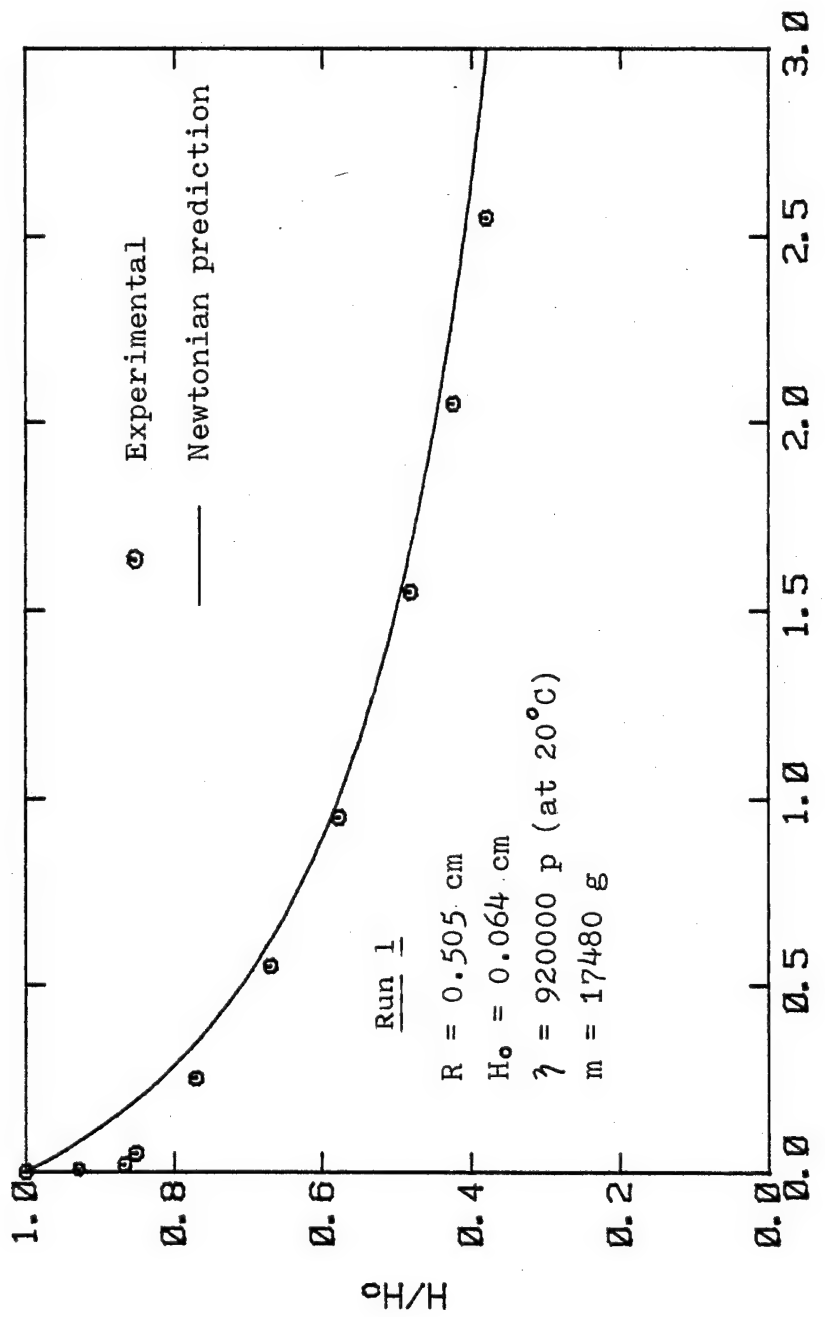

Fig. 5.9 H/H_o vs. time in the unlubricated squeezing of silicone polymer, compared to the corresponding Newtonian fluid.

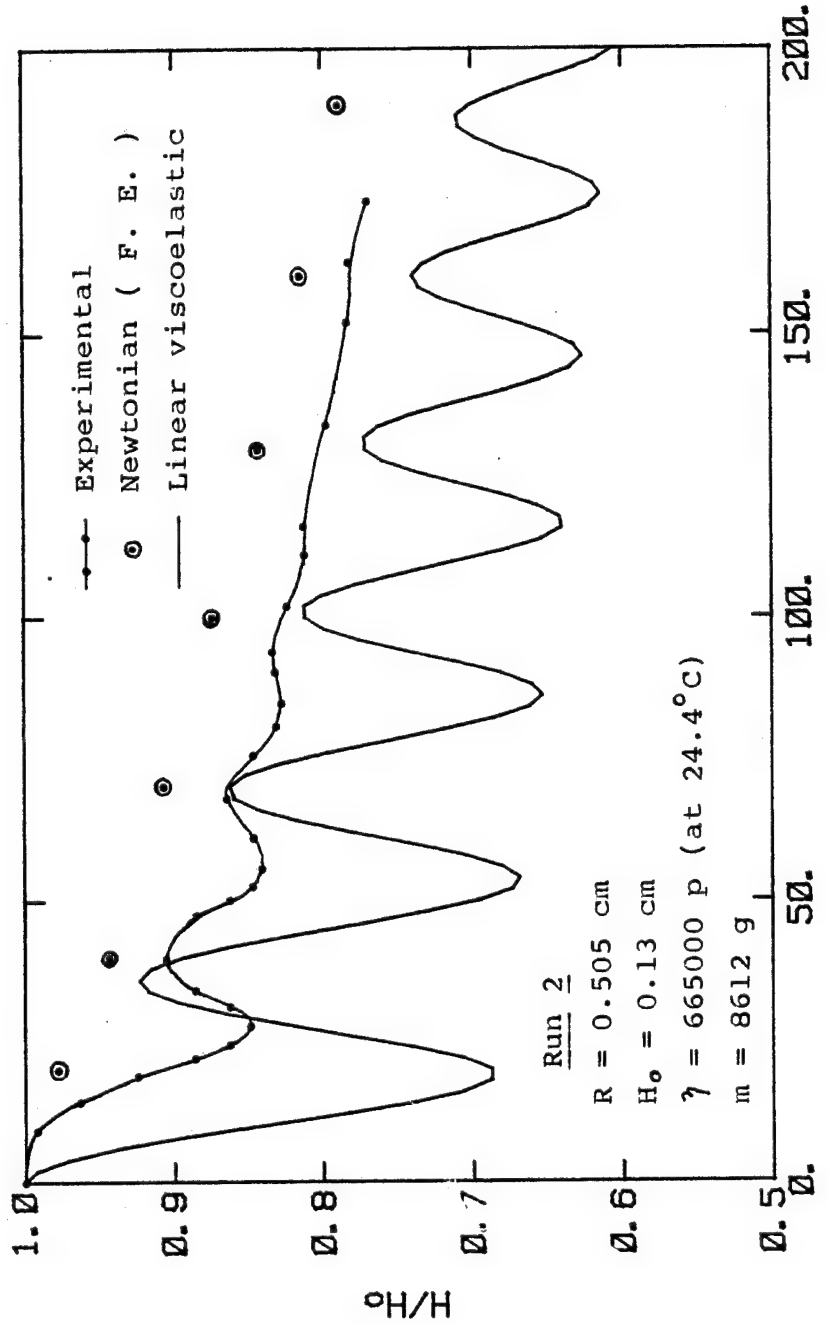

Fig. 5.10 H/H_o vs. time in the unlubricated squeezing of silicone polymer, compared to the corresponding Newtonian and linear viscoelastic cases : short time response.

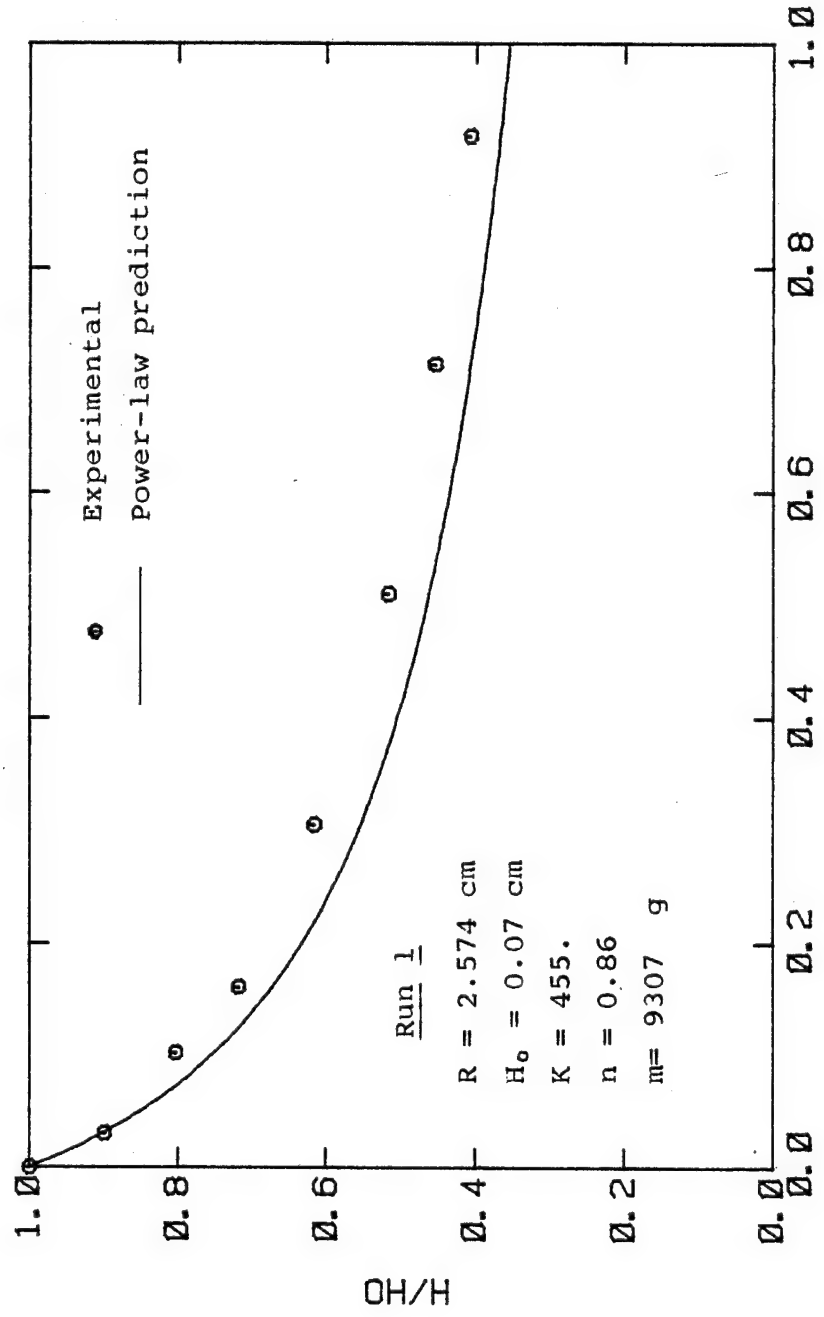

Fig. 5.11 H/H_o vs. time in the unlubricated squeezing of TLA-227, compared to the corresponding power-law case.

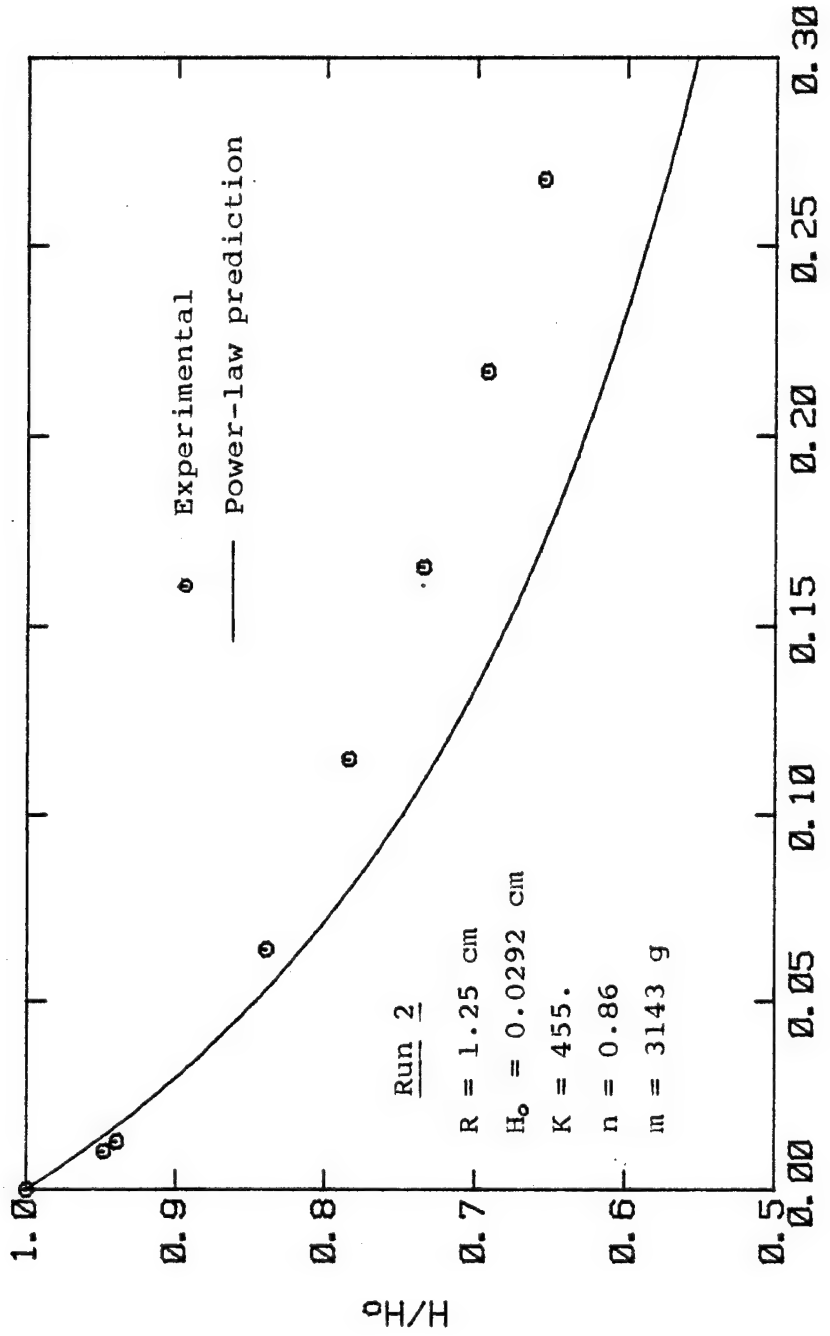

Fig. 5.12 H/H_o vs. time in the unlubricated squeezing of TLA-227, compared to the corresponding power-law case.

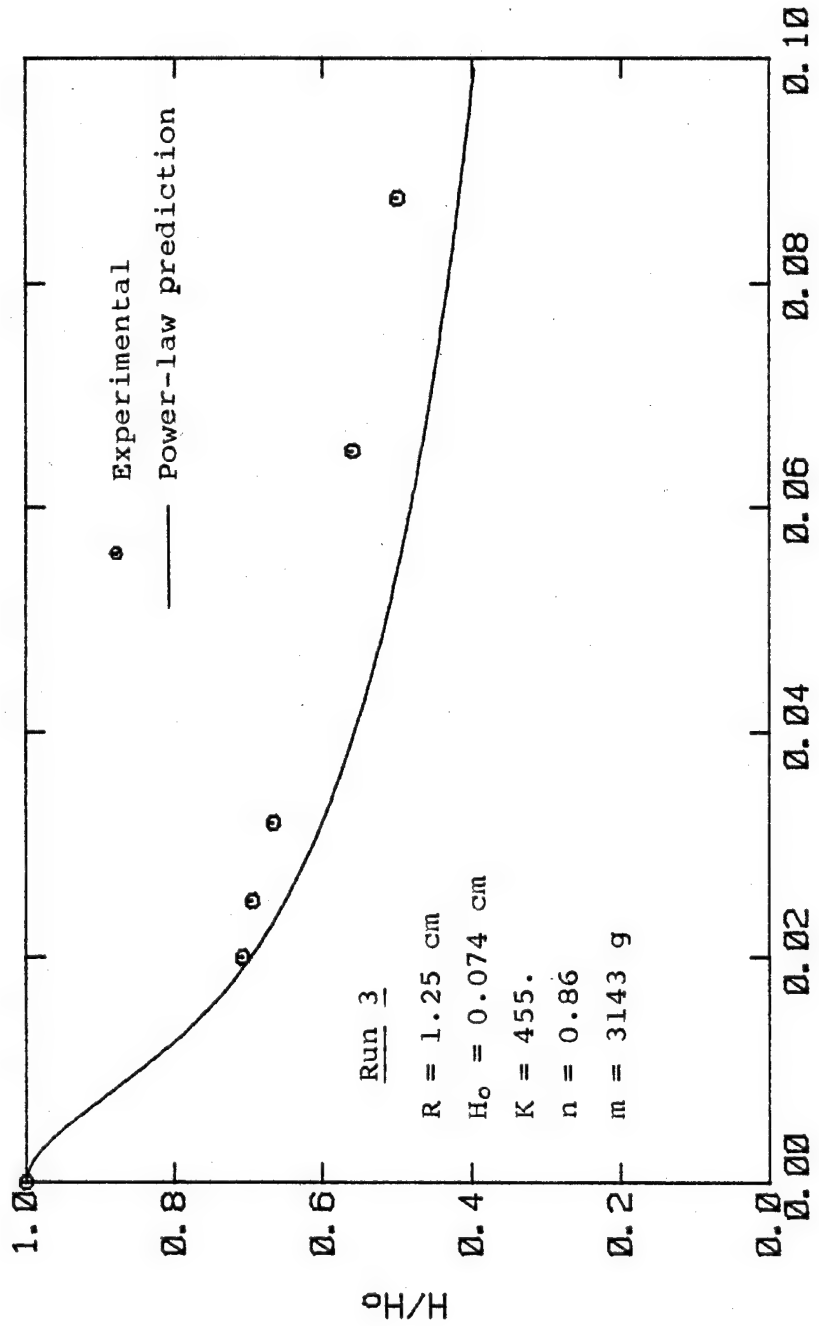

Fig. 5.13 H/H_o vs. time in the unlubricated squeezing of TLA-227, compared to the corresponding power-law case.

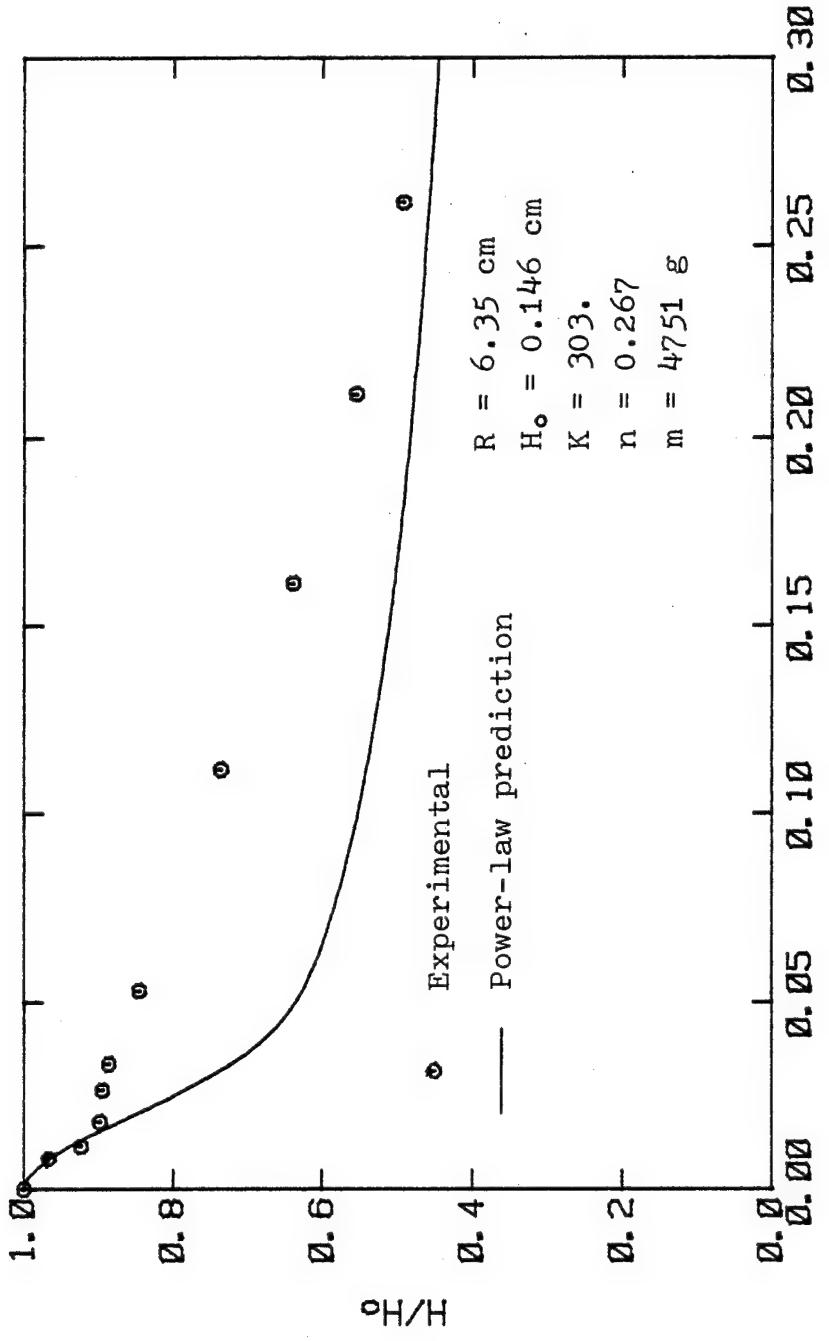

Fig. 5.14 H/H_o vs. time in the unlubricated squeezing of PAA in water solution, compared to the corresponding power-law case.

shear data.

The squeezing curves of TLA-227 are shown in Figs. 5.11 through 5.13. One can see that the experimental curves stay above the corresponding inelastic curves. Fig. 5.14 shows the result for the PAA-water solution, which has the similar characteristic as TLA-227. Most data on these two solutions show an inflection point which probably reflects a very weak oscillation. In Section 4.2.2 we have seen that the Maxwell model predicts the faster squeezing at $\dot{\gamma}_{max}\lambda$ (=21) which is higher than those(=2 ~ 10) in these experiments. Thus, it is not likely, at least in this type of transient flow, that these two polymer solutions are close to Maxwell, or in general White-Metzner, type of fluids.

It is desirable to try more realistic and thus complex models, which can describe the transient behavior more precisely, in finite element calculations in the future. The Phan-Thien-Tanner, Johnson-Segalman, and Marrucci structural models would all be candidates for this purpose.

CHAPTER 6

SUMMARY AND RECOMMENDATIONS

6.1 Summary of present work

1. The unlubricated compressive flows of Newtonian fluids and power-law fluids have been simulated by a finite element technique, verifying that the Stefan equation (Newtonian) and the Scott equation (power-law) based upon an assumption of parallel squeezing are good provided the R/H ratio is large enough. When R/H is small, the edge effect causes slower squeezing than predicted from the Stefan equation or the Scott equation.

2. When there exists a substantial transverse viscosity gradient in the fluid charge, two different flow regimes are predicted depending upon whether the dimensionless group, S ($= \frac{\eta_{max} H^2}{\eta_{min} R^2}$) is small or large compared to unity. When S is small compared to unity, the parallel squeezing assumption is valid and the maximum velocity occurs at the center plane. When S is large compared to unity, the parallel squeezing assumption breaks down and the maximum velocity occurs in the low viscosity fluid near the disks. Thus, a new analysis is necessary in this case. In

the two fluids case, new assumptions other than the parallel squeezing assumption have been made to derive an analytical solution which is found to be in good agreement with the finite element numerical solution.

3. The partially-filled compressive flow of Newtonian fluid has been solved numerically. The flow patterns in the partially-filled compressive flow, or the flow in the mold cavity, are essentially the same as those one observes in the fully-filled case except near the front : here we observe the expected fountain flow phenomenon in the partially-filled case.

4. The lubricated compressive flow of linear viscoelastic material has been solved analytically and numerically. The compressive motion under a constant amount of load may or may not be oscillatory, depending upon the conditions as predicted by equations (3.49-52). When oscillation occurs, it is due to the combined effects of inertia, the elasticity, and the viscosity. The oscillation period is given by $\pi R\sqrt{\frac{\rho^*\lambda}{6\eta}}$. The retardation time plays an important role in the damping of the oscillatory motion.

5. The lubricated compressive flows of non-linear viscoelastic model fluids, including the contravariant convected Maxwell model, White-Metzner model, Johnson-Segalman model (with and without retardation time),

and Marrucci structural model, have been solved numerically. The contravariant convected Maxwell model and White-Metzner model predict faster oscillatory squeezing than the corresponding inelastic cases, except at very small H/H_0 under the extraordinarily high loading conditions. The Johnson-Segalman model and the Marrucci structural model predict slower oscillatory squeezing than the corresponding inelastic cases at high squeezing speed. These different responses seem to be due to the stress overshoot phenomena, since Johnson-Segalman model and Marrucci structural model do predict stress overshoot, but the contravariant convected Maxwell model and White-Metzner model do not.

6. The unlubricated compressive flow of linear viscoelastic materials has been solved analytically, assuming that the velocity field is the same as the Newtonian one. The behavior is very similar to the lubricated case except that the principal length scale is different from the lubricated case. When oscillation occurs, the oscillation period is given by $4\pi H\sqrt{\frac{\rho^*\lambda}{6\eta}}$.

7. The unlubricated compressive flow of the contravariant convected Maxwell model has been solved numerically, using a finite element technique. The results are about the same as in the linear viscoelastic case except that the oscillation amplitude of the Maxwell fluid is somewhat smaller than for the linear viscoelastic material.

8. Squeezing experiments on the viscoelastic materials have shown two different behaviors; silicone polymer, which can be well characterized by the linear Maxwell model, shows faster oscillatory squeezing than the corresponding Newtonian cases, while TLA-227 and PAA-water solution show weak bounces and slower squeezing than the corresponding inelastic cases. The behavior of silicone polymer is predictable from the Maxwell model, but the responses of TLA-227 and PAA-water solution are different from those predicted by the Maxwell model. To explain the latter behavior, we might need a constitutive equation which can predict the transient responses, such as the stress overshoot, more precisely.

9. In conclusion, the slower squeezing of viscoelastic materials, or higher load-bearing capacity of viscoelastic lubricants, seems to be not due to the elasticity of the material, but due to the transient responses of the material. In other words, the dimensionless group $\dot{\gamma}_{max}\lambda$ alone may not be the proper dimensionless group to describe the whole features of the squeezing of viscoelastic materials. We require the ratio of Deborah number to Reynolds number to describe the oscillatory behavior and also require at least one more dimensionless group which can describe the transient responses of the materials such as stress overshoot phenomenon.

6.2 Recommendations for future work

1. The use of the Phan-Thien-Tanner model, Johnson-Segalman model, or Marrucci structural model is recommended for the further study of the compressive flow problems.

2. In all transient problems it may be important to use constitutive equations which describe the transient fluid behavior precisely.

3. The development of a constitutive equation, which can describe the transient responses more precisely, is desirable.

BIBLIOGRAPHY

BIBLIOGRAPHY

Acierno, D., La Mantia, F. P., Marrucci, G., and Titomanlio, G., J. Non-Newtonian Fluid Mech., 1, 125 (1976a).

Acierno, D., La Mantia, F. P., Marrucci, G., Rizzo, G., and Titomanlio, G., ibid., 1, 147 (1976b).

Acierno, D., La Mantia, F. P., Marrucci, G., ibid, 2, 271 (1976c).

Astarita, G., and Marrucci, G., Principles of Non-Newtonian Fluid Mechanics, McGraw-Hill (1974).

Bagley, E. B., J. Appl. Phys., 28, 624 (1957).

Binding, D. M., Davies, J. M., and Walters, K., J. Non-Newtonian Fluid Mech., 1, 259 (1976a).

Binding, D. M., and Walters, K., ibid, 1, 277 (1976b).

Boger, D. V., Tran. Soc. Rheol., 21, 515 (1977).

Brindley, G., Davies, J. M., and Walters, K., J. Non-Newtonian Fluid Mech., 1, 19 (1976).

Chang, P., Patten, T. W., and Finlayson, B. A., Computers and Fluids, 7, 267 (1979a).

Chang, P., Patten, T. W., and Finlayson, B. A., ibid, 7, 285 (1979b).

Chatraei, SH., Macosko, C. W., and Winter, H. H., J. Rheol., 25, 433 (1981).

Cohen, Y., Ph.D. Dissertation, University of Delaware, Newark, Delaware (1981).

Cox, W. P., and Merz, E. H., J. Polym. Sci., 28, 619 (1958).

Crochet, M. J., Finite Elements for Solving Non-Newtonian Flow, Notes prepared for the lecture series on "Non-Newtonian Flows" at the Von Karman Institute (1981).

Crochet, M. J., and Bezy, M., J. Non-Newtonian Fluid Mech.,

5, 201 (1979).

Crochet, M. J., and Keunings, R., J. Non-Newtonian Fluid Mech., 7, 199 (1980).

Crochet, M. J., and Keunings, R., ibid, 10, 85 (1982).

Denn, M. M., Process Fluid Mechanics, 255, Prentice-Hall (1980).

Denn, M. M., and Porteous, K. C., Chem. Eng. J., 2, 280 (1971).

Denn, M. M., Tadmor, Z., and Edelist, I., unpublished research, summarized in the Appendix A (1981).

Denton, D. L., 36th Annual Conference, Soc. Plastics Industry, Sec. 16-A (1981).

Elkouh, A. F., J. Lub. Tech., 98,409 (1976).

Fromm, H., Z. Angew. Math. Mech., 25, 146 (1947).

Gear, C. W., Numerical Initial Value Problems in Ordinary Differential Equations, Prentice-Hall, Englewood Cliffs, New Jersey (1971).

Grimm, R. J., Ph. D. Dissertation, University of Wisconsin-Madison, Madison, Wisconsin (1977).

Grimm, R. J., A.I.Ch.E. Journal, 24, 427 (1978).

Gupta, R. K., Ph.D. Dissertation, University of Delaware, Newark, Delaware (1980).

Irons, B. M., Intern. J. Numer. Meth. Eng., 2, 5 (1970).

Johnson, M. W., and Segalman, D., J. Non-Newtonian Fluid Mech., 2, 255 (1977).

Kawahara, M., and Takeuchi, N., Computers and Fluids, 5, 33 (1977).

Kramer, J. M., Appl. Sci. Res., 30, 1 (1974).

Kuzma, D. C., Appl. Sci. Res., 18, 15 (1967).

Lee, S. J., Denn, M. M., Crochet, M. J., and Metzner, A. B., J. Non-Newtonian Fluid Mech., 10, 3 (1982).

Leider, P. J., Ind. Eng. Chem. Fundam., 13, 342 (1974).

Leider, P. J., and Bird, R. B., Ind. Eng. Chem. Fundam., 13, 336 (1974).

Lodge, A. S., Elastic Liquids, Academic Press., New York (1964).

Marker, L., and Ford, B., 32nd Annual Conference, Soc. Plastics Industry, Sec. 16-A (1981).

Maxwell, J. C., Phil. Trans. R. Soc. London, 157, 49 (1867).

Mendelson, M. A., Yeh, P.-W., Brown, R. A., and Armstrong, R. C., J. Non-Newtonian Fluid Mech., 10, 31 (1982).

Metzner, A. B., J. Lub. Tech., 90, 531 (1968a).

Metzner, A. B., Trans. Soc. Rheol., 12, 57 (1968b).

Metzner, A. B., Rheol. Acta, 10, 434 (1971).

Nickell, R. E., Tanner, R. J., and Caswell, B., J. Fluid Mech., 65, 189 (1974).

Oldroyd, J. G., Proc. Roy. Soc. London, A200, 523 (1950).

Oldloyd, J. G., ibid, A245, 578 (1958).

Parlato, P., M.Ch.E. Thesis, University of Delaware, Newark, Delaware (1969).

Phan-Thien, N., J. Rheol., 22, 259 (1978).

Phan-Thien, N., and Tanner, R. J., J. Non-Newtonian Fluid Mech., 2, 353 (1977).

Riggins, G., B.Ch.E. Thesis, University of Delaware, Newark, Delaware (1982).

Rose, W., Nature, 191, 242 (1961).

Scott, J. R., Trans. Inst. Rubber Ind., 7, 169 (1931).

Segalman, D., Ph.D. dissertation, University of Wisconsin-Madison, Madison, Wisconsin (1978).

Shirodkar, P. P., Ph.D. dissertation, University of Massachusetts, Amherst, Massachusetts (1981).

Shirodkar, P. P., and Middleman, S., J. Rheol., 26, 1 (1982).

Stefan, J., Akad. Wiss. Math. Natur., Wien , 69, 2, 713 (1874).

Tanner, R. I., ASLE Trans., 8, 179 (1965).

Tichy, J. A., Ph.D. dissertation, University of Michigan, Ann Arbor, Michigan (1970).

Tichy, J. A., and Winer, W. O., J. Lub. Tech., 92, 588 (1970).

Tichy, J. A., and Winer, W. O., J. Lub. Tech., 100, 56 (1978).

Tordella, J. P., Rheol. Acta, 3, 216 (1958).

Viriyayuthakorn, M., and Caswell, B., J. Non-Newtonian Fluid Mech., 6, 245 (1980).

Wagner, M. H., Rheol. Acta, 15, 136 (1976).

White, J. L., and Metzner, A. B., J. Appl. Polym. Sci., 7, 1867 (1963).

Williams, G., and Tanner, R. I., J. Lub. Tech., 92, 216 (1970).

Zaremba, S., Bull. Int. Acad. Sci. Cracovie, 594 (1903).

Zienkiewicz, O. C., The Finite Element Method, McGraw-Hill (1977).

APPENDIX A:
CCM REPORT NO. 81-08

COMPRESSIVE FLOW BETWEEN PARALLEL DISKS WITH A TRANSVERSE VISCOSITY GRADIENT

By

S. J. Lee

M. M. Denn

M. J. Crochet*

A. B. Metzner

Center for Composite Materials
University of Delaware
Newark, Delaware

Sponsored By The

Industry-University Research Program
Center for Composite Materials
ACMIP 1980-81

June 1981

*Professor, Université Catholique de Louvain, Louvain-la-neuve, Belgium.

APPENDIX B

GOVERNING EQUATIONS IN THE LUBRICATED CPMPRESSIVE FLOW OF NON-LINEAR MODEL FLUIDS.

Assuming the kinematics given by equations (3.1-3), the lubricated compressive flow of non-linear model fluids are governed by equations (3.19, 16, 22), and the corresponding constitutive equations which calculate τ_{rr} and τ_{zz}. The constitutive equations which will be considered here include White-Metzner model, Johnson-Segalman model (with or without retardation term), and structural model. Since the contravariant convected Maxwell model is just a special case of White-Metzner model (when $\eta(II_d)=\eta_o$), or Johnson-Segalman model (when $\xi=0$), it will not be dealt with separately.

B.1 White-Metzner model

Rewriting equations (3.19, 16, 22),

$$\frac{d\dot{\epsilon}_b}{dt} = \frac{m(g+8H\dot{\epsilon}_b^2) - \frac{1}{4}\pi\rho R^4\dot{\epsilon}_b^2 + \frac{16}{3}\pi\rho R^2H^2\dot{\epsilon}_b^2 - \pi R^2(\tau_{rr}-\tau_{zz})}{\frac{1}{4}\pi R^4\left[\rho+\rho\frac{32}{3}\left(\frac{H}{R}\right)^2+\frac{16mH}{\pi R^4}\right]} \quad (3.19)$$

$$\frac{dH}{dt} = -2H\dot{\epsilon}_b \quad (3.16)$$

$$\frac{dR}{dt} = R\dot{\epsilon}_b \quad (3.22)$$

The τ_{rr} and τ_{zz} in (3.19) are calculated using White-Metzner

constitutive equation given by equation (3.6)

$$\underset{\sim}{\tau} + \frac{\eta(\mathrm{II}_d)}{G} \overset{\nabla}{\underset{\sim}{\tau}} = 2\eta(\mathrm{II}_d)\,\underset{\sim}{d} \tag{3.6}$$

In the lubricated compressive flow,

$$\underset{\sim}{d} = \frac{1}{2}\left(\nabla\underset{\sim}{v} + \nabla\underset{\sim}{v}^{T}\right) = \begin{pmatrix} \dot{\epsilon}_b & 0 & 0 \\ 0 & \dot{\epsilon}_b & 0 \\ 0 & 0 & -2\dot{\epsilon}_b \end{pmatrix} \tag{B.1}$$

and

$$\mathrm{II}_d = -\frac{1}{2}\left[(\mathrm{tr}\underset{\sim}{d})^2 - \mathrm{tr}(\underset{\sim}{d}^2)\right] = +3\dot{\epsilon}_b^{\,2} \tag{B.2}$$

If one assumes that the viscosity is given by the power-law relationship, that is,

$$\eta(\mathrm{II}_d) = K\left|+4\mathrm{II}_d\right|^{\frac{n-1}{2}} \tag{B.3}$$

where K is the consistency factor and n is the power-law index, the radial and axial components of equation (3.65) are written as

$$\frac{d\tau_{rr}}{dt} = 2G\dot{\epsilon}_b - \frac{G}{K(12)^{\frac{n-1}{2}}}\left|\dot{\epsilon}_b\right|^{1-n}\tau_{rr} + 2\dot{\epsilon}_b\,\tau_{rr} \tag{B.4}$$

$$\frac{d\tau_{zz}}{dt} = -4G\dot{\epsilon}_b - \frac{G}{K(12)^{\frac{n-1}{2}}}\left|\dot{\epsilon}_b\right|^{1-n}\tau_{zz} - 4\dot{\epsilon}_b\,\tau_{zz} \tag{B.5}$$

Equations (3.19, 16, 22) and (B.4, 5) are all first order ordinary differential equations and they can be solved simultaneously using the Runge-Kutta method or Gear's method.

B.2 Johnson-Segalman model

Equations (3.19, 16, 22) remain the same and the stress components (rr and zz) of Johnson-Segalman constitutive equation with retardation term (3.55), in the lubricated compressive flow, are given by

$$\tau_{rr} + \lambda_1\left[\frac{d\tau_{rr}}{dt} - 2(1-\xi)\dot{\epsilon}_b\,\tau_{rr}\right] = 2\eta\left[\dot{\epsilon}_b + \lambda_2\left\{\frac{d\dot{\epsilon}_b}{dt} - 2(1-\xi)\dot{\epsilon}_b^2\right\}\right]$$

$$\tau_{zz} + \lambda_1\left[\frac{d\tau_{zz}}{dt} + 4(1-\xi)\dot{\epsilon}_b\,\tau_{zz}\right] = -4\eta\left[\dot{\epsilon}_b + \lambda_2\left\{\frac{d\dot{\epsilon}_b}{dt} + 4(1-\xi)\dot{\epsilon}_b^2\right\}\right]$$

or

$$\frac{d\tau_{rr}}{dt} = 2\frac{\eta}{\lambda_1}\left[\dot{\epsilon}_b + \lambda_2\left\{\frac{d\dot{\epsilon}_b}{dt} - 2(1-\xi)\dot{\epsilon}_b^2\right\}\right] - \frac{1}{\lambda_1}\tau_{rr} + 2(1-\xi)\dot{\epsilon}_b\,\tau_{rr} \quad \text{(B.6)}$$

$$\frac{d\tau_{zz}}{dt} = -4\frac{\eta}{\lambda_1}\left[\dot{\epsilon}_b + \lambda_2\left\{\frac{d\dot{\epsilon}_b}{dt} + 4(1-\xi)\dot{\epsilon}_b^2\right\}\right] - \frac{1}{\lambda_1}\tau_{zz} - 4(1-\xi)\dot{\epsilon}_b\,\tau_{zz} \quad \text{(B.7)}$$

Again it is not difficult to solve the equations (3.19, 16, 22) and (B.6, 7) simultanuously.

B.3 Structural model

First we need to rearrange equation (3.19) in the following form,

$$\frac{d\dot{\epsilon}_b}{dt} = \frac{m(g+8H\dot{\epsilon}_b^2) - \frac{1}{4}\pi\rho R^4\dot{\epsilon}_b^2 + \frac{16}{3}\pi\rho R^2H^2\dot{\epsilon}_b^2 - \pi R^2(\hat{\tau}_{rr}-\hat{\tau}_{zz})G}{\frac{1}{4}\pi R^4\left[\rho + \rho\frac{32}{3}\left(\frac{H}{R}\right)^2 + \frac{16mH}{\pi R^4}\right]} \quad \text{(B.8)}$$

since the constitutive equations are written in terms of $\hat{\tau}_{rr}(=\tau_{rr}/G)$ and $\hat{\tau}_{zz}(=\tau_{zz}/G)$.

In the lubricated compressive flow, the constitutive equations (3.67) become

$$\hat{\tau}_{rr} + \lambda \left[\frac{d\hat{\tau}_{rr}}{dt} - 2\dot{\epsilon}_b \hat{\tau}_{rr} \right] = 2\lambda \dot{\epsilon}_b \tag{B.9}$$

$$\hat{\tau}_{zz} + \lambda \left[\frac{d\tau_{zz}}{dt} + 4\dot{\epsilon}_b \hat{\tau}_{zz} \right] = -4\lambda \dot{\epsilon}_b$$

$$G = G_0 x \quad , \quad \lambda = \lambda_0 x^{1.4}$$

$$\frac{dx}{dt} = \frac{1}{\lambda}(1-x) - a x \frac{1}{\lambda}\sqrt{\frac{E}{G}} \tag{B.10}$$

All the equations are the first order ordinary differential equations again, which can be solved easily.

Computer programs for each model are found in the Appendix E.3. Here, Gear's method has been used to solve given ordinary differential equations simultaneously.

APPENDIX C

THE LUBRICATED COMPRESSIVE FLOW OF MAXWELL FLUID UNDER VERY HIGH LOADING CONDITIONS

The numerical results of the lubricated compressive flow of Maxwell fluid under very high loading conditions are given here. The geometry and the material properties are kept constant as given below. The load varies from 100 to 10000.

Geometry and material properties :

$R = 3.$

$H_o = 0.05$

$\rho = 1.$

$\eta = 10.$

$\lambda = 0.1$

1. m=100.

t	$(H/H_o)_{Newt}$	$(H/H_o)_{Maxwell}$	$(\dot{\epsilon}_b)_{Max}$	$\frac{(H/H_o)_{Max}}{(H/H_o)_{Newt}}$
0.00	1.000	1.000	0.00	1.00
0.01	0.899	0.893	10.93	0.99
0.02	0.694	0.665	17.55	0.96
0.03	0.507	0.459	18.89	0.91
0.04	0.327	0.318	17.59	0.85
0.05	0.281	0.228	15.64	0.81
0.07	0.175	0.131	12.13	0.75
0.1	0.109	0.710E-01	8.60	0.65
0.15	0.522E-01	0.358E-01	5.46	0.69
0.2	0.323E-01	0.226E-01	3.86	0.70
0.3	0.161E-01	0.124E-01	2.36	0.77
0.4	0.979E-02	0.830E-02	1.72	0.85
0.6	0.478E-02	0.474E-02	1.18	0.99
0.8	0.286E-02	0.313E-02	0.93	1.09
1.0	0.191E-02	0.230E-02	0.79	1.20

2. m=500.

t	$(H/H_o)_{Newt}$	$(H/H_o)_{Max}$	$(\dot{\epsilon}_b)_{Max}$	$\frac{(H/H_o)_{Max}}{(H/H_o)_{Newt}}$
0.00	1.000	1.000	0.00	1.00
0.01	0.746	0.738	30.13	0.99
0.02	0.368	0.345	40.18	0.94
0.03	0.187	0.167	32.12	0.89
0.05	0.721E-01	0.604E-01	20.09	0.84
0.1	0.188E-01	0.155E-01	9.48	0.82
0.2	0.488E-02	0.449E-02	4.18	0.92
0.3	0.221E-02	0.233E-02	2.61	1.05
0.4	0.126E-02	0.149E-02	1.93	1.18
0.6	0.569E-03	0.793E-03	1.33	1.53
0.8	0.324E-03	0.497E-03	1.04	1.53
1.0	0.209E-03	0.341E-03	0.86	1.63

3. m=1000.

t	$(H/H_o)_{Newt}$	$(H/H_o)_{Max}$	$(\dot{\epsilon}_b)_{Max}$	$\frac{(H/H_o)_{Max}}{(H/H_o)_{Newt}}$
0.00	1.000	1.000	0.00	1.00
0.01	0.677	0.670	41.76	0.99
0.02	0.251	0.236	51.40	0.94
0.03	0.110	0.988E-01	36.51	0.90
0.05	0.376E-01	0.327E-01	21.26	0.87
0.1	0.903E-02	0.796E-02	9.72	0.88
0.15	0.398E-02	0.372E-02	6.02	0.93
0.2	0.223E-02	0.225E-02	4.27	1.01
0.4	0.560E-03	0.728E-03	1.98	1.30
0.6	0.251E-03	0.381E-03	1.36	1.52
0.8	0.142E-03	0.236E-03	1.06	1.66
1.0	0.911E-04	0.161E-03	0.87	1.77

4. m=10000.

t	$(H/H_o)_{Newt}$	$(H/H_o)_{Max}$	$(\dot{\epsilon}_b)_{Max}$	$\frac{(H/H_o)_{Max}}{(H/H_o)_{Newt}}$
0.00	1.000	1.000	0.00	1.00
0.01	0.541	0.539	80.30	0.996
0.02	0.552E-01	0.534E-01	87.82	0.97
0.03	0.156E-01	0.150E-01	47.25	0.96
0.05	0.414E-02	0.399E-02	24.00	0.96
0.07	0.187E-02	0.184E-02	15.85	0.98
0.1	0.846E-03	0.859E-03	10.30	1.02
0.15	0.353E-03	0.386E-03	6.31	1.09
0.2	0.193E-03	0.228E-03	4.46	1.18
0.4	0.465E-04	0.703E-04	2.06	1.51
0.6	0.204E-04	0.358E-04	1.41	1.75
0.8	0.114E-04	0.219E-04	1.09	1.92
1.0	0.729E-05	0.147E-04	0.89	2.02

APPENDIX D

FINITE ELEMENT FORMULATIONS.

Since our flow of interest is the axisymmetric flow (in r-z coordinate), we will limit ourselves to the axisymmetric flow of incompressible fluids. First, we will consider the flow of generalized Newtonian fluid. The flow of viscoelastic materials will then be considered. The excellent treatments on these subject are given by Crochet(1981), and Zienkiewicz(1977).

D.1 Generalized Newtonian flow

Governing equations : In the compressive flow of inelastic generalized Newtonian fluid, the fluid inertia is considered negligible (Re<<1). The momentum equations then become the quasi-steady state equation, even though the flow itself is time dependent. The momentum equations are given by

$$-\frac{\partial p}{\partial r} + \frac{1}{r}\frac{\partial}{\partial r}(r\tau_{rr}) - \frac{\tau_{\theta\theta}}{r} + \frac{\partial \tau_{rz}}{\partial z} + f_r = 0 \qquad (D.1)$$

$$-\frac{\partial p}{\partial z} + \frac{1}{r}\frac{\partial}{\partial r}(r\tau_{rz}) + \frac{\partial \tau_{zz}}{\partial z} + f_z = 0 \qquad (D.2)$$

where f_r and f_z represent the components of the body force per unit volume.

The constitutive relations of generalized Newtonian fluids are given by

$$\tau_{rr} = 2\eta(\mathrm{II}_d)\, d_{rr} \tag{D.3}$$

$$\tau_{\theta\theta} = 2\eta(\mathrm{II}_d)\, d_{\theta\theta} \tag{D.4}$$

$$\tau_{zz} = 2\eta(\mathrm{II}_d)\, d_{zz} \tag{D.5}$$

$$\tau_{rz} = 2\eta(\mathrm{II}_d)\, d_{rz} \tag{D.6}$$

where

$$\mathrm{II}_d = -\frac{1}{2}\left[(\mathrm{tr}\ \underset{\sim}{d})^2 - \mathrm{tr}(\underset{\sim}{d}^2)\right]$$

$$= \frac{1}{2}\left(d_{rr}^2 + d_{\theta\theta}^2 + d_{zz}^2\right) + d_{rz}^2 \tag{D.7}$$

and

$$d_{rr} = \frac{\partial V_r}{\partial r} \tag{D.8}$$

$$d_{\theta\theta} = \frac{V_r}{r} \tag{D.9}$$

$$d_{zz} = \frac{\partial V_z}{\partial z} \tag{D.10}$$

$$d_{rz} = \frac{1}{2}\left(\frac{\partial V_r}{\partial z} + \frac{\partial V_z}{\partial r}\right) \tag{D.11}$$

The mass conservation is given by

$$\frac{\partial V_r}{\partial r} + \frac{V_r}{r} + \frac{\partial V_z}{\partial z} = 0 \tag{D.12}$$

Galerkin formulation : Let us consider the approximations of V_r, V_z, and p given by

$$V_r \approx \sum_{j=1}^{M} u_j \psi_j \tag{D.13}$$

$$V_z \approx \sum_{j=1}^{M} v_j \psi_j \tag{D.14}$$

$$p \approx \sum_{j=1}^{N} p_j \phi_j \tag{D.15}$$

where ψ_j and ϕ_j are the interpolation functions for the velocity components and the pressure, respectively, and u_j, v_j, and p_j are the nodal values of the velocity components and the pressure. The Galerkin formulation of the momentum equations is then given by

$$\left\langle r\psi_i \, , \, -\frac{\partial p}{\partial r} + \frac{1}{r}\frac{\partial}{\partial r}(r\tau_{rr}) - \frac{\tau_{\theta\theta}}{r} + \frac{\partial \tau_{rz}}{\partial z} + f_r \right\rangle = 0 \tag{D.16}$$

$$\left\langle r\psi_i \, , \, -\frac{\partial p}{\partial z} + \frac{1}{r}\frac{\partial}{\partial r}(r\tau_{rz}) + \frac{\partial \tau_{zz}}{\partial z} + f_z \right\rangle = 0 \tag{D.17}$$

where the brackets denote the integrations over the given domain.

Performing the integration by parts on equations (D.16) and (D.17) and using the divergence theorem, one obtains

$$\left\langle r\frac{\partial \psi_i}{\partial r}, \, -p + \tau_{rr} \right\rangle + \left\langle r\frac{\partial \psi_i}{\partial z}, \, \tau_{rz} \right\rangle + \left\langle \psi_i, \tau_{\theta\theta} \right\rangle - \left\langle \psi_i, p \right\rangle = \left\langle r\psi_i, f_r \right\rangle + \left\langle\!\left\langle r\psi_i, t_r \right\rangle\!\right\rangle \tag{D.18}$$

$$\left\langle r\frac{\partial \psi_i}{\partial r}, \, \tau_{rz} \right\rangle + \left\langle r\frac{\partial \psi_i}{\partial z}, \, -p + \tau_{zz} \right\rangle = \left\langle r\psi_i, f_z \right\rangle + \left\langle\!\left\langle r\psi_i, t_z \right\rangle\!\right\rangle \tag{D.19}$$

where t_r and t_z are the r and z component of the contact force vector and the double brackets denote the integrations

along the boundary of the domain.

Substituting the constitutive relations (D.3-6) into equations (D.18) and (D.19) gives the final form of Galerkin equations,

$$\langle r\frac{\partial \psi_i}{\partial r},\ -p+2\eta\frac{\partial V_r}{\partial r}\rangle + \langle r\frac{\partial \psi_i}{\partial z},\ \eta\left(\frac{\partial V_r}{\partial z}+\frac{\partial V_z}{\partial r}\right)\rangle + \langle \psi_i, 2\eta\frac{V_r}{r}\rangle - \langle \psi_i, p\rangle = \langle r\psi_i, f_r\rangle + \ll r\psi_i,\ t_r \gg \tag{D.20}$$

$$\langle r\frac{\partial \psi_i}{\partial r},\ \eta\left(\frac{\partial V_r}{\partial z}+\frac{\partial V_z}{\partial r}\right)\rangle + \langle r\frac{\partial \psi_i}{\partial z},\ -p+2\eta\frac{\partial V_z}{\partial z}\rangle = \langle r\psi_i,\ f_z\rangle + \ll r\psi_i,\ t_z\gg \tag{D.21}$$

Galerkin form of the mass conservation becomes

$$\langle r\phi_i,\ \frac{\partial V_r}{\partial r}+\frac{V_r}{r}+\frac{\partial V_z}{\partial z}\rangle = 0 \tag{D.22}$$

Further substituting the approximations of (D.13-15) into (D.20-22), one obtains the following algebraic system

$$\sum_{j=1}^{M}\left(A_{ij}u_j + C_{ij}v_j\right) - \sum_{j=1}^{N} D_{ij}p_j = X_i,\quad i:1\sim M \tag{D.23}$$

$$\sum_{j=1}^{M}\left(C_{ji}u_j + B_{ij}v_j\right) - \sum_{j=1}^{N} E_{ij}p_j = Y_i,\quad i:1\sim M \tag{D.24}$$

$$\sum_{j=1}^{M}\left(-D_{ji}u_j - E_{ji}v_j\right) = 0,\quad i:1\sim N \tag{D.25}$$

where

$$A_{ij} = 2\langle \eta r\frac{\partial \psi_i}{\partial r},\frac{\partial \psi_j}{\partial r}\rangle + \langle \eta r\frac{\partial \psi_i}{\partial z},\frac{\partial \psi_j}{\partial z}\rangle + \langle \eta\psi_i, \frac{1}{r}\psi_j\rangle$$

$$B_{ij} = 2\langle \eta r\frac{\partial \psi_i}{\partial z},\frac{\partial \psi_j}{\partial z}\rangle + \langle \eta r\frac{\partial \psi_i}{\partial r},\frac{\partial \psi_j}{\partial r}\rangle$$

$$C_{ij} = \langle \eta r\frac{\partial \psi_i}{\partial z},\frac{\partial \psi_j}{\partial r}\rangle,\quad D_{ij} = \langle r\frac{\partial \psi_i}{\partial r},\phi_j\rangle + \langle \psi_i,\phi_j\rangle$$

$$E_{ij} = \langle r\frac{\partial \psi_i}{\partial z},\phi_j\rangle$$

$$X_i = \langle r\psi_i, f_r\rangle + \ll r\psi_i, t_r\gg,\quad Y_i = \langle r\psi_i, f_z\rangle + \ll r\psi_i, t_z\gg$$

The solution of the system (D.23-25) can be obtained by a certain iteration technique, since the viscosity is a function of the velocity field in general. One can assume a constant viscosity to obtain the velocity field in the first iteration and the new viscosities are obtained from the previously obtained velocity field. One then repeats this procedure until the solution or the viscosity converges within a given error allowance. This technique has been used successfully to solve the unlubricated compressive flows of the power-law fluids in Section 2.3.

Solving equations (D.23-25) requires the calculation of all the matrices, which are the integrations in the domain, and the selection of the appropriate elements and shape functions ψ_i and ϕ_i . Numerical integration, using quadrature points, is the effective way of performing integations. Two types of elements have been successful in the past. The first element is a triangle on which the velocity components are represented by complete second order polynomials, while the pressure is given by complete first order polynomials. The second element is a quadrilateral with biquadratic velocity components and bilinear pressure. The functions ψ_i and ϕ_i are given in Tables D.1 and D.2 for the triangular and the quadrilateral element, respectively.

D.2 Viscoelastic flow : Maxwell fluid

Governing equations : Let us consider the compressive flow of the contravariant convected Maxwell fluid. One then requires to retain the material time derivative terms in the momentum equations and in the constitutive equations. They are given in the following.

Momentum:

$$\rho \frac{DV_r}{Dt} = -\frac{\partial p}{\partial r} + \frac{1}{r}\frac{\partial}{\partial r}(r\tau_{rr}) - \frac{\tau_{\theta\theta}}{r} + \frac{\partial \tau_{rz}}{\partial z} + f_r \qquad (D.26)$$

$$\rho \frac{DV_z}{Dt} = -\frac{\partial p}{\partial z} + \frac{1}{r}\frac{\partial}{\partial r}(r\tau_{rz}) + \frac{\partial \tau_{zz}}{\partial z} + f_z \qquad (D.27)$$

Constitutive:

$$\tau_{rr} + \lambda\left[\frac{D\tau_{rr}}{Dt} - 2\tau_{rr}\frac{\partial V_r}{\partial r} - 2\tau_{rz}\frac{\partial V_r}{\partial z}\right] = 2\eta\frac{\partial V_r}{\partial r} \qquad (D.28)$$

$$\tau_{\theta\theta} + \lambda\left[\frac{D\tau_{\theta\theta}}{Dt} - 2\tau_{\theta\theta}\frac{V_r}{r}\right] = 2\eta\frac{V_r}{r} \qquad (D.29)$$

$$\tau_{zz} + \lambda\left[\frac{D\tau_{zz}}{Dt} - 2\tau_{rz}\frac{\partial V_z}{\partial r} - 2\tau_{zz}\frac{\partial V_z}{\partial z}\right] = 2\eta\frac{\partial V_z}{\partial z} \qquad (D.30)$$

$$\tau_{rz} + \lambda\left[\frac{D\tau_{rz}}{Dt} - \tau_{rr}\frac{\partial V_z}{\partial r} - \tau_{zz}\frac{\partial V_r}{\partial z} - \tau_{rz}\left(\frac{\partial V_r}{\partial r} + \frac{\partial V_z}{\partial z}\right)\right] = \eta\left(\frac{\partial V_r}{\partial z} + \frac{\partial V_z}{\partial r}\right) \qquad (D.31)$$

The continuity equation is given by

$$\frac{\partial V_r}{\partial r} + \frac{V_r}{r} + \frac{\partial V_z}{\partial z} = 0 \qquad (D.32)$$

A mixed finite element method : In this method, first proposed by Kawahara and Takeuchi, the extra stress

components are considered as unknown functions to the same degree as the velocity components and the pressure. Thus, we consider 7 unknown fields for axisymmetric flow: 4 stress components, 2 velocity components, and the pressure. We use the following approximations for these unknown fields,

$$V_r \approx \Sigma\, u_j \psi_j \tag{D.33}$$

$$V_z \approx \Sigma\, v_j \psi_j \tag{D.34}$$

$$p \approx \Sigma\, p_j \phi_j \tag{D.35}$$

$$\tau_{rr} \approx \Sigma\, R_j \tau_j \tag{D.36}$$

$$\tau_{zz} \approx \Sigma\, S_j \tau_j \tag{D.37}$$

$$\tau_{rz} \approx \Sigma\, T_j \tau_j \tag{D.38}$$

$$\tau_{\theta\theta} \approx \Sigma\, Q_j \tau_j \tag{D.39}$$

The Galerkin form of the constitutive and field equations may then be obtained as follows,

$$\left\langle r\tau_i,\ \tau_{rr} + \lambda\left[\frac{D\tau_{rr}}{Dt} - 2\tau_{rr}\frac{\partial V_r}{\partial r} - 2\tau_{rz}\frac{\partial V_r}{\partial z}\right] - 2\eta\frac{\partial V_r}{\partial r}\right\rangle = 0 \tag{D.40}$$

$$\left\langle r\tau_i,\ \tau_{\theta\theta} + \lambda\left[\frac{D\tau_{\theta\theta}}{Dt} - 2\tau_{\theta\theta}\frac{V_r}{r}\right] - 2\eta\frac{V_r}{r}\right\rangle = 0 \tag{D.41}$$

$$\left\langle r\tau_i,\ \tau_{zz} + \lambda\left[\frac{D\tau_{zz}}{Dt} - 2\tau_{rz}\frac{\partial V_z}{\partial r} - 2\tau_{zz}\frac{\partial V_z}{\partial z}\right] - 2\eta\frac{\partial V_z}{\partial z}\right\rangle = 0 \tag{D.42}$$

$$\langle r\tau_i,\ \tau_{rz}+\lambda\left[\frac{D\tau_{rz}}{Dt}-\tau_{rr}\frac{\partial V_z}{\partial r}-\tau_{zz}\frac{\partial V_r}{\partial z}-\tau_{rz}\left(\frac{\partial V_r}{\partial r}+\frac{\partial V_z}{\partial r}\right)\right] \qquad (D.43)$$
$$-\eta\left(\frac{\partial V_r}{\partial z}+\frac{\partial V_z}{\partial r}\right)\rangle = 0$$

$$\langle r\frac{\partial \psi_i}{\partial r},\ -p-\tau_{rr}\rangle+\langle r\frac{\partial \psi_i}{\partial z},\ \tau_{rz}\rangle+\langle \psi_i,\ \tau_{\theta\theta}\rangle-\langle r\psi_i,\ \rho\frac{DV_r}{Dt}\rangle \qquad (D.44)$$
$$-\langle \psi_i,\ p\rangle=\langle r\psi_i,\ f_r\rangle+\ll r\psi_i,\ t_r\gg$$

$$\langle r\frac{\partial \psi_i}{\partial r},\ \tau_{rz}\rangle+\langle r\frac{\partial \psi_i}{\partial z},\ -p+\tau_{zz}\rangle-\langle r\psi_i,\ \rho\frac{DV_z}{Dt}\rangle \qquad (D.45)$$
$$=\langle r\psi_i,\ f_z\rangle+\ll r\psi_i,\ t_z\gg$$

$$\langle r\phi_i,\ \frac{\partial V_r}{\partial r}\rangle+\langle r\phi_i,\ \frac{V_r}{r}\rangle+\langle r\phi_i,\ \frac{\partial V_z}{\partial z}\rangle=0 \qquad (D.46)$$

By replacing V_r, V_z, τ_{rr}, τ_{zz}, τ_{rz}, $\tau_{\theta\theta}$, and p in terms of their approximations given by (D.33-39) it is possible to obtain a non-linear algebraic system of equations in terms of the unknowns, u_j, v_j, R_j, S_j, T_j, Q_j, and p_j, which is solved by means of Newton-Raphson iterative method.

The material time derivatives are treated by a finite difference scheme in the time coordinate. Their discretization, using the implicit three point recurrence scheme with variable time steps, is given by equation (3.72).

The same types of elements as used in the generalized Newtonian flow have been shown to work well with the mixed method, using the same interpolation functions for the velocity components and the stress components; that is, $\tau_i = \psi_i$.

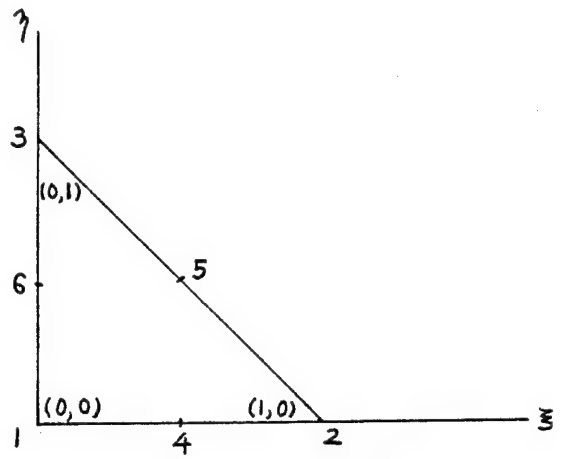

parent triangular element

$$\phi_1 = 1 - \xi - \eta$$

$$\phi_2 = \xi$$

$$\phi_3 = \eta$$

$$\psi_1 = 1 - 3(\xi+\eta) + 2(\xi+\eta)^2$$

$$\psi_2 = \xi(2\xi - 1)$$

$$\psi_3 = \eta(2\eta - 1)$$

$$\psi_4 = 4\xi(1-\xi-\eta)$$

$$\psi_5 = 4\xi\eta$$

$$\psi_6 = 4\eta(1-\xi-\eta)$$

Table D.1 Shape functions, ϕ_i and ψ_i, in the parent triangular element.

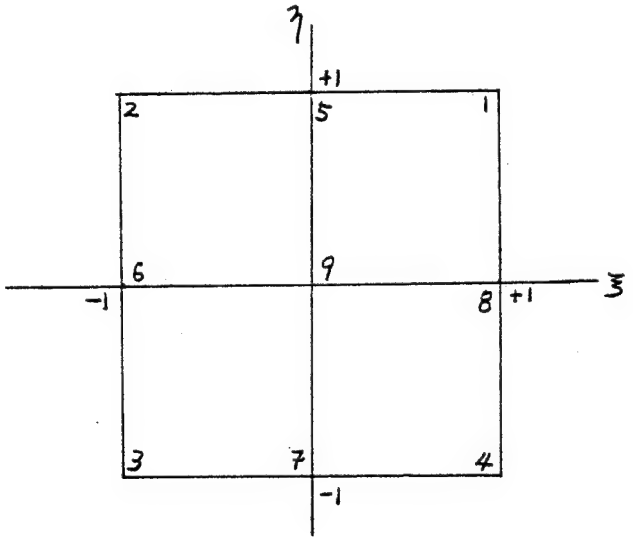

parent quadrilateral element

$$\phi_1 = (1+\xi)(1+\eta)/4 \quad , \qquad \phi_2 = (1-\xi)(1+\eta)/4$$

$$\phi_3 = (1-\xi)(1-\eta)/4 \quad , \qquad \phi_4 = (1+\xi)(1-\eta)/4$$

$$\psi_1 = \xi(1+\xi)\eta(1+\eta)/4 \, , \qquad \psi_2 = -\xi(1-\xi)\eta(1+\eta)/4$$

$$\psi_3 = \xi(1-\xi)\eta(1-\eta)/4 \, , \qquad \psi_4 = -\xi(1+\xi)\eta(1-\eta)/4$$

$$\psi_5 = (1-\xi^2)\eta(1+\eta)/2 \, , \qquad \psi_6 = -\xi(1-\xi)(1-\eta^2)/2$$

$$\psi_7 = -(1-\xi)^2\eta(1-\eta)/2 \, , \qquad \psi_8 = \xi(1+\xi)(1-\eta^2)/2$$

$$\psi_9 = (1-\xi^2)(1-\eta^2)$$

Table D.2 Shape functions, ϕ_i and ψ_i, in the quadrilateral element.

APPENDIX E

COMPUTER PROGRAMS

The computer programs for the lubricated compressive flows of the White-Metzner, Johnson-Segalman, Marrucci structural models, and their corresponding inelastic cases are given here. Subroutine DGEAR, the differential equation solver by Gear method, from IMSL subroutine package has been used in these programs. Each program deals with the following case:

Program	Description
WMSLP.FOR	White-Metzner model with power-law viscosity
PWLSLP.FOR	inelastic power-law fluid
JSSLP.FOR	Johnson-Segalman model
NJSSLP.FOR	inelastic case corresponding to Johnson-Segalman model
SMSLP.FOR	Marrucci structural model
NSMSLP.FOR	inelastic case corresponding to Marrucci model

Programs used in the lubricated compressive flows

```
C*************************************************************
C
C      PROGRAM WMSLP.FOR
C
C                LUBRICATED SQUEEZING OF WHITE-METZNER FLUIDS.
C
C*************************************************************
      INTEGER N,METH,MITER,INDEX,IWK(5),IER,IRV
      REAL Y(5),WK(115),T,TOL,TEND,DELT
      DOUBLE PRECISION PRINT,THH0
      EXTERNAL FCN,FCNJ
      COMMON/AB/A,B
      COMMON/AM/AMASS
      COMMON/G/GM
      COMMON/VR/VISC,GSHEAR,PLI
C************************************
      TYPE 10
10    FORMAT(' INITIAL CONDITIONS'/' ENTER T0,EB0,PRR0
     1,PZZ0,H0,R0')
      ACCEPT *,T0,EB0,PRR0,PZZ0,H0,R0
      TYPE 11
11    FORMAT(' ENTER DENSITY, SHEAR MODULUS, VISCOSITY OR'
     1       ' CONSISTENCY FACTOR, POWER LAW INDEX, MASS')
      ACCEPT *,DENS,GSHEAR,CONF,PLI,AMASS
      VISC=CONF*(12.)**((PLI-1.)/2.)
      TYPE 12
12    FORMAT(' ENTER TOLERANCE, DELT')
      ACCEPT *,TOL,DELT
      TYPE 15
15    FORMAT(' ENTER NPRT,INTERVAL')
      ACCEPT *,NPRT,AINTR
      TYPE 16
16    FORMAT(' ENTER FILENAMES FOR PRINT / T VS. HH0')
      ACCEPT 117,PRINT,THH0
117   FORMAT(A10/A10)
C**********************************
      OPEN(UNIT=31,DEVICE='DSK',FILE=PRINT)
      OPEN(UNIT=32,DEVICE='DSK',FILE=THH0)
      WRITE(31,17)
17    FORMAT(' LUBRICATED SQUEEZING OF WHITE-METZNER FLUID')
      WRITE(31,25) DENS,GSHEAR,CONF,PLI,AMASS
25    FORMAT(' DENSITY = ',E14.5/' SHEAR MODULUS = ',E14.5/
     1   ' CONSISTENCY FACTOR = ',E14.5/' POWER LAW INDEX = ',
     1   E14.5/' MASS = ',E14.5)
      WRITE(31,27) TOL
27    FORMAT(' TOLERANCE = ',E14.5)
C****************************************
      PI=3.14159265357989
```

```
      N=5
      METH=1
      MITER=0
      INDEX=1
      WRITE(31,28) METH,MITER,INDEX
28    FORMAT(/' METH = ',I4/' MITER = ',I4/' INDEX = ',I4/)

      T=T0
      Y(1)=EB0
      Y(2)=PRR0
      Y(3)=PZZ0
      Y(4)=H0
      Y(5)=R0

      GM=980.*AMASS
      A=PI*DENS
      B=PI*VISC

      EB=Y(1)
      PRR=Y(2)
      PZZ=Y(3)
      H=Y(4)
      R=Y(5)
      HH0=H/H0
      WRITE(5,20)
      WRITE(31,20)
20    FORMAT(//7X,'TIME',12X,'EB',11X,'PRR',11X,'PZZ',
     1         13X,'H',13X,'R',10X,'H/H0',10X,'DELT'/)
      WRITE(5,21) T,EB,PRR,PZZ,H,R,HH0,DELT
      WRITE(31,21) T,EB,PRR,PZZ,H,R,HH0,DELT
      WRITE(32,*) T,HH0
21    FORMAT(8E14.5)
C************************************
      DO 100 I=1,NPRT
      TEND=FLOAT(I)*AINTR+T0
      CALL DGEAR(N,FCN,FCNJ,T,DELT,Y,TEND,TOL,METH,MITER,
     1          INDEX,IWK,WK,IER)
      EB=Y(1)
      PRR=Y(2)
      PZZ=Y(3)
      H=Y(4)
      R=Y(5)
      HH0=H/H0
      WRITE(31,21) TEND,EB,PRR,PZZ,H,R,HH0,DELT
      WRITE(32,*) TEND,HH0
100   WRITE(5,21) TEND,EB,PRR,PZZ,H,R,HH0,DELT
      CLOSE(UNIT=31,DISPOSE='PRINT')
      CLOSE(UNIT=32)
      STOP
      END
C*********************************************
```

```
      SUBROUTINE FCN(N,T,Y,YPRIME)
C*********************************************
      INTEGER N
      REAL Y(5),YPRIME(5),T
      COMMON/AB/A,B
      COMMON/AM/AMASS
      COMMON/G/GM
      COMMON/VR/VISC,GSHEAR,PLI
C************************************
      PI=3.14159265357989
      EB=Y(1)
      EB2=EB*EB
      PRR=Y(2)
      PZZ=Y(3)
      H=Y(4)
      H2=H*H
      R=Y(5)
      R2=R*R
      R4=R2*R2

      YPRIME(1)=(GM+4.*AMASS*H*EB2-A*R4*EB2/4.
     1           +4.*A*R2*H2*EB2/3.-PI*R2*(PRR-PZZ))
     1           /(A*R4/4.+2.*A*R2*H2/3.+2.*AMASS*H)
      YPRIME(2)=2.*GSHEAR*EB-GSHEAR/VISC*ABS(EB)**(1.-PLI)*
     1           PRR+2.*EB*PRR
      YPRIME(3)=-4.*GSHEAR*EB-GSHEAR/VISC*ABS(EB)**(1.-PLI)*
     1           PZZ+-4.*EB*PZZ
      YPRIME(4)=-2.*EB*H
      YPRIME(5)=EB*R

      RETURN
      END
C*********************************************
      SUBROUTINE FCNJ(N,T,Y,PD)
      INTEGER N
      REAL Y(5),PD(N,N),T
      RETURN
      END
```

```
C*************************************************************
C
C     PROGRAM PWLSLP.FOR
C
C                LUBRICATED SQUEEZING OF POWER LAW FLUIDS.
C
C*************************************************************
      INTEGER N,METH,MITER,INDEX,IWK(3),IER,IRV
      REAL Y(3),WK(63),T,TOL,TEND,DELT
      DOUBLE PRECISION PRINT,THH0
      EXTERNAL FCN,FCNJ
      COMMON/AB/A,B
      COMMON/AM/AMASS
      COMMON/G/GM
      COMMON/P/PLI
C************************************
      TYPE 10
10    FORMAT(' INITIAL CONDITIONS'/' ENTER T0,EB0,H0,R0')
      ACCEPT *,T0,EB0,H0,R0
      TYPE 11
11    FORMAT(' ENTER DENS, VISC OR CONSISTENCY FACTOR,'
     1          ' POWER LAW INDEX, MASS OF LOAD')
      ACCEPT *,DENS,VISC,PLI,AMASS
      TYPE 12
12    FORMAT(' ENTER TOLERANCE, DELT')
      ACCEPT *,TOL,DELT
      TYPE 15
15    FORMAT(' ENTER NPRT,INTERVAL')
      ACCEPT *,NPRT,AINTR
      TYPE 16
16    FORMAT(' ENTER FILENAMES FOR PRINT & T VS. HH0')
      ACCEPT 117,PRINT,THH0
117   FORMAT(A10/A10)
C************************************
      OPEN(UNIT=31,DEVICE='DSK',FILE=PRINT)
      OPEN(UNIT=32,DEVICE='DSK',FILE=THH0)
      IF(PLI.EQ.1.) WRITE(31,17)
      IF(PLI.NE.1.) WRITE(31,18)
17    FORMAT(/' LUBRICATED SQUEEZING OF NEWTONIAN FLUID'//)
18    FORMAT(/' LUBRICATED SQUEEZING OF POWER LAW FLUID'//)
      IF(PLI.EQ.1.) WRITE(31,25) DENS,VISC,AMASS
      IF(PLI.NE.1.) WRITE(31,26) DENS,VISC,PLI,AMASS
25    FORMAT(' DENSITY = ',E14.5/' VISCOSITY = ',E14.5/
     1          ' MASS = ',E14.5)
26    FORMAT(' DENS =',E14.5/' CONSISTENCY FACTOR =',E14.5/
     1          ' POWER LAW INDEX = ',E14.5/' MASS = ',E14.5)
      WRITE(31,27) TOL
27    FORMAT(' TOLERANCE = ',E14.5)
C************************************
      PI=3.14159265357989
      N=3
```

```
      METH=1
      MITER=0
      INDEX=1
      WRITE(31,28) METH,MITER,INDEX
28    FORMAT(/' METH = ',I4/' MITER = ',I4/' INDEX = ',I4)

      T=T0
      Y(1)=EB0
      Y(2)=H0
      Y(3)=R0

      GM=980.*AMASS
      A=PI*DENS
      B=PI*VISC

      EB=Y(1)
      H=Y(2)
      R=Y(3)
      HH0=H/H0
      WRITE(5,20)
      WRITE(31,20)
20    FORMAT(//7X,'TIME',12X,'EB',12X,'H',13X,'R',10X,
     1          'H/H0',10X,'DELT'/)
      WRITE(5,21) T,EB,H,R,HH0,DELT
      WRITE(31,21) T,EB,H,R,HH0,DELT
      WRITE(32,*) T,HH0
21    FORMAT(6E14.5)
C*************************************
      DO 100 I=1,NPRT
      TEND=FLOAT(I)*AINTR
      CALL DGEAR(N,FCN,FCNJ,T,DELT,Y,TEND,TOL,METH,MITER,
     1          INDEX,IWK,WK,IER)
      EB=Y(1)
      H=Y(2)
      R=Y(3)
      HH0=H/H0
      WRITE(31,21) TEND,EB,H,R,HH0,DELT
      WRITE(32,*) TEND,HH0
100   WRITE(5,21) TEND,EB,H,R,HH0,DELT
      CLOSE(UNIT=31)
      CLOSE(UNIT=32)
      STOP
      END
C*********************************************
      SUBROUTINE FCN(N,T,Y,YPRIME)
C*********************************************
      INTEGER N
      REAL Y(3),YPRIME(3),T
      COMMON/AB/A,B
      COMMON/AM/AMASS
      COMMON/G/GM
```

```
      COMMON/P/PLI
C**************************************
      EB=Y(1)
      EB2=EB*EB
      H=Y(2)
      H2=H*H
      R=Y(3)
      R2=R*R
      R4=R2*R2
      AAA=1.
      IF(ABS(EB).EQ.0.) AAA=0.

      YPRIME(1)=(GM+4.*AMASS*H*EB2-A*R4*EB2/4.
     1             +4.*A*R2*H2*EB2/3.-6.*B*R2*
     1             (12.)**((PLI-1.)/2.)*EB*
     1             ABS(EB)**(AAA*(PLI-1.)))
     1             /(A*R4/4.+2.*A*R2*H2/3.+2.*AMASS*H)
      YPRIME(2)=-2.*EB*H
      YPRIME(3)=EB*R

      RETURN
      END
C************************************************
      SUBROUTINE FCNJ(N,T,Y,PD)
      INTEGER N
      REAL Y(3),PD(N,N),T
      RETURN
      END
```

```
C*********************************************************
C
C      PROGRAM JSSLP.FOR
C
C                LUBRICATED COMPRESSIVE FLOW OF
C                JOHNSON-SEGALMAN MODEL.
C
C*********************************************************
       INTEGER N,METH,MITER,INDEX,IWK(5),IER,IRV
       REAL Y(5),WK(115),T,TOL,TEND,DELT,MASS
       DOUBLE PRECISION PRINT,THH0
       EXTERNAL FCN,FCNJ
       COMMON/AB/A,B
       COMMON/M/MASS
       COMMON/G/GM
       COMMON/VR/VISC,RTIME1,RTIME2
       COMMON/MP/G,RTIME,XI,EPS
C************************************
7      TYPE 10
10     FORMAT(' INITIAL CONDITIONS'/' ENTER T0,EB0,PRR0,PZZ0,H0,R0')
       ACCEPT *,T0,EB0,PRR0,PZZ0,H0,R0
       TYPE 11
11     FORMAT(' ENTER DENSITY, AND MASS OF LOAD')
       ACCEPT *,DENS,MASS
       TYPE 111
111    FORMAT(' ENTER SHEAR MODULUS, RELAXATION TIME, AND',
      1        ' RETARDATION TIME')
       ACCEPT *,G,RTIME1,RTIME2
       TYPE 112
112    FORMAT(' ENTER XI')
       ACCEPT *,XI
       TYPE 12
12     FORMAT(' ENTER TOLERANCE, DELT')
       ACCEPT *,TOL,DELT
       TYPE 15
15     FORMAT(' ENTER NPRT,INTERVAL')
       ACCEPT *,NPRT,AINTR
       TYPE 16
16     FORMAT(' ENTER FILENAMES FOR PRINT / T VS. HH0')
       ACCEPT 117,PRINT,THH0
117    FORMAT(A10/A10)
C************************************
       OPEN(UNIT=31,DEVICE='DSK',FILE=PRINT)
       OPEN(UNIT=32,DEVICE='DSK',FILE=THH0)
       WRITE(31,17)
17     FORMAT(/' LUBRICATED COMPRESSIVE FLOW OF JOHNSON-',
      1         'SEGALMAN MODEL'//)
       WRITE(31,25) DENS,G,RTIME1,RTIME2,XI,MASS
25     FORMAT(' DENSITY = ',E14.5/' SHEAR MODULUS = ',
      1        E14.5/' RELAXATION TIME = ',E14.5/
      1        ' RETARDATION TIME = ',E14.5/' XI = ',
```

```
     1          E14.5/' MASS = ',E14.5)
      WRITE(31,27) TOL
27    FORMAT(' TOLERANCE = ',E14.5)
C**************************************
      PI=3.14159265357989
      N=5
      METH=2
      MITER=0
      INDEX=1
      WRITE(31,28) METH,MITER,INDEX
28    FORMAT(/' MWTH = ',I4/' MITER = ',I4/' INDEX = ',I4/)

      T=T0
      Y(1)=EB0
      Y(2)=PRR0
      Y(3)=PZZ0
      Y(4)=H0
      Y(5)=R0

      GM=980.*MASS
      A=PI*DENS

      EB=Y(1)
      PRR=Y(2)
      PZZ=Y(3)
      H=Y(4)
      R=Y(5)
      HH0=H/H0
      WRITE(5,20)
      WRITE(31,20)
20    FORMAT(//7X,'TIME',12X,'EB',11X,'PRR',11X,'PZZ',
     1          13X,'H',13X,'R',10X,'H/H0',10X,'DELT'/)
      WRITE(5,21) T,EB,PRR,PZZ,H,R,HH0,DELT
      WRITE(31,21) T,EB,PRR,PZZ,H,R,HH0,DELT
      WRITE(32,*) T,HH0
21    FORMAT(8E14.5)
C**********************************
      DO 100 I=1,NPRT
      TEND=FLOAT(I)*AINTR+T0
      CALL DGEAR(N,FCN,FCNJ,T,DELT,Y,TEND,TOL,METH,MITER,
     1          INDEX,IWK,WK,IER)
      EB=Y(1)
      PRR=Y(2)
      PZZ=Y(3)
      H=Y(4)
      R=Y(5)
      HH0=H/H0
      WRITE(31,21) TEND,EB,PRR,PZZ,H,R,HH0,DELT
      WRITE(32,*) TEND,HH0
100   WRITE(5,21) TEND,EB,PRR,PZZ,H,R,HH0,DELT
        CLOSE(UNIT=31,DISPOSE='PRINT')
```

```
      CLOSE(UNIT=32)
      STOP
      END
C*********************************************
      SUBROUTINE FCN(N,T,Y,YPRIME)
C*********************************************
      INTEGER N
      REAL Y(5),YPRIME(5),T,MASS
      COMMON/AB/A,B
      COMMON/M/MASS
      COMMON/G/GM
      COMMON/VR/VISC,RTIME1,RTIME2
      COMMON/MP/G,RTIME,XI
C************************************
      PI=3.14159265357989
      EB=Y(1)
      EB2=EB*EB
      PRR=Y(2)
      PZZ=Y(3)
      H=Y(4)
      H2=H*H
      R=Y(5)
      R2=R*R
      R4=R2*R2

      YPRIME(1)=(GM+4.*MASS*H*EB2-A*R4*EB2/4.
     1           +4.*A*R2*H2*EB2/3.-PI*R2*(PRR-PZZ))
     1           /(A*R4/4.+2.*A*R2*H2/3.+2.*MASS*H)
      YPRIME(2)=2.*G*(EB+RTIME2*(YPRIME(1)-2.*(1.-XI)
     1           *EB2))+2.*(1.-XI)*EB*PRR-PRR/RTIME1
      YPRIME(3)=-4.*G*(EB+RTIME2*(YPRIME(1)+4.*(1.-XI)
     1           *EB2))-4.*(1.-XI)*EB*PZZ-PZZ/RTIME1
      YPRIME(4)=-2.*EB*H
      YPRIME(5)=EB*R

      RETURN
      END
C*********************************************
      SUBROUTINE FCNJ(N,T,Y,PD)
C*********************************************
      INTEGER N
      REAL Y(5),PD(N,N),T
      RETURN
      END
```

```
C*****************************************************************
C
C     PROGRAM NJSSLP.FOR
C
C               LUBRICATED SQUEEZING OF INELASTIC FLUIDS
C               WITH JOHNSON-SEGALMAN VISCOSITY.
C
C*****************************************************************
      INTEGER N,METH,MITER,INDEX,IWK(3),IER,IRV
      REAL Y(3),WK(63),T,TOL,TEND,DELT
      DOUBLE PRECISION PRINT,THH0
      EXTERNAL FCN,FCNJ
      COMMON/AB/A,B
      COMMON/AM/AMASS
      COMMON/G/GM
      COMMON/RX/RTIME1,RTIME2,XI
C************************************
      TYPE 10
10    FORMAT(' INITIAL CONDITIONS'/' ENTER T0,EB0,H0,R0')
      ACCEPT *,T0,EB0,H0,R0
      TYPE 11
11    FORMAT(' ENTER DENS, ZERO VISC, MASS OF LOAD')
      ACCEPT *,DENS,VISC0,AMASS
      TYPE 111
111   FORMAT(' ENTER RTIME1,RTIME2,XI')
      ACCEPT *,RTIME1,RTIME2,XI
      TYPE 12
12    FORMAT(' ENTER TOLERANCE, DELT')
      ACCEPT *,TOL,DELT
      TYPE 15
15    FORMAT(' ENTER NPRT,INTERVAL')
      ACCEPT *,NPRT,AINTR
      TYPE 16
16    FORMAT(' ENTER FILENAMES FOR PRINT & T VS. HH0')
      ACCEPT 117,PRINT,THH0
117   FORMAT(A10/A10)
C************************************
      OPEN(UNIT=31,DEVICE='DSK',FILE=PRINT)
      OPEN(UNIT=32,DEVICE='DSK',FILE=THH0)
      WRITE(31,17)
17    FORMAT(/' LUBRICATED SQUEEZING OF INELASTIC FLUIDS',
     1        /' WITH JOHNSON-SEGALMAN VISCOSITY')
      WRITE(31,18) DENS,VISC0,AMASS
18    FORMAT(' DENSITY = ',E14.5/' ZERO VISCOSITY = ',E14.5/
     1        ' MASS OF LOAD = ',E14.5)
      WRITE(31,25) RTIME1,RTIME2,XI
25    FORMAT(' RELAXATION TIME = ',E14.5/
     1        ' RETARDATION TIME = ',E14.5/' XI = ',E14.5)
      WRITE(31,27) TOL
27    FORMAT(' TOLERANCE = ',E14.5)
C************************************
```

```
      PI=3.14159265357989
      N=3
      METH=1
      MITER=0
      INDEX=1
      WRITE(31,28) METH,MITER,INDEX
28    FORMAT(/' METH = ',I4/' MITER = ',I4/' INDEX = ',I4)

      T=T0
      Y(1)=EB0
      Y(2)=H0
      Y(3)=R0

      GM=980.*AMASS
      A=PI*DENS
      B=PI*VISC0

      EB=Y(1)
      H=Y(2)
      R=Y(3)
      HH0=H/H0
      WRITE(5,20)
      WRITE(31,20)
20    FORMAT(//7X,'TIME',12X,'EB',12X,'H',13X,'R',10X,
     1       'H/H0',10X,'DELT'/)
      WRITE(5,21) T,EB,H,R,HH0,DELT
      WRITE(31,21) T,EB,H,R,HH0,DELT
      WRITE(32,*) T,HH0
21    FORMAT(6E14.5)
C*************************************
      DO 100 I=1,NPRT
      TEND=FLOAT(I)*AINTR
      CALL DGEAR(N,FCN,FCNJ,T,DELT,Y,TEND,TOL,METH,MITER,
     1           INDEX,IWK,WK,IER)
      EB=Y(1)
      H=Y(2)
      R=Y(3)
      HH0=H/H0
      WRITE(31,21) TEND,EB,H,R,HH0,DELT
      WRITE(32,*) TEND,HH0
100   WRITE(5,21) TEND,EB,H,R,HH0,DELT
      CLOSE(UNIT=31,DISPOSE='PRINT')
      CLOSE(UNIT=32)
      STOP
      END
C*********************************************
      SUBROUTINE FCN(N,T,Y,YPRIME)
C*********************************************
      INTEGER N
      REAL Y(3),YPRIME(3),T
      COMMON/AB/A,B
```

```
      COMMON/AM/AMASS
      COMMON/G/GM
      COMMON/RX/RTIME1,RTIME2,XI
C*************************************
      EB=Y(1)
      EB2=EB*EB
      H=Y(2)
      H2=H*H
      R=Y(3)
      R2=R*R
      R4=R2*R2

      YPRIME(1)=(GM+4.*AMASS*H*EB2-A*R4*EB2/4.
     1           +4.*A*R2*H2*EB2/3.-6.*B*R2*EB
     1           *(1.+12.*XI*(2.-XI)*RTIME1*
     1           RTIME2*EB2)
     1           /(1.+12.*XI*(2.-XI)*RTIME1*
     1           RTIME1*EB2))
     1           /(A*R4/4.+2.*A*R2*H2/3.+2.*AMASS*H)
      YPRIME(2)=-2.*EB*H
      YPRIME(3)=EB*R

      RETURN
      END
C*************************************************
      SUBROUTINE FCNJ(N,T,Y,PD)
C*************************************************
      INTEGER N
      REAL Y(3),PD(N,N),T
      RETURN
      END
```

```
C*************************************************************
C
C     PROGRAM SMMSLP.FOR
C
C               LUBRICATED COMPRESSIVE FLOW OF
C               MARRUCCI STRUCTURAL MODEL.
C
C*************************************************************
      INTEGER N,METH,MITER,INDEX,IWK(6),IER,IRV
      REAL Y(6),WK(144),T,TOL,TEND,DELT,MASS
      DOUBLE PRECISION PRINT,THH0
      EXTERNAL FCN,FCNJ
      COMMON/AB/A,B
      COMMON/M/MASS
      COMMON/G/GM
      COMMON/VR/VISC,RTIME1,RTIME2
      COMMON/MP/G0,RTIME0,XI,EPS
C************************************
      TYPE 1
1     FORMAT(' LUBRICATED COMPRESSIVE FLOW OF'/
     1       ' MARRUCCI STRUCTURAL MODEL'//
     1       ' ALL INPUT DATA IN CGS UNITS'/)
7     TYPE 10
10    FORMAT(' INITIAL CONDITIONS'/
     1       ' ENTER T0,EB0,PRR0,PZZ0,H0,R0,X0')
      ACCEPT *,T0,EB0,PRR0,PZZ0,H0,R0,X0
      TYPE 11
11    FORMAT(' ENTER DENSITY, AND MASS OF LOAD')
      ACCEPT *,DENS,MASS
      TYPE 111
111   FORMAT(' ENTER ZERO SHEAR MODULUS, ZERO RELAX TIME')
      ACCEPT *,G0,RTIME0
      TYPE 12
12    FORMAT(' ENTER TOLERANCE, DELT')
      ACCEPT *,TOL,DELT
      TYPE 15
15    FORMAT(' ENTER NPRT,INTERVAL')
      ACCEPT *,NPRT,AINTR
      TYPE 16
16    FORMAT(' ENTER FILENAMES FOR PRINT / T VS. HH0')
      ACCEPT 117,PRINT,THH0
117   FORMAT(A10/A10)
C************************************
      OPEN(UNIT=31,DEVICE='DSK',FILE=PRINT)
      OPEN(UNIT=32,DEVICE='DSK',FILE=THH0)
      WRITE(31,17)
17    FORMAT(/' LUBRICATED COMPRESSIVE FLOW OF ',
     1        'MARRUCCI STRUCTURAL MODEL'//)
      WRITE(31,25) DENS,G0,RTIME0,MASS
25    FORMAT(' DENSITY = ',E14.5/' ZERO SHEAR MODULUS = ',
     1       E14.5/' ZERO RELAXATION TIME = ',E14.5/
```

```
     1          ' MASS = ',E14.5)
      WRITE(31,27) TOL
27    FORMAT(' TOLERANCE = ',E14.5)
C*************************************
      PI=3.14159265357989
      N=6
      METH=2
      MITER=0
      INDEX=1
      WRITE(31,28) METH,MITER,INDEX
28    FORMAT(/' METH = ',I4/' MITER = ',I4/' INDEX = ',I4/)

      T=T0
      Y(1)=EB0
      Y(2)=PRR0/(G0*X0)
      Y(3)=PZZ0/(G0*X0)
      Y(4)=X0
      Y(5)=H0
      Y(6)=R0

      GM=980.*MASS
      A=PI*DENS

      EB=Y(1)
      PRRH=Y(2)
      PZZH=Y(3)
      X=Y(4)
      H=Y(5)
      R=Y(6)
      G=G0*X
      PRR=PRRH*G
      PZZ=PZZH*G
      HH0=H/H0
      WRITE(5,20)
      WRITE(31,20)
20    FORMAT(//7X,'TIME',12X,'EB',11X,'PRR',11X,'PZZ',
     1         13X,'H',13X,'R',10X,'H/H0',10X,'DELT',12X,'X'/)
      WRITE(5,21) T,EB,PRR,PZZ,H,R,HH0,DELT,X
      WRITE(31,21) T,EB,PRR,PZZ,H,R,HH0,DELT,X
      WRITE(32,*) T,HH0
21    FORMAT(9E14.5)
C*************************************
      DO 100 I=1,NPRT
      TEND=FLOAT(I)*AINTR+T0
      CALL DGEAR(N,FCN,FCNJ,T,DELT,Y,TEND,TOL,METH,MITER,
     1         INDEX,IWK,WK,IER)
      EB=Y(1)
      PRRH=Y(2)
      PZZH=Y(3)
      X=Y(4)
      H=Y(5)
```

```
      R=Y(6)
      G=G0*X
      PRR=PRRH*G
      PZZ=PZZH*G
      HH0=H/H0
      WRITE(31,21) TEND,EB,PRR,PZZ,H,R,HH0,DELT,X
      WRITE(32,*) TEND,HH0
100   WRITE(5,21) TEND,EB,PRR,PZZ,H,R,HH0,DELT,X
      CLOSE(UNIT=31)
      CLOSE(UNIT=32)
      STOP
      END
C*********************************************
      SUBROUTINE FCN(N,T,Y,YPRIME)
C*********************************************
      INTEGER N
      REAL Y(6),YPRIME(6),T,MASS
      COMMON/AB/A,B
      COMMON/M/MASS
      COMMON/G/GM
      COMMON/VR/VISC,RTIME1,RTIME2
      COMMON/MP/G0,RTIME0,XI,EPS
C*************************************
      PI=3.14159265357989
      EB=Y(1)
      EB2=EB*EB
      PRRH=Y(2)
      PZZH=Y(3)
      X=Y(4)
      X14=X**1.4
      RX14=RTIME0*X14
      H=Y(5)
      H2=H*H
      R=Y(6)
      R2=R*R
      R4=R2*R2

      YPRIME(1)=(GM+4.*MASS*H*EB2-A*R4*EB2/4.
     1            +4.*A*R2*H2*EB2/3.-PI*R2*G0*X*(PRRH-PZZH))
     1            /(A*R4/4.+2.*A*R2*H2/3.+2.*MASS*H)
      YPRIME(2)=2.*EB-PRRH/RX14+2.*EB*PRRH
      YPRIME(3)=-4.*EB-PZZH/RX14-4.*EB*PZZH
      YPRIME(4)=(1.-X)/RX14-0.25*X*SQRT(2.*PRRH+PZZH)/RX14
      YPRIME(5)=-2.*EB*H
      YPRIME(6)=EB*R

      RETURN
      END
C*********************************************
      SUBROUTINE FCNJ(N,T,Y,PD)
      INTEGER N
```

```
REAL Y(6),PD(N,N),T
RETURN
END
```

```
C*************************************************************
C
C     PROGRAM NSMSLP.FOR
C
C               LUBRICATED SQUEEZING OF INELASTIC FLUIDS
C               WITH STRUCTURE-DEPENDENT VISCOSITY.
C
C*************************************************************
      INTEGER N,METH,MITER,INDEX,IWK(3),IER,IRV
      REAL Y(3),WK(63),T,TOL,TEND,DELT
      DOUBLE PRECISION PRINT,THH0
      EXTERNAL FCN,FCNJ
      COMMON/AB/A,B
      COMMON/AM/AMASS
      COMMON/G/GM
      COMMON/RT/RTIME0
      COMMON/X/X
C************************************
      TYPE 10
10    FORMAT(' INITIAL CONDITIONS'/' ENTER T0,EB0,H0,R0,X0')
      ACCEPT *,T0,EB0,H0,R0,X0
      TYPE 11
11    FORMAT(' ENTER DENSITY, MASS OF LOAD')
      ACCEPT *,DENS,AMASS
      TYPE 111
111   FORMAT(' ENTER ZERO VISCOSITY, ZERO RELAXATION TIME')
      ACCEPT *, VISC0, RTIME0
      TYPE 12
12    FORMAT(' ENTER TOLERANCE, DELT')
      ACCEPT *,TOL,DELT
      TYPE 15
15    FORMAT(' ENTER NPRT,INTERVAL')
      ACCEPT *,NPRT,AINTR
      TYPE 16
16    FORMAT(' ENTER FILENAMES FOR PRINT & T VS. HH0')
      ACCEPT 117,PRINT,THH0
117   FORMAT(A10/A10)
C************************************
      OPEN(UNIT=31,DEVICE='DSK',FILE=PRINT)
      OPEN(UNIT=32,DEVICE='DSK',FILE=THH0)
      WRITE(31,25)
25    FORMAT(/' LUBRICATED SQUEEZING OF INELASTIC FLUIDS'
     1       /' WITH STRUCTURE-DEPENDENT VISCOSITY.')
      WRITE(31,26) DENS,VISC0,AMASS,RTIME0
26    FORMAT(/' DENS = ',E14.5/' ZERO VISC = ',E14.5/
     1        ' MASS OF LOAD = ',E14.5/
     1        ' ZERO RELAXATION TIME = ',E14.5)
      WRITE(31,27) TOL
27    FORMAT(' TOLERANCE = ',E14.5)
C************************************
      PI=3.14159265357989
```

```
      N=3
      METH=1
      MITER=0
      INDEX=1
      WRITE(31,28) METH,MITER,INDEX
28    FORMAT(/' METH = ',I4/' MITER = ',I4/' INDEX = ',I4)

      T=T0
      Y(1)=EB0
      Y(2)=H0
      Y(3)=R0
      X=X0

      GM=980.*AMASS
      A=PI*DENS
      B=PI*VISC0

      EB=Y(1)
      H=Y(2)
      R=Y(3)
      HH0=H/H0
      WRITE(5,20)
      WRITE(31,20)
20    FORMAT(//7X,'TIME',12X,'EB',12X,'H',13X,'R',10X,
     1          'H/H0',10X,'DELT',12X,'X'/)
      WRITE(5,21) T,EB,H,R,HH0,DELT,X
      WRITE(31,21) T,EB,H,R,HH0,DELT,X
      WRITE(32,*) T,HH0
21    FORMAT(7E14.5)
C*************************************
      DO 100 I=1,NPRT
      TEND=FLOAT(I)*AINTR
      CALL DGEAR(N,FCN,FCNJ,T,DELT,Y,TEND,TOL,METH,MITER,
     1          INDEX,IWK,WK,IER)
      EB=Y(1)
      H=Y(2)
      R=Y(3)
      HH0=H/H0
      WRITE(31,21) TEND,EB,H,R,HH0,DELT,X
      WRITE(32,*) TEND,HH0
100   WRITE(5,21) TEND,EB,H,R,HH0,DELT,X
      CLOSE(UNIT=31)
      CLOSE(UNIT=32)
      STOP
      END
C*********************************************
      SUBROUTINE FCN(N,T,Y,YPRIME)
C*********************************************
      INTEGER N
      REAL Y(3),YPRIME(3),T
      COMMON/AB/A,B
```

```
      COMMON/AM/AMASS
      COMMON/G/GM
      COMMON/RT/RTIME0
      COMMON/X/X
C**************************************
      EB=Y(1)
      EB2=EB*EB
      H=Y(2)
      H2=H*H
      R=Y(3)
      R2=R*R
      R4=R2*R2
1002  XN=X-(1.38564*RTIME0*EB*X**2.4+X-1.)/
     1       (2.4*1.38564*RTIME0*EB*X**1.4+1.)
      IF(ABS((XN-X)/XN).LT.0.001) GO TO 1001
1005  X=XN
      GO TO 1002
1001  X=XN

1000  YPRIME(1)=(GM+4.*AMASS*H*EB2-A*R4*EB2/4.
     1             +4.*A*R2*H2*EB2/3.-6.*B*R2*
     1             (1.-X)/(1.38564*RTIME0))
     1             /(A*R4/4.+2.*A*R2*H2/3.+2.*AMASS*H)
      YPRIME(2)=-2.*EB*H
      YPRIME(3)=EB*R

      RETURN
      END
C**********************************************
      SUBROUTINE FCNJ(N,T,Y,PD)
C**********************************************
      INTEGER N
      REAL Y(3),PD(N,N),T
      RETURN
      END
```

APPENDIX F

RHEOLOGICAL DATA

F.1 Oscillatory shear data on silicone polymer

(1) Temperature = 18°C

CIRCULAR FREQUENCY, ω (RAD/SEC)	STORAGE MODULUS, G' (DYN/CM2)	LOSS MODULUS, G'' (DYN/CM2)	COMPLEX VISCOSITY, η^* (POISE)
0.1	0.750E+04	0.113E+07	0.113E+07
0.31	0.400E+05	0.360E+07	0.117E+07
1.0	0.275E+06	0.107E+07	0.110E+07
3.1	0.145E+07	0.230E+07	0.877E+06
10.	0.395E+07	0.275E+06	0.481E+06
31.	0.600E+07	0.185E+06	0.203E+06
100.	0.620E+07	0.860E+06	0.626E+05

Horizontal shift factor (a_T) = 1.60

(2) Temperature = 23°C

CIRCULAR FREQUENCY, ω (RAD/SEC)	STORAGE MODULUS, G' (DYN/CM2)	LOSS MODULUS, G'' (DYN/CM2)	COMPLEX VISCOSITY, η^* (POISE)
0.1	0.240E+04	0.730E+05	0.730E+06
0.31	0.130E+05	0.230E+06	0.743E+06
1.0	0.101E+06	0.700E+06	0.707E+06
3.1	0.710E+06	0.185E+07	0.639E+06
10.	0.296E+07	0.310E+07	0.429E+06
31.	0.590E+07	0.265E+07	0.208E+06
100.	0.650E+07	0.135E+07	0.664E+05

Horizontal shift factor (a_T) = 1.0

(3) Temperature = 35°C

CIRCULAR FREQUENCY, ω (RAD/SEC)	STORAGE MODULUS, G' (DYN/CM2)	LOSS MODULUS, G'' (DYN/CM2)	COMPLEX VISCOSITY, η^* (POISE)
0.1	0.100E+03	0.325E+05	0.325E+06
0.31	0.305E+04	0.100E+06	0.323E+06
1.0	0.109E+05	0.330E+06	0.330E+06
3.1	0.173E+06	0.940E+06	0.308E+06
10.	0.115E+07	0.230E+07	0.257E+06
31.	0.390E+07	0.320E+07	0.163E+06
100.	0.570E+07	0.210E+07	0.607E+05

Horizontal shift factor (a_T) = 0.44

F.2 Steady shear data on TLA-227

(1) Temperature = 23.5°C

SHEAR RATE, $\dot{\gamma}$ (SEC^{-1})	SHEAR STRESS, τ_{12} (DYN/CM^2)	NORMAL STRESS, $\tau_{11}-\tau_{22}$ (DYN/CM^2)	REMARK
32.1	0.934E+04	-	CAPILLARY
37.6	0.105E+05	-	($L/R = 268$)
51.0	0.136E+05	-	"
74.8	0.192E+05	-	"
118.2	0.286E+05	-	"

(2) Temperature = 27°C

SHEAR RATE, $\dot{\gamma}$ (SEC^{-1})	SHEAR STRESS, τ_{12} (DYN/CM^2)	NORMAL STRESS, $\tau_{11}-\tau_{22}$ (DYN/CM^2)	REMARK
1.0	0.260E+03	0.110E+03	CONE & PLATE
2.5	0.600E+03	0.300E+03	"
6.3	0.145E+04	0.120E+04	"
16.	0.336E+04	0.440E+04	"
25.	0.463E+04	0.880E+04	"
34.5	0.751E+04	-	CAPILLARY
70.5	0.140E+05	-	($L/R = 268$)
98.	1.83E+05	-	"
122.8	0.224E+05	-	"
168.	0.291E+05	-	"
195.3	0.333E+05	-	"
62.8	0.119E+05	-	CAPILLARY
123.3	0.212E+05	-	($L/R = 160$)
194.5	0.316E+05	-	"
259.1	0.423E+05	-	"
357.9	0.557E+05	-	"

(3) Temperature = 30°C

SHEAR RATE, $\dot{\gamma}$ (SEC^{-1})	SHEAR STRESS, τ_{12} (DYN/CM^2)	NORMAL STRESS, $\tau_{11}-\tau_{22}$ (DYN/CM^2)	REMARK
1.6	0.304E+03	0.800E+02	CONE & PLATE
2.5	0.500E+03	0.180E+03	"
6.3	0.113E+04	-	"
10.	0.185E+04	0.150E+04	"
16.	0.272E+04	0.320E+04	"
25.	0.400E+04	0.588E+04	"

(4) Temperature = 35°C

SHEAR RATE, $\dot{\gamma}$ (SEC^{-1})	SHEAR STRESS, τ_{12} (DYN/CM^2)	NORMAL STRESS, $\tau_{11}-\tau_{22}$ (DYN/CM^2)	REMARK
1.6	0.216E+03	-	CONE & PLATE
4.	0.488E+03	0.206E+03	"
10.	0.115E+04	0.940E+03	"

F.3 Steady shear data on 3.3 wt. % PAA in water solution

Temperature = 25 °C

SHEAR RATE, $\dot{\gamma}$ (SEC^{-1})	SHEAR STRESS, τ_{12} (DYN/CM^2)	NORMAL STRESS, $\tau_{11} - \tau_{22}$ (DYN/CM^2)	REMARK
1.05	0.262E+03	-	CONE & PLATE
2.1	0.330E+03	-	〃
5.28	0.447E+03	-	〃
10.5	0.561E+03	-	〃
21.	0.683E+03	-	〃
52.8	0.879E+03	0.574E+04	〃
105.	0.105E+04	0.862E+04	〃
210.	0.126E+04	0.137E+05	〃
419.	0.151E+04	0.211E+05	〃

APPENDIX G

EXPERIMENTAL DATA ON THE SQUEEZING FLOW

G.1 Newtonian Fluids

(1) Viscasil 60000

Run 1 :

R = 1.252 cm
$2H_o$ = 0.102 cm
m = 6289 g
η = 580 poise (at 25°C)

t (sec)	2H (cm)
0.	0.1021
0.0388	0.0760
0.102	0.0584
0.204	0.0455
0.306	0.0385
0.408	0.0340
0.612	0.0282
0.816	0.0247

Run 2 :

R = 1.252 cm
$2H_o$ = 0.101 cm
m = 6289 g
η = 580 poise (at 25°C)

t (sec)	2H (cm)
0.	0.101
0.0408	0.0750
0.112	0.0569
0.214	0.0448
0.316	0.0375
0.418	0.0329
0.520	0.0297

(2) Dow Corning 200 fluid, 12500

Run 1

$R = 2.534$ cm
$2H_o = 0.211$ cm
$m = 3676$ g
$\eta = 130$ poise (at 22.5°C)

t (sec)	2H (cm)
0.	0.211
0.0214	0.188
0.0897	0.148
0.2254	0.112
0.3274	0.0969
0.429	0.0855
0.5314	0.0775
0.633	0.0719

Run 2

$R = 1.252$ cm
$2H_o = 0.122$ cm
$m = 6290$ g
$\eta = 121$ poise (at 25.5°C)

t (sec)	2H (cm)
0.	0.122
0.0612	0.0403
0.1632	0.0244
0.2652	0.0201
0.3672	0.0171

G.2 Viscoelastic materials

(1) Silicone polymer

Run 1

$R = 0.505$ cm
$2H_o = 0.128$ cm
$m = 17480$ g
$\eta = 920000$ poise (at 20°C)
$\lambda = 0.12$ sec

t (sec)	2H (cm)
0.	0.128
0.02	0.111
0.05	0.109
0.25	0.0986
0.55	0.0858
0.95	0.0740
1.55	0.0617
2.05	0.0543
2.55	0.0486
3.05	0.0444

$V_{max} = 1.$ cm/sec
$\dot{\gamma}_{max} = 105.$ sec^{-1}
$\dot{\gamma}_{max}\lambda = 12.6$

Run 2

$R = 0.505$ cm
$2H_o = 0.26$ cm
$m = 8612$ g
$\eta = 665000$ poise (at 24.4°C)
$\lambda = 0.1$ sec

t (msec)	2H (cm)
0.	0.26
9.2	0.258
14.3	0.250
18.9	0.240
21.9	0.230
24.5	0.224
27.8	0.220
31.1	0.224
34.4	0.230
35.7	0.234
39.8	0.236
44.9	0.234
47.4	0.230
50.0	0.224
52.5	0.220
55.6	0.218
61.0	0.220
67.9	0.224
75.5	0.220
80.6	0.216
84.7	0.215
90.3	0.216
93.8	0.216
102.	0.214
111.2	0.211
116.3	0.211
134.1	0.207
152.	0.204
162.2	0.203
172.9	0.20

$V_{max} = 3.3$ cm/sec
$\dot{\gamma}_{max} = 90.$ sec^{-1}
$\dot{\gamma}_{max}\lambda = 9.$

(2) TLA-227

Run 1

$R = 2.534$ cm
$2H_o = 0.14$ cm
$m = 9307$ g
$\eta = 455(\dot{\gamma})^{0.86-1}$ (at 23.4°C)

t (sec)	2H (cm)
0.	0.14
0.0306	0.126
0.102	0.1124
0.161	0.1005
0.306	0.0864
0.510	0.0724
0.714	0.0636
0.918	0.0570
1.122	0.0519

$V_{max} = 0.46$ cm/sec
$\dot{\gamma}_{max} = 218.$ sec^{-1}
$\dot{\gamma}_{max}\lambda = 2.2$

Run 2

$R = 1.25$ cm
$2H_o = 0.0584$ cm
$m = 3143$ g
$\eta = 455(\dot{\gamma})^{0.86-1}$

t (sec)	2H (cm)
0.	0.0584
0.01275	0.0549
0.06375	0.0490
0.1148	0.0458
0.1658	0.0429
0.2168	0.0404
0.2678	0.0382

$V_{max} = 0.275$ cm/sec
$\dot{\gamma}_{max} = 347.$ sec^{-1}
$\lambda = 2.95$

Run 3

$R = 1.252$ cm
$2H_o = 0.148$ cm
$m = 3143$ g
$\eta = 455(\dot{\gamma})^{0.267-1}$

t (sec)	2H (cm)
0.	0.148
0.02	0.105
0.025	0.103
0.032	0.0986
0.065	0.0829
0.0875	0.074

$V_{max} = 2.16$ cm/sec
$\dot{\gamma}_{max} = 594.$ sec^{-1}
$\dot{\gamma}_{max}\lambda = 3.6$

(3) PAA-water solution

Run 1

$R = 6.35$ cm
$2H_o = 0.2915$ cm
$m = 4751$ g
$\eta = 302.7(\dot{\gamma})^{0.267 - 1}$

t (sec)	2H (cm)
0.	0.2915
0.0115	0.2693
0.0265	0.261
0.0335	0.2584
0.053	0.2466
0.112	0.2145
0.162	0.1864
0.212	0.1618
0.262	0.1435
0.312	0.131

$V_{max} = 1.93$ cm/sec
$\dot{\gamma}_{max} = 898.$ sec^{-1}
$\dot{\gamma}_{max}\lambda = 8.7$